Development and Verification of a High-Resolution X-ray Spectroscopy Line Scanner

Thomas Nesjø

Thesis submitted for the degree of

Master in Mikroelektronikk og Sensorteknologi

60 credits

Fysisk Institutt

Faculty of mathematics and natural sciences

UNIVERSITY OF OSLO

Spring 2023

Development and Verification of a High-Resolution X-ray Spectroscopy Line Scanner

Thomas Nesjø

Development and Verification of a High-Resolution X-ray Spectroscopy Line Scanner

http://www.duo.uio.no/

Printed: Reprosentralen, University of Oslo

Sammendrag

Spektroskopi, målingen av spektrene til elektromagnetisk stråling, har omfattende anvendelser innen astrofysikk, kjerneforskning og industriell tomografi. Innen industriell tomografi brukes strålingsdetektorer i en linjeskannende konfigurasjon. Dette gjør det mulig å inspisere rørledninger og nøyaktig analysere innholdet, for eksempel vann, olje eller stein, ved hjelp av variasjoner i røntgenabsorpsjon. IDEAS tilbyr allerede en kompakt linjeskanner som benytter ROSSPAD-systemet. Nå skal systemet videreutvikles ved å integrere den avlesningsintegrerte kretsen APOCAT. Prosjektet har som mål å demonstrere APOCATs egenskaper, en foton-deteksjonsbasert integrert krets for avlesning, ved å lage en linjeskanner for røntgen- og gammastråler. Linjeskanner-konfigurasjonen muliggjør detaljert analyse og deteksjon av røntgen- og gammastråler i spektroskopiske målinger. I kombinasjon med ROSSPAD-systemet muliggjør det presis og nøyaktig karakterisering av strålingskilder og deres spektrale egenskaper. Et kretskort (Chip-on-board) er designet basert på APOCAT, som muliggjør avlesning av 16 SiPM (Silisium fotomultiplikator). Detektorenhetene er integrert med kretskortet og eksisterende datainnsamlings utstyr og programvare. Ytelsen til scintillatorene, SiPM-ene og avlesningene i laboratoriet karakteriserer systemet. Tester med elektriske pulser og radioaktive kilder utføres for å teste energiområdet, linearitet, terskel og oppløsning. Basert på de forhåndsdefinerte spesifikasjonene oppnår systemet gode resultater. Full bredde halv maksimum (FWHM) er under 10%, og energiområdet strekker seg fra 50 keV til 1.5 MeV. Den ikke-lineære energikarakteristikken (ENL) er langt under spesifikasjonen på 2% og er nær 0,2%. I tillegg demonstrerte systemet pålitelig terskelfunksjonalitet over hele det dynamiske området, noe som gjør det i stand til å detektere og registrere energisignaler over den forhåndsbestemte terskelen. Dette bekrefter at systemet oppfyller kravene til høykvalitets og nøyaktig måling av røntgen- og gammastråler.

Abstract

Spectroscopy, the measurement of the spectra of electromagnetic radiation, finds extensive applications in astrophysics, nuclear research, and industrial tomography. In industrial tomography, radiation detectors are employed in a line-scanning configuration. This allows for inspecting pipelines that enable accurate analysis of their contents, such as water, oil, or rock, using X-ray absorption variations. IDEAS already offers a compact line scanner utilising the ROSSPAD system. Now, the system is further enhanced by integrating a photon detection-based readout integrated circuit, APOCAT. The project aims to demonstrate the capabilities of APOCAT by creating an X-ray and gamma-ray line scanner. The line-scanner configuration allows for highly detailed analysis and detection of X-rays and gamma rays in spectroscopic measurements. Combined with the ROSSPAD system, it enables precise and accurate characterisation of radiation sources and their spectral properties. A circuit board (Chip-on-board) is designed based on APOCAT, which enables a readout of 16 SiPM(Silicon Photomultiplier). The detector units are integrated with the circuit board and existing acquisition hardware and software. The performance of the scintillators, the SiPMs and the readouts in the laboratory characterises the system. Tests with electrical pulses and radioactive sources are conducted to test the energy range, linearity, threshold and resolution. Based on the predefined specifications, the system achieves good results. The full-width half maximum (FWHM) is below 10%, and the energy range extends from 50 keV to 1.5 MeV. Energy Non-Linearity (ENL) is well below the specification of 2% and is close to 0.2%. In addition, the system demonstrated reliable threshold functionality over the entire dynamic range, allowing it to detect and register energy signals above the predetermined threshold. This confirms that the system meets the requirements for high-quality and accurate measurement of X-rays and gamma rays.

Forord

Jeg ønsker først å takke mine veiledere Anja Kohfeldt og Codin Gheorghe for deres veiledning og tips gjennom oppgaven. Jeg ønsker også takke IDEAS for å ha stilt til rådighet med passende utstyr og labplass.

Denne oppgaven har vært fylt med mange utfordringer, men har også vært utrolig spennende og har åpnet døren for enda flere spennende utfordringer. En spesiell takk til Petter Øya, Thorbjørn Østmoe, Tor Magnus Johansen og Jan-Erik Holter for deres tålmodighet og assistanse da dere hørte mitt skrik om hjelp. Til slutt vil jeg takke mine venner, familie og resten av IDEAS for deres motiverende støtte gjennom hele prosessen.

"Success is not final. Failure is not fatal: It is the courage to continue that counts."

- *Winston Churchill* -

Terminology

Abbreviation	Term
ADC	Analog to Digital converter
ASIC	Application-specific integrated circuit
CI	Current integrator
CMIS	Charge Sensitive Amplifier
CMOS	Complementary Metal-Oxide-Semiconductor
CsI(Tl)	Thallium doped cesium iodide
CSA	Charge Sensitive Amplifier
Cs137	Caesium 137
DAC	Digital to analog converter
DetCarrier	Detector Carrier Board
ENC	Equivalent Noise Charge
ENL	Energy Non-Linearity
FEB	Front end Board
FWHM	Full width half maximum
GCU	Gain calibration unit
IC	Integrated circuit
LVDS	Low Voltage Differential Signaling
Msps	Mega-samples per second
PD	Peak detector
PMT	Photo multiplier tube
Pz	Pole zero cancellation
ROIC	A Readout integrated circuit (ROIC)
ROSSHIP	Readout System Spectroscopic High-resolution Pulse-height
ROSSPAD	Readout System for Silicon Photomultiplier Arrays in Detectors
SAR ADC	Successive Approximation Register (Analog-to-Digital Converter).
SHA	Shaper optimizes the signal-to-noise ratio
SiPMs	Silicon photomultipliers
SPI	Serial peripheral interface
TOR	Logic OR'ed-signal of triggers from all 17 channels.

Table 0.1: Terminology in alphabetic order

Contents

1 Introduction

Spectroscopy is a technique that involves the interaction between matter and electromagnetic radiation, including the absorption, emission and scattering of electromagnetic radiation by atoms or molecules. Spectroscopy measurement is a versatile technique that finds applications in various fields. For example, it is widely used in astrophysics, nuclear research, medical imaging and security applications. Radiation detectors in a line-scanning configuration make it possible to inspect pipelines in the context of pipeline tomography. By studying their unique characteristics, this method enables accurate analysis of the pipeline contents, including water, oil, or rock. With the line-scanning configuration, the detector system moves methodically across the pipeline, collecting numerous data points along a designated path. This approach allows for the creation of high-quality images and enables precise analysis of X-ray absorption changes in various parts of the pipeline.

The motivation for this thesis aims to explore new aspects of APOCAT. By integrating APOCAT into the ROSSPAD system, IDEAS aims to showcase enhanced performance and capabilities for X-ray and gamma-ray detection. While IDEAS already possesses a system with a line-scanning configuration, utilising APOCAT offers the potential for further improvements, particularly in handling high count rates. Additionally, the internal ADC of APOCAT enables standalone operation without additional components, thus reducing system costs. The assignment seeks to examine and evaluate the integration of APOCAT with the scintillator-based detectors in the ROSSPAD system by assessing factors such as energy range, linearity, threshold and resolution. The results of this research will help advance the ROSSPAD system and demonstrate APOCATs potential for future high-resolution X-ray spectroscopy applications.

1.1 Task Description

The primary goal of this project is to showcase the capabilities of the APOCAT readout integrated circuit. This will be accomplished by developing an X-ray and gamma-ray line scanner that utilises photon detection principles, scintillator arrays, and silicon photomultipliers (SiPM). The line scanning configuration, implemented with the ROSSPAD system, will serve as a demonstration platform to highlight the versatility and performance of the readout integrated circuit, APOCAT.

In the first phase, existing designs of scintillator arrays and SiPM arrays are utilised, and necessary modifications are carried out. A small batch of detector units is produced with appropriate scintillators and SiPMs.

The second phase involves designing and producing a circuit board (Chip-on-board, COB) that enables the readout of 16 SiPMs, based on the existing integrated readout circuit APOCAT.

The detector units are integrated with the circuit board and existing acquisition hardware and software in the third phase.

The final phase focus on characterising the performance of the scintillators, the SiPMs and the readout in the laboratory environment. Tests with electrical pulses and radioactive sources are performed to confirm factors such as energy range, linearity, threshold and resolution of the X-ray and gamma-ray measurements. Calibration and determination of the energy distribution are performed using the ROSSPAD ADC.

System Requirements

The system requirements for this project are driven by the limitations of the scintillators and the specifications provided by APOCAT. The proposed system must meet or exceed the existing system's performance delivered by IDEAS. The goal is to achieve a minimum level of performance that is either better or at least comparable to the current system. This ensures that the new system has accurate measurements of X-rays and gamma-rays.

- Scintillator linear array made of 8 crystals of CsI:Tl.
- SiPM linear array, made of 8 SiPMs.
- Energy range: 50keV to 1.5MeV
- Energy non-linearity less than 2%
- Energy threshold: programmable in the range from 50 keV to 1.5 MeV
- Energy resolution: better than 10% full-width-half-maximum FWHM for energy around 662 keV

1.2 Structure of this Work

This report follows the IMRAD (Introduction, Method, Results, Discussion) format, although the sections are somewhat integrated due to the complex system design. The theoretical background chapter combines physics concepts, analysis techniques, and unit explanations while incorporating information about the Readout Integrated Circuit (ROIC) and system description as part of the theory. The system verification section presents the test plan, which outlines the structure and approach of the testing process. It provides a detailed description of the experimental setup, including the equipment used and measurement procedures. The results are discussed throughout the test results and summarised in an achievements table, followed by a system comparison discussion chapter. The appendix includes additional system information in the form of figures, codes, and tables.

Various software programs were utilised for different purposes. For example, Cadstar was used for the schematics and layout design of the front-end board, Xilinx ISE for hardware implementation, IDEAS-Testbench for analysis, and Python for data analysis.

2 Theoretical Background in Radiation Detection

2.1 The Photon

The Photon is an elementary particle and the quantum of the electromagnetic field, including electromagnetic radiation such as light and radio waves, and the force carrier for the electromagnetic force. Photons are mass-less, so they always move at the speed of light in a vacuum, which is approximately 299,792,458 meters per second.

Photon energy [1, Ch. 1] is the energy carried by a single photon. The Planck–Einstein relation states that the amount of energy is directly proportional to the photon's electromagnetic frequency (eq 2.1) and inversely proportional to its wavelength. So, therefore the higher the photon's frequency, the higher its energy. Equivalently, the longer the photon's wavelength, the lower its energy.

$$
\begin{aligned}
&E = hf \\
&E = \frac{hc}{\lambda}
\end{aligned}
\qquad
\begin{aligned}
E &= (\text{Photon energy}) \\
h &= 6.62607015 \cdot 10^{-34} [J \cdot Hz^{-1}] \text{ (Planck constant)} \\
f &= (\text{frequency})[\text{Hz}] \\
c &= (\text{Speed of light in vacuum})[\text{m/s}] \\
\lambda &= (\text{Photon's wavelength})[\text{m}]
\end{aligned}
\tag{2.1}
$$

The unit for measurement of radiation energy is in electron volt (eV), defined as the kinetic energy gained by an electron by its acceleration through a potential of 1 volt and corresponds to a minimal amount of energy.
An elementary charge (proton or electron) is defined as ($1.6 \cdot 10^{-19}$ Coulomb), and we know that volt can be expressed as $1\,\text{V} = 1\frac{J}{C}$, which defines electron volt in terms of joules.

$$
\begin{aligned}
1\,\text{eV} &= 1.602 \cdot 10^{-19}[C] \cdot 1\frac{J}{C} \\
1\,\text{eV} &= 1.602 \cdot 10^{-19}[J]
\end{aligned}
\tag{2.2}
$$

Figure 2.1 shows the electromagnetic spectrum with the wavelength, frequency, and energy of common types of electromagnetic radiation. X-rays have frequencies ranging from $3 \cdot 10^{16}$ Hz to $3 \cdot 10^{19}$ Hz corresponding to energies in the range of 100 eV to 100 keV. In comparison, the human eye is sensitive to electromagnetic radiation with wavelengths between approximately 390 and 750 nm ($400–790 \cdot 10^{12}$ Hz).

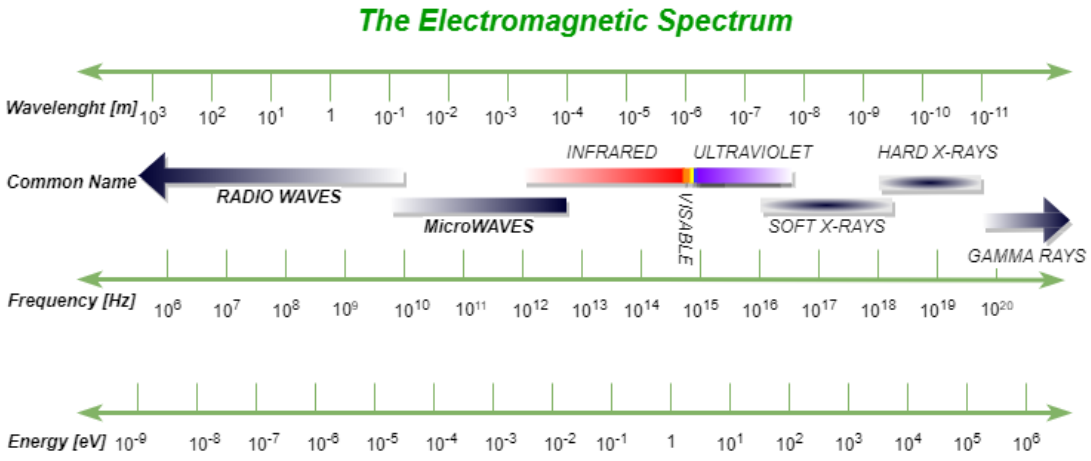

Figure 2.1: The electromagnetic spectrum

2.2 Radiation Detection Methods

Methods for detecting the intensity and characteristics of ionizing radiation, such as alpha, beta, and gamma rays or neutrons, are often referred to as the ionizing process.
The process of electromagnetic radiation involves removing an electron from an initially neutral atom or molecule, and the energy required for this process varies depending on the material being interacted with.
Ionizing radiation can take the form of electromagnetic radiation, such as X-rays or gamma rays. X-rays are emitted when electrons transition between energy levels in an atom, while gamma rays are emitted from the nuclei of atoms during radioactive decay. In both cases, the radiation takes the form of photons of electromagnetic energy.

Electromagnetic energy can be detected as pulses by a radiation detector, and the distribution of pulse heights can be interpreted as a plot between the number of ionizing radiation pulses and the energy from the radioactive source, as depicted in figure 2.2. This plot is referred to as a radiation spectrum and can be used to detect various forms of ionizing radiation, including X-rays and gamma rays. Radiation detectors are commonly used in medical imaging, particularly in

X-ray imaging techniques such as computed tomography (CT) and radiography. These detectors are used to measure the intensity of X-ray beams that pass through the body and create an image based on the differences in X-ray absorption between different tissues. This can aid in the detection and characterization of diseases, as abnormal tissue may have different X-ray absorption properties than healthy tissue.

Another usage area would be the field of space-based gamma-ray astronomy, and an example is in the All-sky medium-energy Gamma-Ray observatory (AMEGO) mission where an AMEGO calorimeter subsystem measures gamma-rays [2]. Measurement of gamma rays is of particular interest in astrophysical studies because sources such as pulsars, active galactic nuclei, and supernova remnants emit them, allowing insight into these cosmic objects.

2.2.1 Radiation Sources and Their Spectrum Properties

Another application of radiation detection techniques is detecting and determining specific radioactive isotopes. One such isotope is caesium-137 (Cs^{137}), a radioactive isotope produced by nuclear fission. To calibrate and test the sensitivity of radiation detectors, Cs^{137} is commonly used in small amounts due to its strong gamma radiation emissions. The resulting gamma radiation can be detected and measured by placing a probe of Cs^{137} near the detector. These instruments measure the ionizing radiation produced by Cs^{137}, which can be used to determine the level of radiation exposure. By analyzing the energy spectrum of the detected gamma rays, the peak at 662 keV can be identified as the characteristic peak of Cs^{137}. The height and shape of the peak in the energy spectrum provide information about the intensity and distribution of the Cs^{137} source, which can be used to calibrate the detector and determine the level of radiation exposure. The precision and accuracy of the radiation detection system are ensured by using a well-characterized

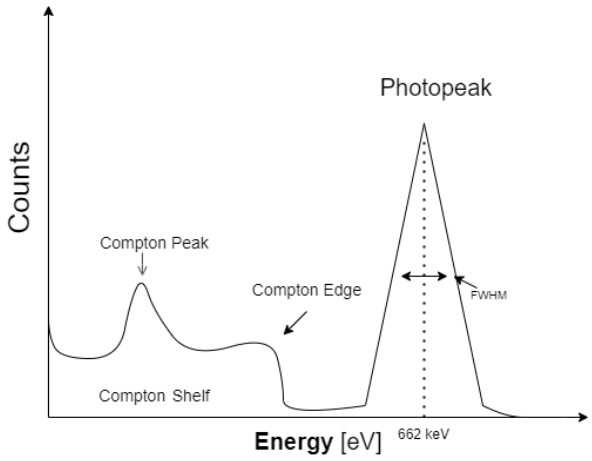

Figure 2.2: Gamma spectrum of Cs^{137} shows a very clear peak at 662keV, makes it a good calibration source. The lower energy peak shows Compton scatter and backscattering events.

and calibrated radiation source, and Cs^{137} is particularly valuable for this purpose due to its well-defined energy spectrum and high gamma-ray yield. Using multiple calibration sources for calibration purposes is also a good approach for calibration, and the table 5.1 shows other sources used in this thesis.

2.2.2 The Compton Effect

Figure 2.2 shows a clear peak for Cs^{137} at 662 keV, which is the characteristic peak of Cs^{137}, but it also displays other areas with lower energy. These areas are caused by Compton scattering shown in figure 2.3, where the photons interact with matter and lose some of their energy. The relationship of the scattered photon E' and the scattering angle θ can be derived as the formula 2.3. Back-scattering is another phenomenon observed in figure 2.2. It occurs when the photons interact with matter and change direction, causing them to bounce back toward the detector. This can result in a peak at lower energies than the main peak, also known as the back-scatter or -Compton peak. [3] This occurs when the angle θ is approximately 180 degrees, where the scattered photon is reflected back towards the detector. The back-scatter peak intensity is affected by the detector's geometry and the sample being measured. Therefore, it can offer valuable information regarding the properties of the measured samples.

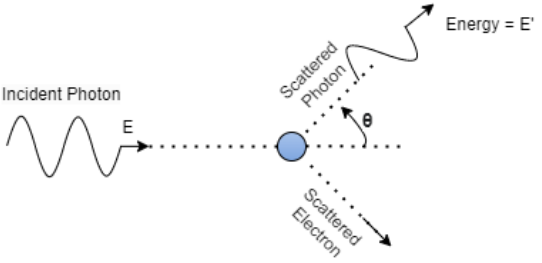

Figure 2.3: The Compton effect where a gamma ray photon is deflected through an angle θ with respect to its original direction

The Compton peak occurs at an intermediate scattering angle between the Compton edge and the Compton shelf. Specifically, the Compton peak occurs at a scattering angle corresponding to the maximum energy transfer from the photon to the electron, which depends on the photon's initial energy and the electron's rest mass energy.

At low angles of scattering (θ near 0), the Compton scattering process results in a small transfer of energy from the photon to the electron, which gives rise to the Compton shelf. Energy transfer is maximized at high scattering angles (θ near π), resulting in the Compton edge.

$$E' = \frac{E}{1 + \frac{E}{mc^2}(1 - cos(\theta))} \qquad (2.3)$$

E = initial energy of incident gamma photon
E' = energy of scattered photon
θ = angle of scattering
m = rest mass of electron
c = speed of light

2.2.3 Spectral Analysis Techniques

An important parameter that is often measured during radiation detection and analysis is the **"Full width half maximum"** (FWHM). This is because the FWHM provides information about the detector's resolution or ability to distinguish between different energy levels of ionizing radiation. A narrow FWHM indicates high resolution, while a broad FWHM indicates lower resolution.

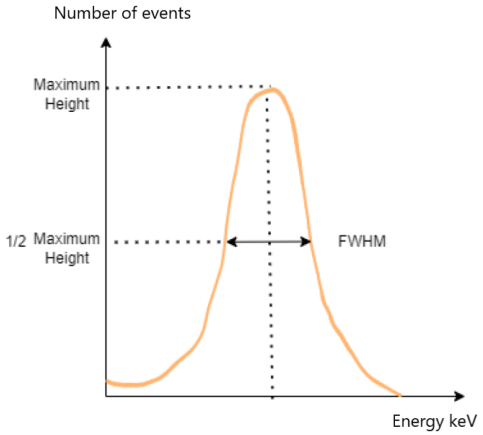

Figure 2.4: Full width at half maximum (FWHM)

In equation 2.4, the resolution FWHM is defined as the full width at half maximum ΔE of the energy peak E_p

$$\text{FWHM} = \frac{\Delta E}{E_p} \qquad (2.4)$$

The result of the FWHM is often expressed in a percentage, and for scintillation detectors, its common below 10% [4, Ch.4] for energy's around 662 keV. Still, it is also expected to see a variation of FWHM based on the energy. Peak variation due to the statistical variation in the number of electrons created at the photocathode and higher energy gamma rays create more electrons at the photocathode than lower energy gamma rays. Therefore the FWHM of a given detector will be more significant for lower energy photo-peaks than for higher energy photo-peaks. Since it's clear that a variation of FWHM is based on energy, it's common to use Cs^{137} as a reference for determining the resolution.

Therefore, by measuring the FWHM of the Cs^{137} peak, we can determine the radiation detector's

quality and performance and ensure accurate ionizing radiation measurements. In the case of Cs^{137}, measuring the FWHM of the 662 keV peak can provide information about the energy resolution of the detector and its ability to accurately measure the intensity of the radiation. In addition to the factors that affect the sensitivity and resolution of radiation detectors, there is another important consideration to consider when reading a gamma spectrum. The baseline noise or pedestals is the output signal produced by the detector in the absence of any radiation source. It can arise from various sources, including electronic noise, dark current, or leakage current. The presence of pedestals can increase the background noise level, making it difficult to distinguish between the signal from the radiation source and the noise. To solve this problem, measuring and accounting for pedestals in the radiation data is crucial. One common approach is subtracting the pedestal signal from the total signal received from the detector. This can improve the signal-to-noise ratio and provide more accurate measurements of the radiation source. There are different methods for measuring the pedestal signal, such as taking measurements with no radiation source present or using statistical techniques based on multiple measurements.

2.2.4 Scintillators

Scintillators is a group of materials that can convert high energy radiation (x- and gamma-rays) to a near visible or visible light. These materials emit light when they absorb particles or electromagnetic waves, which creates free electrons in the material. [4, ch.9]
When an external particle enters a scintillator medium, the scintillator medium absorbs the energy of the incident particle and converts it into a photon burst. The wavelength of the photon burst depends on the specific scintillator material and the energy of the incident particle. The photon bursts are then detected by a photodetector, which converts the emitted light into an electrical current pulse. The current pulse can be amplified, processed, and analyzed to determine the energy and other properties of the incident ionizing radiation.

CsI(tl) Scintillator

One of the brightest scintillation materials is the thallium-doped caesium iodide, (CsI(Tl)) . Together with a silicon photomultiplier (SiPM) detector, it has an emission peak at 550nm, which gives it a wide usage area. It has a relatively high light output, fast response time, and good energy resolution for gamma rays. Usages might be security inspection for example, homeland security and custom border protection, other usage might be nuclear medicine, particle physics, and environmental monitoring, among others.

2.2.5 The Silicon Photomultiplier (SiPM)

SIPMs are a type of photodetector capable of detecting single photons. SiPMs consist of several hundred to thousands of micro-cells, all connected in parallel. Each micro-cell (Figure 2.5) is an avalanche photo-diode with its quench resistor and a capacitively coupled fast output. When a photon enters the photo-diode, it creates an "avalanche" of electron-hole pairs. Due to a large number of carriers generated due to ionization, a gain factor of 10^6 is achieved, which is almost the same as for a classical Photo multiplier tube (PMT) (gain of 10^7). The avalanche is stopped with the quenching resistor, which is switched off due to the current floating through the PN junction in the photodiode.
Since a micro-cell only gives information about whether there was

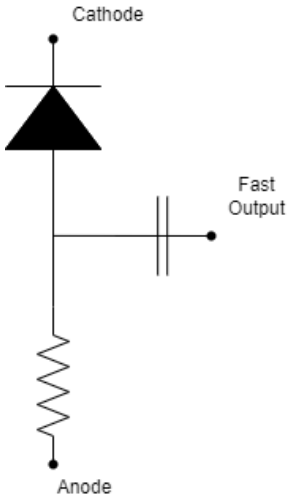

Figure 2.5: Circuit schematic of the Microcell[5]

a photon, they are connected in parallel so multiple incidences can be detected simultaneously, which is what's called a Silicon Photomultiplier [6].

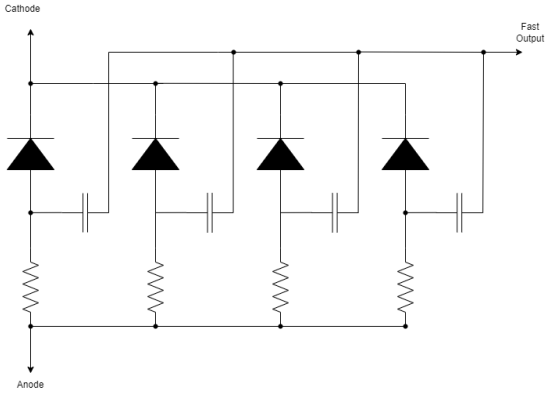

Figure 2.6: Simplified Circuit Schematic of a SiPM showing four microcells in parallel, typically SiPM sensors have hundred to thousands of microcells

When compared to a PMT, a SiPM has several advantages, where the SiPMs have an operating voltage below 70 V compared to above 1000 V for PMT. While PMTs have a large photosensitive area, SiPMs achieve a similar result by using an array of many individual microcells. In addition, SiPMs are also more compact and robust than traditional PMT, where PMTs have a more complex arrangement of dynodes and electrodes. The SIPMs consist, as mentioned above, of arrays of tiny microcells. SiPMs are also less sensitive to magnetic fields than PMTs and are less complex (Figure 2.6). On the other hand, SiPM is highly temperature sensitive, with a temperature-dependent noise rate in the MHz region compared to PMTs kHz rates. PMTs are typically used for detecting and measuring radiation intensity and offer a higher dynamic range and gain than SiPMs but do not provide spatial information about the distribution or location. SiPMs have higher quantum efficiency, higher temporal resolution, and response time than PMTs, leading to improved spatial resolution in Compton imaging. [7]

2.2.6 Matrix Vs Line Configuration for SiPMs

For radiation applications, both the linear and matrix arrangements of SiPMs have their advantages and disadvantages.

In a linear array of SiPMs, each SiPMs is directly measuring the radiation intensity at a specific point along a line which gives better spatial resolutions in a specific direction compared to a matrix. The detector can also more accurately determine the position and direction of the radiation source. Additionally, lining up the SiPMs in a single row can simplify the readout electronics and reduce costs compared to a matrix configuration, as fewer readout channels are required.

In a matrix configuration, a larger volume of radiation is detected, leading to an increased sensitivity for detecting low radiation levels. As a larger area is covered, the location of the radiation can more easily be pinpointed. This is particularly useful in applications where the source of the radiation needs to be located precisely. Another thing about the matrix configuration is the possibility of cross-talk. When the SiPMs are arranged in a matrix, the signals from the neighboring SiPMs can interfere with each other, which can cause cross-talk and degrade the spatial resolution of the measurement.

2.2.7 Pulse processing

Under irradiation, a series of transient current pulses are injected into the pulse processing system, as shown in Figure 2.7. The system's output is usually a count rate or an energy spectrum. In count mode, the number of pulses that meets a certain discriminator threshold criteria increments a counter. The energy spectrum mode is a measurement of the distribution of energies deposited by the pulses in the detector. The figure shows the chain of the main signal processing performed in a system and how the pulses are processed along the way.

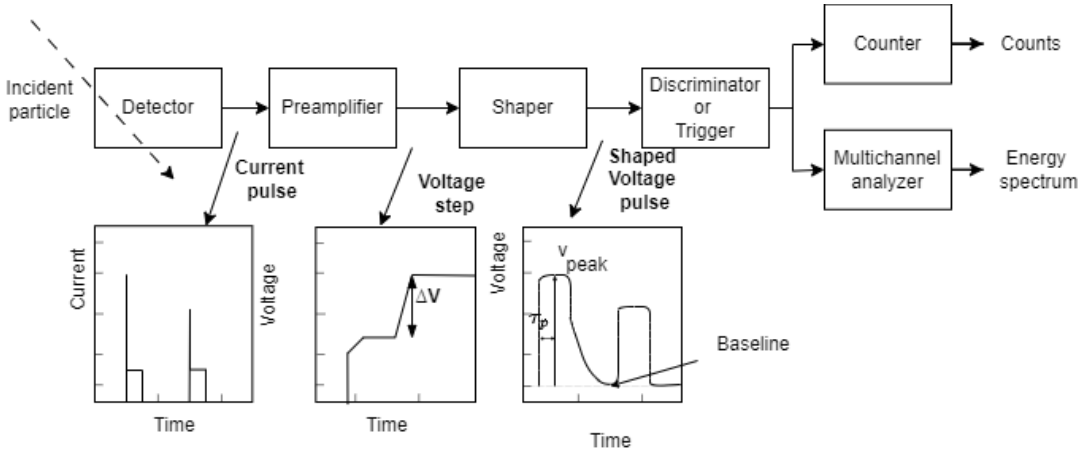

Figure 2.7: Schematic diagram of the detector and electronics shows a typical output stage of the processing electronic. Showing two pulses in time

An incident particle interacts with the detector, and deposit energy is converted into a current pulse as explained in chapter 2.2.4. Since the current charge is so low that it cannot be sensed directly, it is sent to the preamplifier. The preamplifier integrates the current pulse to produce a voltage step. The shaper converts the preamplifier output into a measurable form making a voltage pulse with pulse height V_{peak}. The pulse height is proportional to the initial charge, making pulse height distribution a useful method of providing information about the energy from the incident particle. To prevent overlapping pulses, the shaper must quickly return to baseline before the next event occurs. The discriminator selects all pulses with pulse height above a certain threshold, and the selected events are processed in a counter that implements events over a finite period. The processing result is a histogram or, as we know, the pulse height spectrum. [4, ch. 16]. To achieve a compact readout with multiple SiPMs, a multi-channel readout integrated circuit is necessary, and the ideal solution is to use an application-specific integrated circuit (ASIC) designed for this purpose.

3 Readout Integrated Circuit (ROIC)

ASIC

An application specific integrated circuits (ASIC) has the benefit of integrating a maximum amount of circuitry for a particular function on a single IC. As mentioned in chapter 2.2.5, several SiPMs are to be read out, and a multichannel circuit is required. ASICs provide size and space efficiency since they can be designed with a smaller footprint than equivalent discrete components, making them an obvious choice. It can be optimized for specific tasks, allowing them to operate with greater power efficiency than an equivalent circuit made up of discrete components. ASICs can be designed to perform specific functions with greater speed and accuracy than a circuit of discrete components. In addition, for specialized scientific applications where instrument performance is limited by factors such as form factor and signal/cable length, an ASIC can be a suitable choice as it can be designed to fit into small spaces and minimize signal degradation over long cable lengths. However, ASIC design can be expensive and time-consuming, making it most suitable for high-volume applications where the benefits outweigh the initial investment.

ROIC

A Readout Integrated Circuit (ROIC) is an integrated circuit specifically used for reading detectors of a particular type, such as scintillation detectors for gamma-ray and X-ray detection. ROICs play a critical role in converting the weak signals generated by radiation detectors into digital data that can be processed and analyzed. This project uses an ASIC-based ROIC as a high-performance readout circuit for scintillation detectors. The ROIC has been optimized for low noise and high sensitivity to the specific type of radiation being detected and includes features such as pulse shaping and pulse height analysis to distinguish between different types of radiation. As a result, the ROIC provides a compact and efficient solution for reading out signals from multiple scintillation detectors and is expected to offer superior performance compared to an equivalent circuit made up of discrete components.

3.1 Introducing SIPHRA

The ROIC, called SIPHRA [8], is a general-purpose IC for the readout of Photon detectors, such as PMTs, SiPMs, and multi-pixel photon counters (MPPCs). As an example of its versatile usage SIPHRA is utilized as the front-end readout for the detector system in the GMOD study [9], facilitating the accurate measurement and analysis of gamma-ray signals. SIPHRA has 16 input channels and a summing channel which sums the current from the 16 channels. Every channel has programmable channel outputs, and the readout module can perform various functions, including waveform sampling and digitization, pulse height and time spectroscopy, pulse counting, triggering, and time-over-threshold analysis.

The readout module includes a 12-bit internal Analog to digital converter (ADC) for digitization, providing a convenient and efficient solution for many applications. However, for applications where higher resolution is required, the module also has the capability to interface with an external ADC, allowing for even greater precision in digitization. The ROIC includes an SPI interface for register programming. This interface allows for easy configuration of the ROIC's internal settings and features. In addition, it uses a serial data transmission line that enables fast readouts from the detector. SIPHRAs output channels are shown in the figure below.

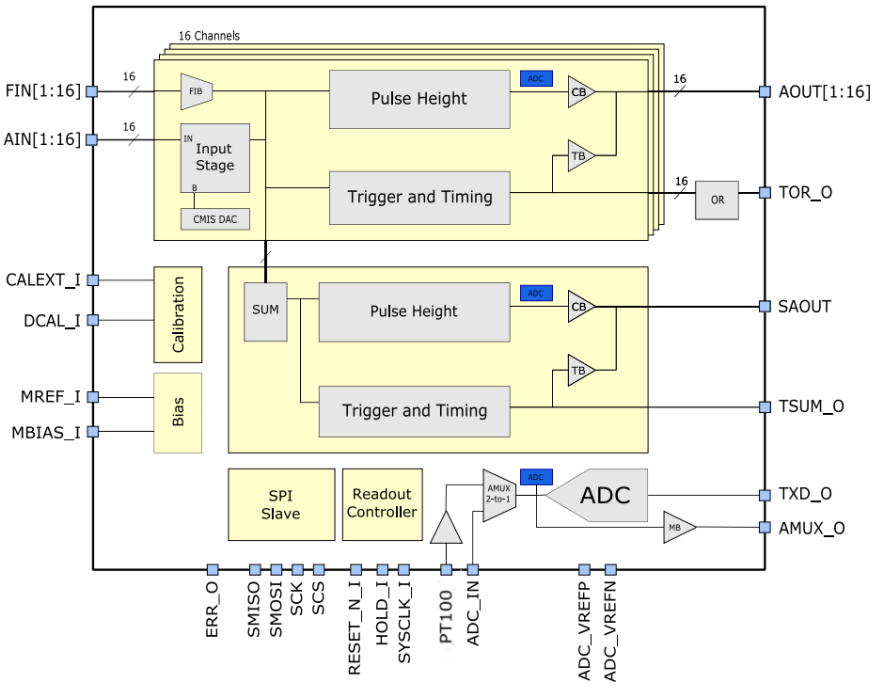

Figure 3.1: Block diagram for the output channel in SIPHRA

3.2 Introducing APOCAT

Introducing another ROIC designed for high-performance readout of photon detectors, The APOCAT [10] is used in missions such as the ASO-S mission to study the relationships among the solar magnetic field, solar flares, and coronal mass ejections [11]. The ROIC features a range of improvements over the previous model, including higher rate capability in each channel thanks to pole-zero cancellation, baseline holder, dc compensation, and a peak detector. In addition, the APOCAT includes a charge-sensitive amplifier (CSA) with individually adjustable gains for greater accuracy and flexibility when correcting for gain variations among multiple detectors. APOCAT also features a faster SAR ADC for more rapid and precise digitization of detector signals. Furthermore, each channel includes four counters for more advanced data processing capabilities. By setting different threshold values for each counter, one can adjust the sensitivity of each channel to match the expected signal level. Due to the addition of counters, the ROIC has both an analog and digital output for each channel. The analog output provides pulse height information for external digitization, while the digital output offers a range of options for time spectroscopy, pulse counting, triggering, and time-over-threshold measurements. APOCATs output channels are shown in the figure below.

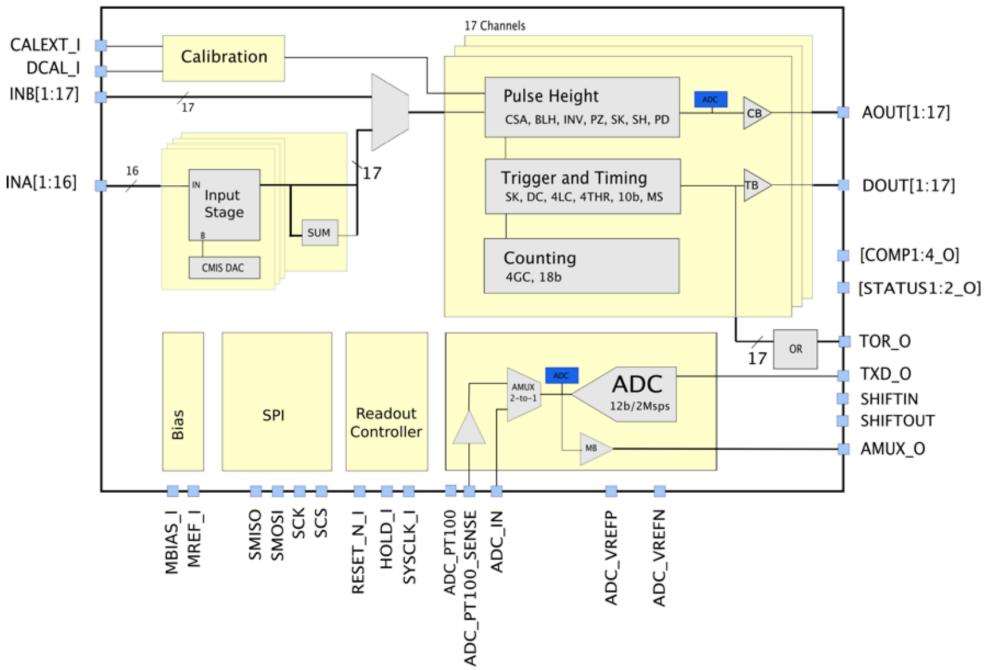

Figure 3.2: Overall block diagram for the Readout output channels in APOCATs

3.3 Pulse Height Spectroscopy Readout

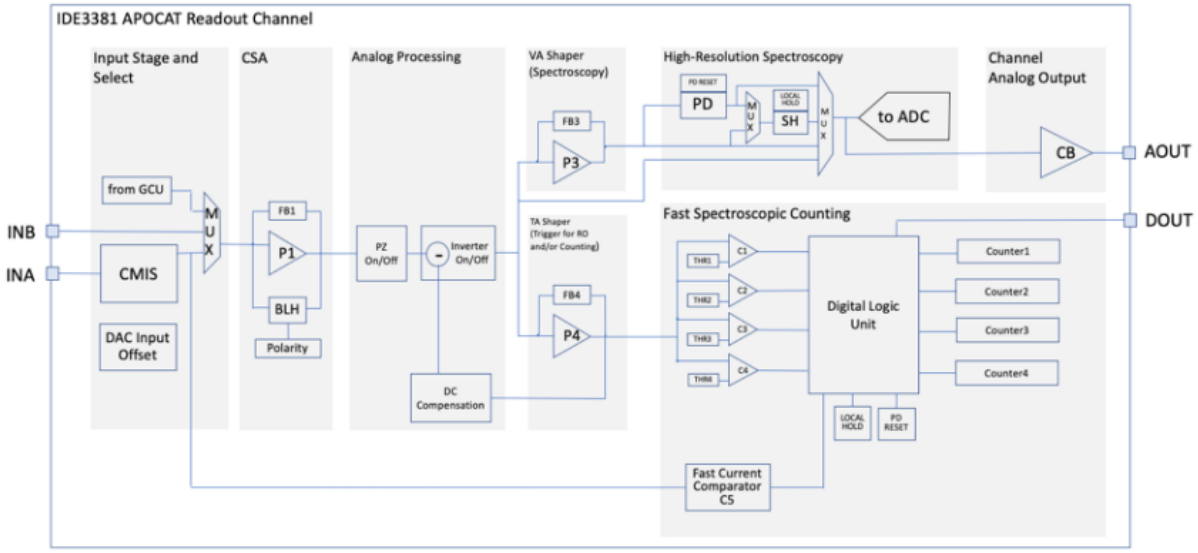

Figure 3.3: Detailed block diagram for the readout output channels in APOCAT

From the more detailed block diagram for APOCAT (Figure 3.3), the analog processing output feeds the Va(slow) shaper for spectroscopy and the TA(fast) shaper for triggering and counting. The pulse-height spectrometer block consists of the VA shaper (P3), multiplexers (MUX), a peak detector (PD), a sample-and-hold unit (SH) and a channel output buffer (CB). The different aspects of AOUT can be looked at by changing the ROIC configuration register as seen in the figure 3.4

Gain Calibration Unit

In the **FIRST STAGE**, in Figure 3.3, one can choose to use the input stage from the Gain Calibration Unit (GCU). This unit offers the possibility to measure gain variations and non-linear responses from channel to channel. This is achieved by injecting a calibration charge internally or externally at the Charge Sensitive Amplifier (CSA) input. "The voltage step can be adjusted using a 10-bit digital-to-analog converter (DAC), providing programmable options between 0 and 3.3 V for generating the calibration charge."

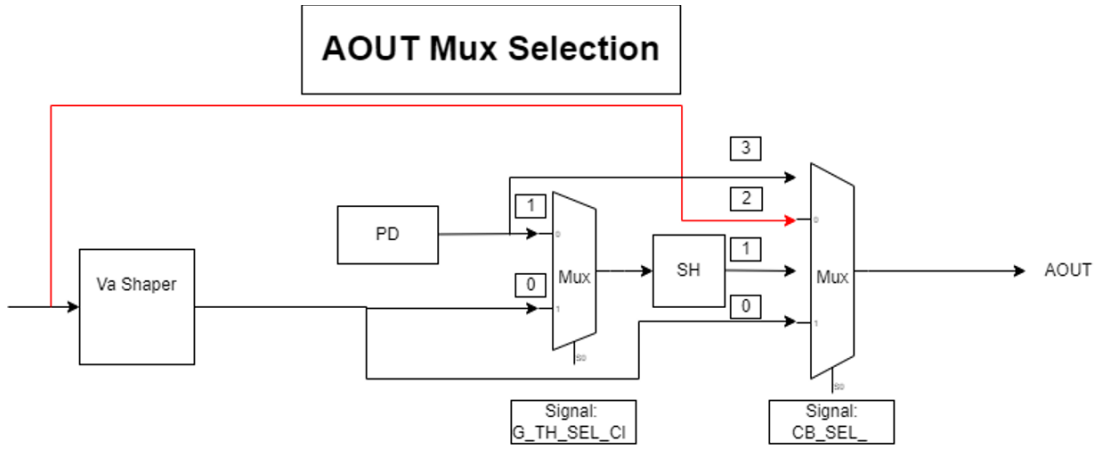

Figure 3.4: The mux selection of the analog output in each channels, showing a configuration of the MUX output for AOUT. There are two Mux the first chooses the output for Peak detecting or not. The second MUX can choose between output or input of the Shaper, as well as output of Sample and hold or peak detector.

Triggering Readout And Counting

Each channel is equipped with four level comparators, which allow for pulse height discrimination. Each comparator is capable of generating a trigger pulse that starts the readout process and increments a counter.

The comparators serve three main purposes. Firstly, they generate an internal hold signal that triggers the track and hold function and initiates digitization in the ADC. Secondly, they produce a timing trigger pulse that signals the occurrence of an event to the system through the logic OR operation. TOR_O is a logic OR of triggers from all 17 channels. When a signal from any comparator is detected, the corresponding channel is enabled for data readout. By combining the triggers from all channels, the logic OR operation ensures that all relevant events are captured and recorded for analysis. Finally, they provide a time-over-threshold (TOT) measurement at DOUT[1:17], which is proportional to the input charge. A block diagram of the digital logic is shown in the figure below.

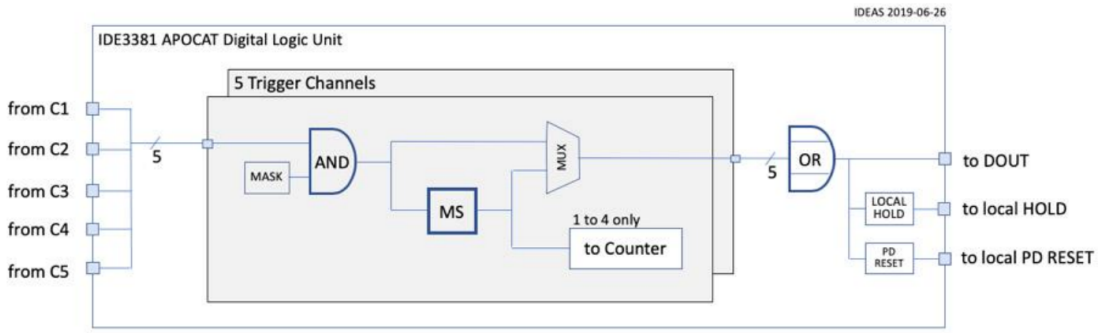

Figure 3.5: APOCATs block diagram for the digital logic for each channel, where the five comparators feed the input (four for counters and one for TOT). The five digital signals are combined in a logic which drives the digital outputs.

3.4 ASIC Mode Selection

The APOCAT offers multiple modes, with both internal Hold and internal ADC but offers also the possibility to use external Hold and external ADC. Figure 3.6 shows the different mode possible within APOCAT, all channels have the opportunity to be read out through the multiplexer (AMUX), and the output can either be to the internal or an external ADC. Another option is to read out each channel directly with multiple external ADCs. Each analog channel contains an analog sample and hold circuit, and the triggering of this hold may come from several sources, depending on the configuration. Another option is to use an external hold. The readout mode implemented for spectroscopy in this thesis is with the external ADC and internal hold, highlighted in the figure with red colors. Where all channels are multiplexed out to the ADC after a trigger event, the Shift signal controls the multiplexer when the internal ADC is not in use.

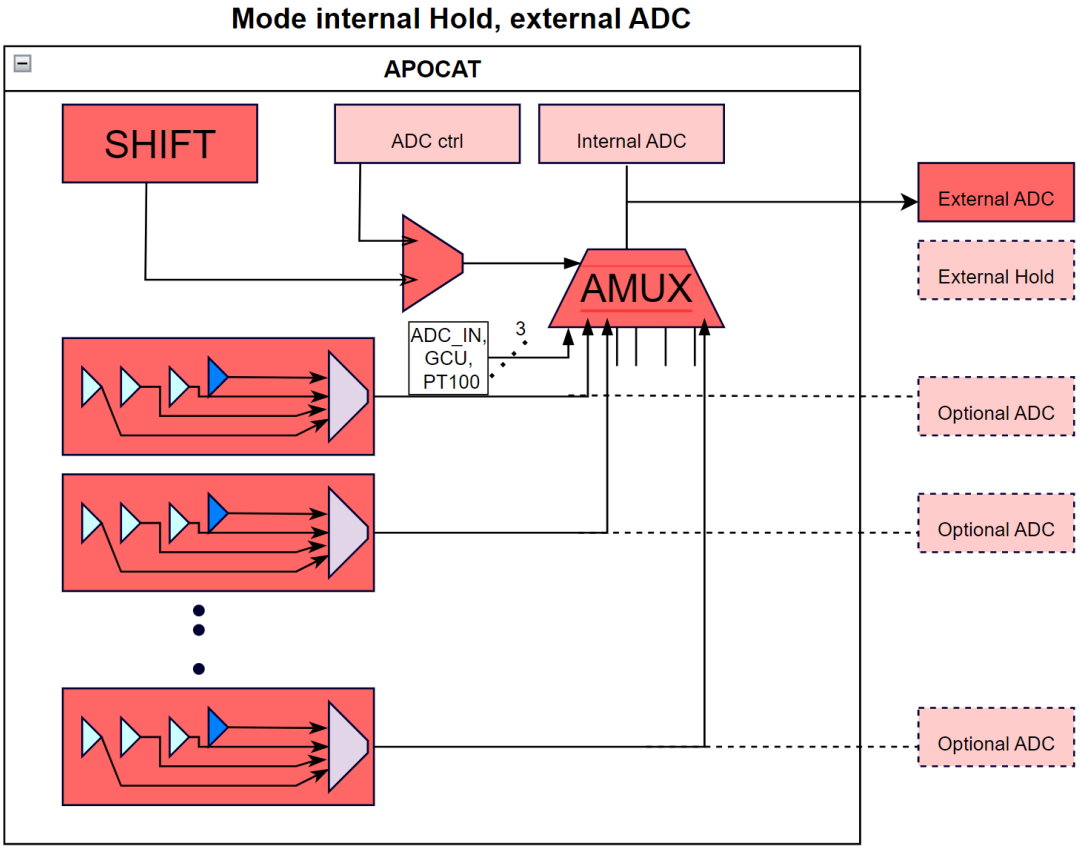

Figure 3.6: The Mode internal Hold with External ADC readout process highlighted in red .

3.5 APOCAT Vs SIPHRA

The main differences between the SIPHRA and APOCAT ROICs are highlighted in table 3.1. As differs from SIPHRA, APOCAT has four counters in each channel. Having counters with programmable threshold values in a system provides flexibility and enables the system to better adapt to specific requirements and conditions. The APOCAT has a CSA with individually adjustable gains which can correct for gain variations among multiple detectors, followed by more analog processing. The SIPHRA has only the current integrator for this purpose, the current integrator is a simpler and more power efficient approach to signal processing, which may be more suitable for certain applications where power consumption is a concern. Other than the new features the APOCAT also have direct access to the digital output and with the addition of 4 counters for each channel the ROIC has gained in size. The die size is 7.600 x 6.8 x 0.3[mm] for SIPHRA while for APOCAT the die size is 16.420 x 14.030 x 0.3 [mm]

Overall, the APOCAT ROIC has more advanced features and capabilities than the SIPHRA ROIC, but it also has a larger size. The APOCAT is designed for higher resolution and energy-resolved counting, while the SIPHRA is more general-purpose and designed for lower power consumption.

Table 3.1:
SIPHRA vs APOCAT comparison table where green color highlight the superior feature

Aspect	**Details**	SIPHRA	APOCAT
Features			
	Input channels	16	16
	Summing channel	Yes	Yes
	Digitization	Yes	Yes
	Pulse height-Spectroscopy	Yes	Yes
	Pulse time-Spectroscopy	Yes	Yes
	Pulse counting	Yes	Yes
	Triggering	Yes	Yes
	Counter channels	No	4x18bit per input channel
	Size	7.600 x 6.8 x 0.3 [mm]	16.420 x 14.030 x 0.3 [mm]
Analog processing			
CMIS			
	Programmable Gain	$\frac{1}{10}$, $\frac{1}{100}$, $\frac{1}{200}$, $\frac{1}{400}$	1, 2.5, 5, 10, 20
	Charge ranges	-0.4, -4, -8, -16 [nC]	-0.8, -0.4, -0.2, -0.1, -0.04 [nC]
Current Integrator		Yes	No
Charge Sensitive Amplifier		No	Yes
Pole-zero cancellation		No	Yes
Baseline holder		No	Yes
Dc compensation		No	Yes
Peak detector		No	Yes
Shaper	Programmable Peaking time	200, 400, 800, 1600 [ns]	50, 150, 300, 2000 [ns]
ADC			
	Type	SAR ADC	SAR ADC
	Resolution	12bit	12bit
	Sampling rate	50ksps	2Msps
Power Consumption			
	Voltage	3.3V	3.3V
	With CMIS active	30mW	230mW
	With CMIS inactive	15mW	142mW

4 ROSSPAD System Description

Today an already available readout module for x-ray/gamma-ray Spectroscopy and Imaging is developed from IDEAS called the ROSSPAD (Read-out Module for Silicon Photo-multiplier Avalanche Diode arrays). The ROSSPAD is a readout module for detecting and measuring the signals from (SiPMs) and multi-pixel-photon-counters (MPPCs). As shown in figure 4.1, ROSSPAD has the possibility for a setup with a total of 64 channel readouts.
The scintillators are attached to the SIPMs at the detector board.
The Front end board(FEB) is the board with the assembled ROIC('s).
The controller board is responsible for data acquisition and processing. It contains an SAR ADC of type LTC2325-12, power handling, trigger receivers, cal pulse generator and digital processing. Additionally, the controller board includes a piggyback system on module (SOM) that is based on a Xilinx Zync system on chip (SoC) [12].
The SoC features a dual-core ARM Cortex-A9 processor, programmable logic fabric (FPGA), and various other hardware peripherals and interfaces. The Interface Board acts as a bridge between the Controller Board and the user's computer system. It provides Ethernet connectivity for control and data acquisition. In addition, the Interface Board includes circuits for power conversion, detector bias generation and buffers for synchronisation signals.

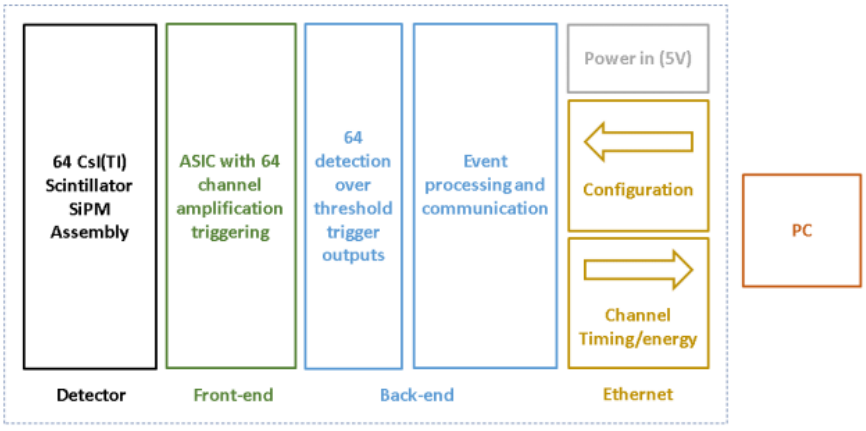

Figure 4.1: Figure gathered from ROSSPAD user manual document
Detector board has the (64 CsI(TI)) scintillators, which are attached to the SiPMs.
The front-end board contains of 4 of the readout circuits of type IDE3380 (SiPHRA)
The back-end board contains the ADC, power handling, trigger receivers, cal pulse generation and digital processing.
The Interface board handles the control and configuration of the module and the data communication.

4.1 ROSSPAD FEB with SIPHRA

The setup given today with the ROSSPAD system is with 4 SIPHRAs implemented on the FEB. Since each SIPHRA has 16 channels, it can have a total of 64 channels readout. The event rate is then up to 20 000 frames per second in all channel spectroscopic mode at 12-bit resolution. A readout sequence is triggered when an event with a pulse height above the threshold is detected. Each channel has the possibility to set its individually triggering threshold. The module saves a data package with pulse height information and a timestamp. The FEB has two detector interfaces to a detector carrier board which holds the SIPMs in an 8x8 detector array as shown in 4.2. The compact design of the ROSSPAD stack is 50mm x 50mm x48.5mm(without the detector)

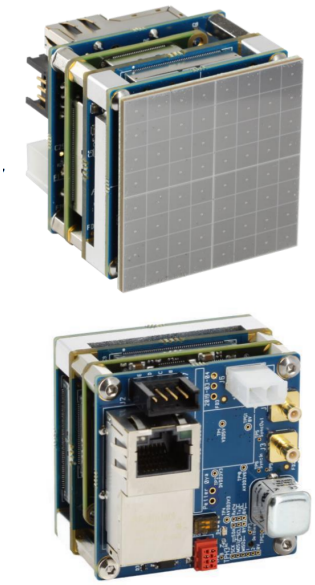

Figure 4.2:
The ROSSPAD system stack with the Hamamatsu S14161-6050HS-04-SiPM

The ROSSPAD ADC

The external ADC in the ROSSPAD system is an LTC2325-12 ADC

The LTC2325-12 is a high-speed, low-noise, quad-channel ADC that can simultaneously sample 5Msps (mega-samples per second) per channel and uses a differential input architecture to achieve a high level of performance in terms of signal-to-noise ratio and spurious-free dynamic rang. The ADC also has a high-speed SPI-compatible serial interface that supports CMOS or LVDS(Low Voltage Differential Signaling). In the ROSSPAD configuration with SIPHRA, all four channels are used simultaneously with four SIPHRA. In the configuration with one APOCAT, only two of the ADC channels are used. One channel is a multiplex of all analog channels, and one is for the summing channel only. The two remaining channels may be used for feature work.

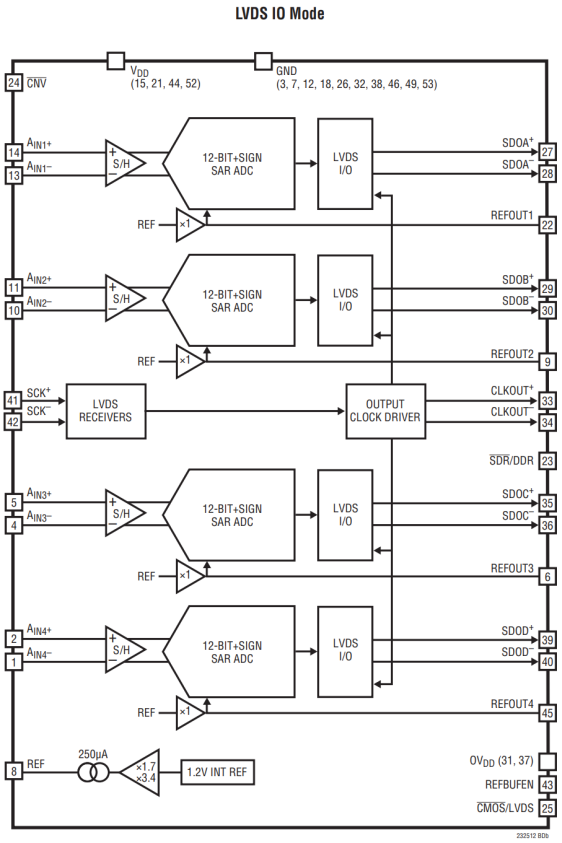

Figure 4.3: The ROSSPAD ADC, which is located on the controller board of the system, is a four-channel SAR ADC

The ADC's timing diagram in figure 4.4 shows that the sampling phase starts during a "high" CNV signal where the input signal is acquired and held constant by the internal sample-and-hold circuitry of the ADC. When the CNV signal transitions from high to low, the ADC starts the conversion phase and converts the sampled analog input signal to digital output data. The ADC outputs one bit of digital data on each SCK pulse, starting from the MSB and ending with the LSB of the 16-bit output word. After the 16th SCK pulse, the complete 16-bit output word is available on the falling edge of the last SCK pulse. The output data format is 16 bits, with the first 12 bits containing the actual conversion result, a "don't care" bit in the 13th position. The remaining 3 bits in the output word are constantly driven to zero and are used to pad the output to 16 bits for compatibility with other digital systems.

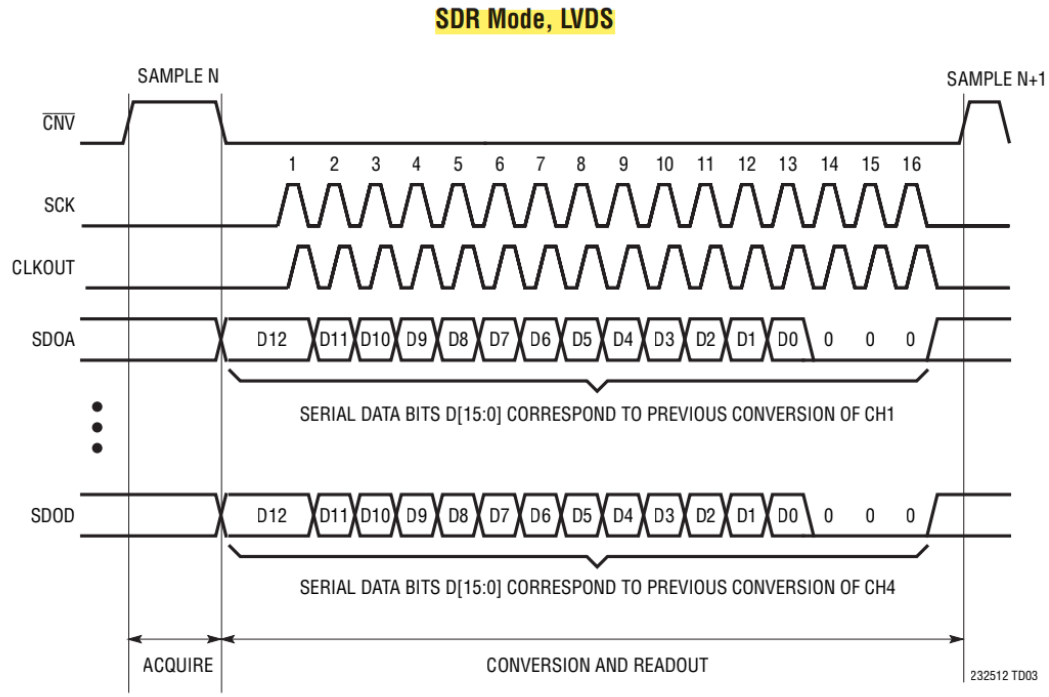

Figure 4.4: Timing of the ROSSPAD ADC gathered from the ADC data sheet [13]

The 12-bit resolution means the ADC can distinguish between 2^{12} (4096) different voltage levels in the analog input signal. This means that the analog input signal is quantised into 4096 digital steps, and each step represents a voltage range equal to the ADC's reference voltage divided by 4096.

$$\frac{\text{Resulution of the ADC}}{\text{System voltage}} = \frac{\text{ADC Reading}}{\text{Analog voltage measured}} \tag{4.1}$$

For a 3.3 v system

$$\frac{4096}{3.3v} = \frac{\text{ADC Reading}}{\text{Voltage output}}$$

$$\text{Voltage output} = \frac{3.3v}{4096} \cdot \text{ADC Reading}$$

4.2 The IDEAS-Testbench

Another system that will be used with the ROSSPAD system is the IDEAS-Testbench, a framework software. IDEAS-Testbench is generally used to read and control devices from IDEAS, such as radiation spectrometers, gamma and X-ray cameras, and ASIC development systems. IDEAS Testbench software offers functionality that allows users to control the system configuration registers and read out data. This can be done either through scripts written in the Python programming language or manually through the testbench-GUI. This allows users to write Python scripts to interact with the IDEAS-Testbench software, manipulate the system configuration registers and retrieve data as needed. Using Python scripts, the user can write code to set specific configuration values, trigger actions, and retrieve data from the system. For the ROSSHIP system, an updated framework was needed from the previous ROSSPAD version, as different system registers and the pixel map now include 20 channels. The system registers tab can be used to read/write the ROSSPAD register values or view the current values of all system registers. A separate tab is available for showing only the ASIC configuration, where also the registers are displayed but also modified if needed. The output data from the system also shows framed and spectroscopy imaging, as shown in the picture below.

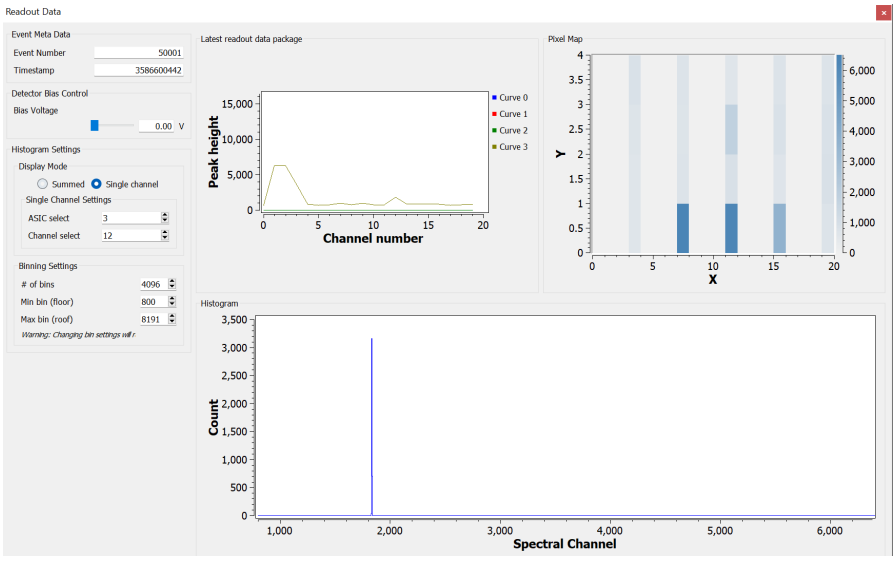

Figure 4.5: Visualisation of the IDEAS Testbench, showing a pulse on channel 12 with an ADC value of ca 1800 (Histogram). In the pixelMap, three channels show clearer blue colours than the rest, which means they have a higher ADC value. These three channels are mentioned as "extra channels" (ADC_In, GCU, Pt100).
Another pixel is showing a higher blue colour than the other channel, which is channel 12, the channel with the charge.

4.3 The new APOCAT Demonstrator

To demonstrate the use of APOCAT ROIC, it was implemented in the ROSSPAD system with scintillator detectors in a line scanning detection configuration. For this, a new Front end board (FEB) was made as seen in figure 4.6 (See Schematics and Layout in Appendix), the new FEB (Green block in Fig 4.7) includes one APOCAT which replaces the previous SIPHRA's. Although substituting one APOCAT from 4 SIPHRA led to a lack of channels compared to today's ROSSPAD system (From 64 to 16 channels), the main point was to showcase APOCAT and its features in a system. After assembling APOCAT with the ROSSPAD system, the system now has all the superior features that APOCAT had over SIPHRA. The system has been named ROSSHIP, Readout System Spectroscopic High-resolution Pulse-height. Further implementation of the system will be detailed in this chapter.

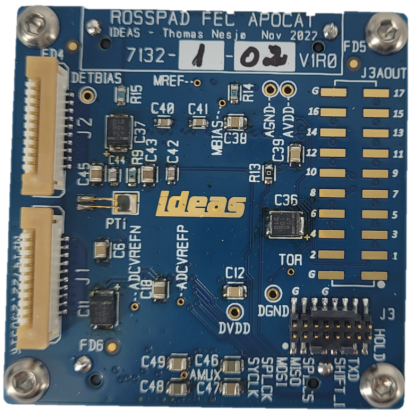

Figure 4.6: A new front-end board was made, which includes APOCAT, connectors to both the controller board and SiPMs and test points/headers for testing.

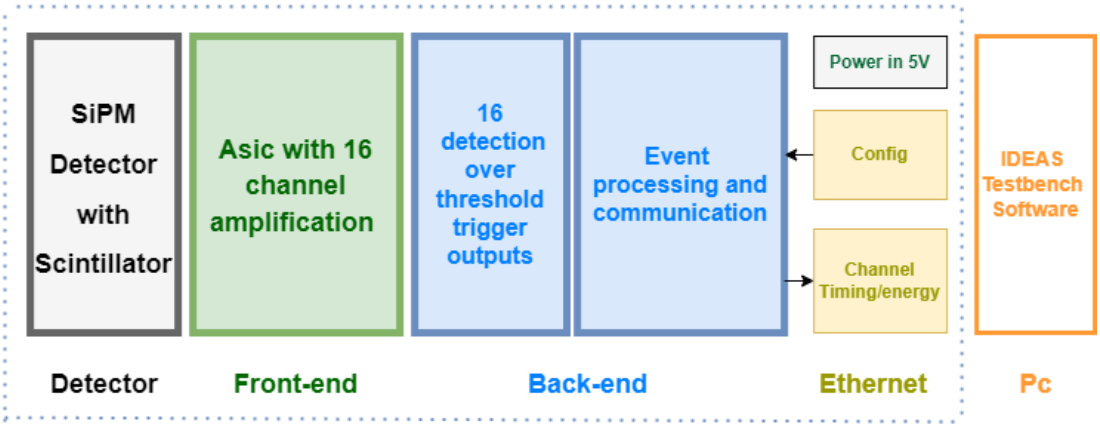

Figure 4.7: Block diagram of ROSSHIP, with the new FEB colored green and the ASIC APOCAT implemented.

4.4 Detector carrier board

The solution for implementing multiple SiPMs in the system was to use IDEAS detector carrier boards, which consist of 8 SiPMs of type J series from SensL. The board has 1x8 pix-elated scintillator array and connectors to the readout module where the module can be connected directly to the FEB with a jump cable. Two DetCarrier boards will be placed in a line giving a total of 16 pixels.

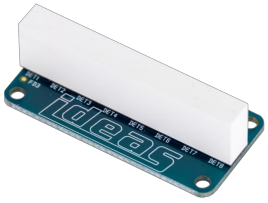

Figure 4.8:
DetCarrier SiPM scintillator assembly

4.5 Expectations of APOCAT Compared to SIPHRA

The APOCAT and SIPHRA ROICs differ in their features and capabilities, which may affect their performance when used in the ROSSPAD system for spectroscopy. For example, APOCAT has a CSA with individually adjustable gains and more advanced analog processing, which may result in higher resolution than the SIPHRA. On the other hand, the SIPHRA's more straightforward approach with a current integrator may be more power efficient but may not provide the same level of performance as the APOCAT.

The APOCAT has four counters in each channel with programmable threshold values, providing greater flexibility to adapt to specific experimental requirements. Using count mode only with the implementation of counters in APOCAT, the APOCAT have a higher counting efficiency than the SIPHRA (though this is not implemented in this thesis).

When comparing the APOCAT and SIPHRA readouts in the ROSSPAD system, the expected spectroscopy results are similar, with differences potentially due to the differences in the ROICs themselves. Overall, the APOCAT may provide higher resolution and energy resolution, while the SIPHRA may be more power-efficient but may not provide the same level of performance as the APOCAT.

4.6 Hardware Implementations

4.6.1 Matching the Sampling Rate ROSSPAD to APOCAT

The APOCAT's analog values for each channel can be multiplexed out at AMUX_O (Figure 3.6) with a nominal frequency of 5 MHz, while the LTC2325-12 ADC has a maximum sampling rate of 5Msps for each channel, which means that the ADC can convert an analog input signal into a 12-bit digital value at a rate of 5 million times per second. The Nyquist frequency formula [14] states that the maximum frequency that can be accurately sampled is half of the sampling rate, which can be expressed as

$$\begin{aligned} f_{max} &= f_s/2 \\ f_{max} &= 5\,\text{MHz}/2 \\ f_{max} &= 2.5\,\text{MHz} \end{aligned} \tag{4.2}$$

Where f_max is the maximum frequency that can be accurately sampled and f_s is the sampling rate.

In this case, the Nyquist frequency is 2.5MHz, which means that the LTC2325-12 ADC cannot accurately sample any analog signal with a frequency above 2.5MHz. Therefore, it's important to ensure that the analog signal being measured has a frequency content within this range to avoid aliasing and ensure accurate data acquisition.

To match the sampling rate of the ROSSPAD ADC to APOCAT, the readout frequency of the APOCAT's analog channels should be decreased to 2.5MHz, which can be achieved by adjusting the readout frequency of the ASIC to a period of 400ns. This will ensure that the LTC2325-12 ADC can properly sample the analog signal and that the Nyquist frequency requirement is met.

A notice is that APOCAT has the potential to achieve an even higher readout with a high-speed data readout of up to 16 Mbit/s via a serial data transmission line such as LVDS(Low Voltage Differential Signaling). This feature can be advantageous for future work requiring high-speed data acquisition. However, it is important to note that the current LTC2325-12 ADC cannot handle data rates beyond 5 Msps. Therefore, an even higher speed ADC would need to be implemented to utilise this feature. Though the typical signal bandwidth for CsI(Tl) scintillators is much lower than the sampling rate of the ADC, meaning the ADC sampling rate is already fast enough for most spectroscopy applications.

4.6.2 System Design Overview and Features

The System Top module defines and manages the communication of all signals with the FPGA and processing system with the Asic. An overview of the system can be seen below (complete overview and code are found in the appendix 9.5). Since the ROSSPAD system is reused most of the modules can be reused, with minor justifications. But the main module for controlling the new FEB with its features needs to be rewritten.

The new module for the ROSSHIP is to be shown here as the ROSSPAD_OS_wrapper.

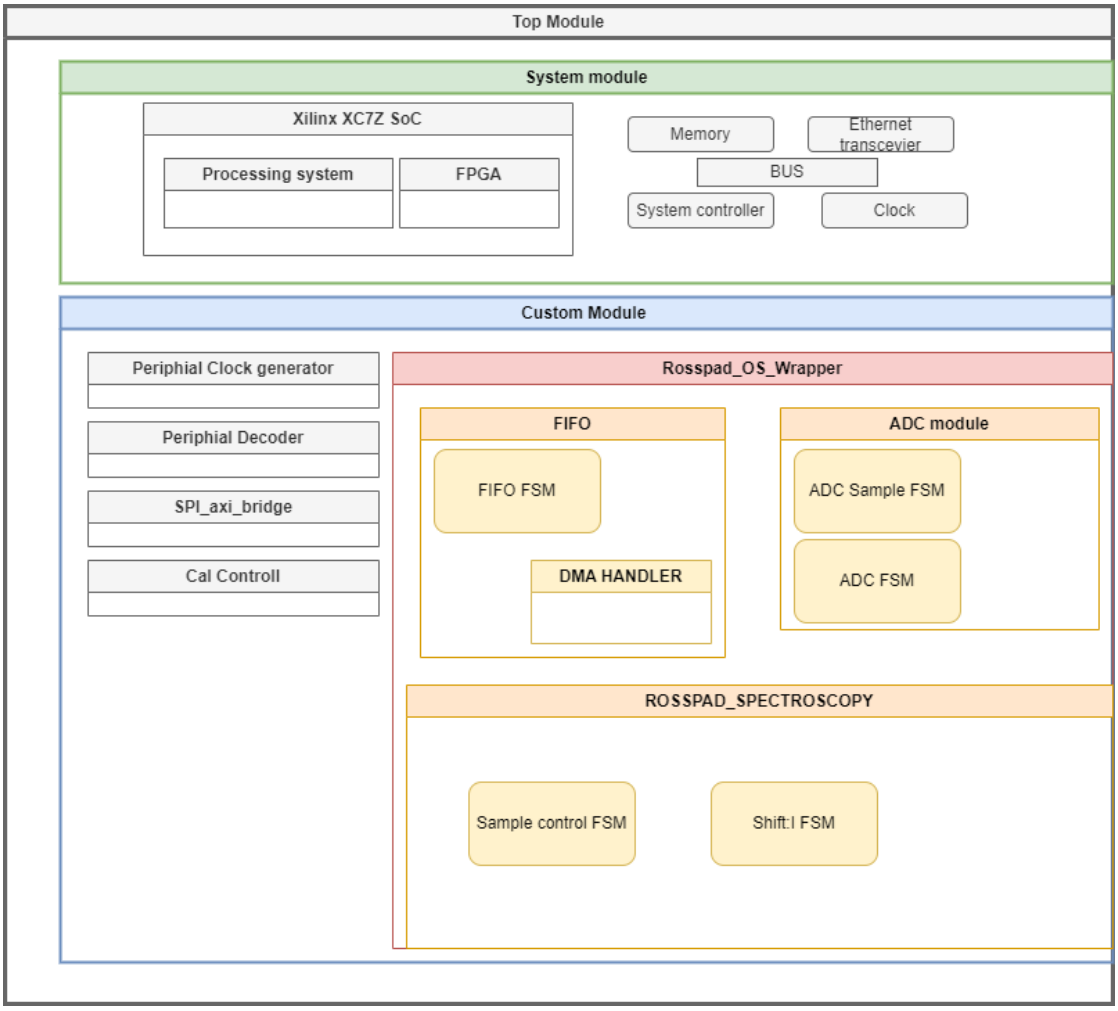

Figure 4.9: System Architecture Overview:
A high-level view of the system design showcasing the key components and their interconnections. The system module consists, among other things, of a Xilinx SoC, memory, Ethernet transceiver, system controller, clock and buses that connect the key components.
The Custom module serves as the primary interface between the ASIC and the rest of the system, while the OS_Wrapper module provides key functionality for managing data flow and timing.

4.6.3 Data Flow And Timing

The module Rosspad_OS_Wrapper module in figure 4.9 handles trigger events from the SIPM, while the ROSSPAD_SPECTROSCOPY module controls the event timing and activates the ADC module. The ADC module performs conversions and sends the data to the FIFO module, which formats and sends it to the DMA handler. The DMA handler (Direct Memory Access) manages data transfer between the FIFO and the memory.

As mentioned in chapter 3.3, the occurrence of an event triggers the TOR_O signal, and for the external ADC to multiplex out the analog data after a trigger event, a token bit is used to signalise when the internal hold is set, called Shift_I. The state machine in figure 4.10 shows how the module reacts on a trigger to activate the Internal hold signal to an external ADC readout module. When a trigger event is detected at TOR_O, Shift_I goes high after a programmable delay. The state machine transitions to the RESET_Shift state after a configurable duration of the Shift_I signal."

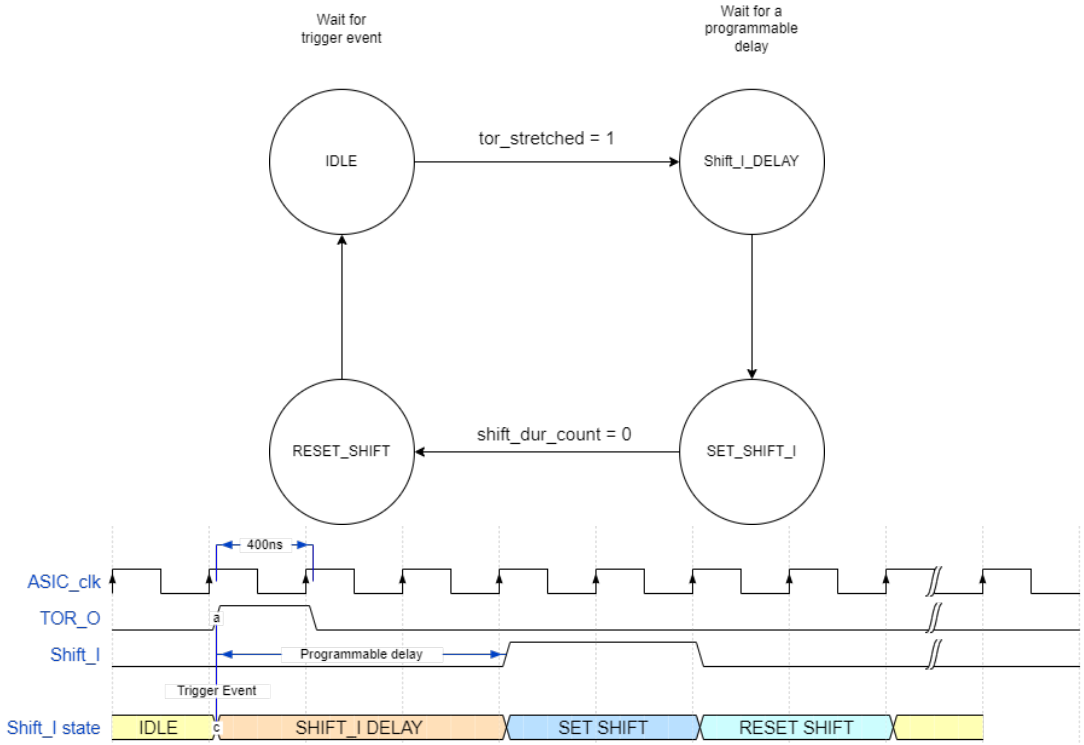

Figure 4.10: The Shift_I state machine detects a trigger of an event, and the external ADC can start sampling the analog data. The wave diagram shows the transactions between the different states at the start of a trigger

The sample control state machine

The finite state machine(FSM) in figure 4.11 shows how the module should react on a trigger to activate the ADC readout module. When a trigger event occurs, and TOR_O goes high, the state change from IDLE to the Wait_Shift_I, there it stays until the Shift_I signal set by the Shift_I FSM 4.10 goes high. In the Sample state, the FSM checks if all channels are done and if not, it goes to the next state, where it waits for a rising edge of the ASIC clk. This is for synchronising the multiplexed output from the ASIC with the ADC sampling, as explained in chapter 4.6.1. Also, the last state is for ADC sample timing, where a programmable delay can make a phase shift from the Asic clock. The FSM goes back to the sample state, and if all channels were now sampled, it
returns to the IDLE state

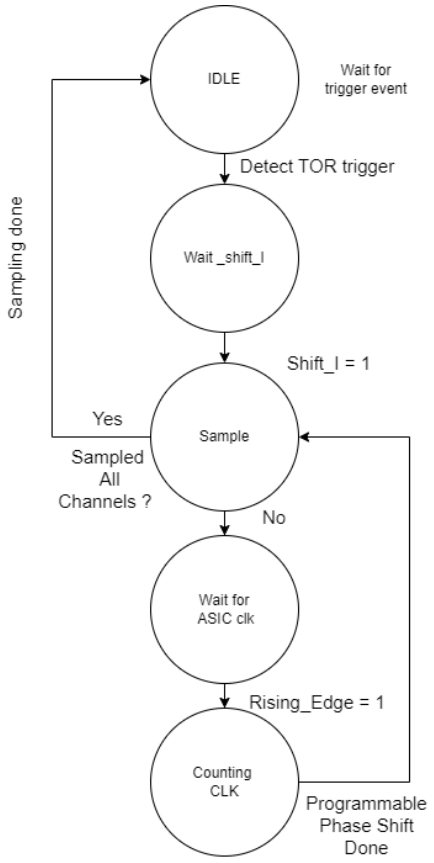

With a simulation of the two state machines, a wave diagram showing a triggering event's response signals the ADC to start sampling.

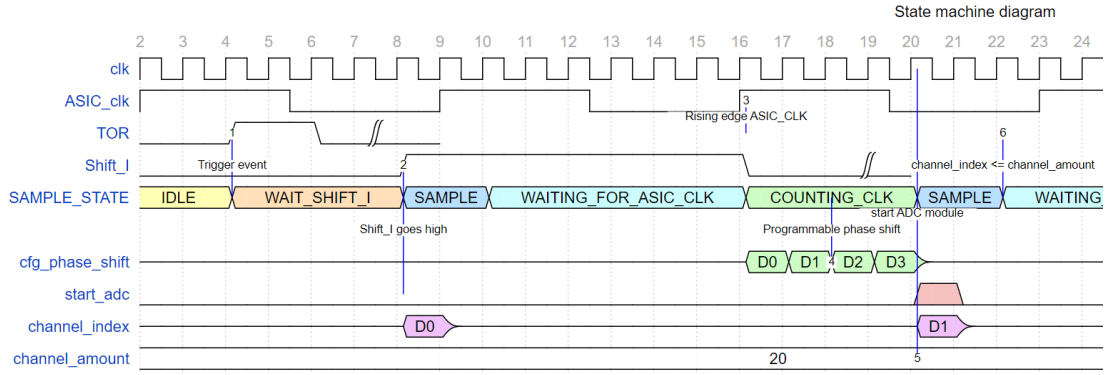

Figure 4.11: The Sample control state FSM
1. Trigger event, TOR_O goes high
2. After a programable delay, Shift_I goes high
3. Rising edge of the ASIC clock changes state to Counting clock
4. The phase shift counter counts the number of clocks cycles programmed by the user
5. The Start ADC signal is sent to the ADC Module and goes back
to the sample state, where it checks if this was the last channel

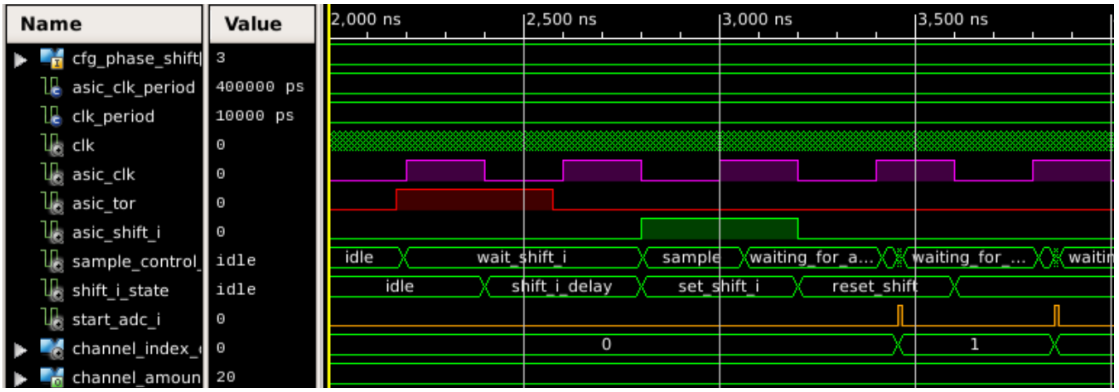

Figure 4.12: The sequence of starting the ADC readout,
Asic clk highlighted in Purple color shows that all signals for Shift_I_State(Higlihted in blue) is set at falling clock edge of the ASIC_clk, while signal in Sample_control_state is sat at rising clock edge for the Clk
Asic Tor After a trigger on TOR, the two state machines start, and Sample_control_state is then waiting for the shift_I signal
Asic_Shift_I is set after a programmable delay and Sample_control_state is then going to Sample state.
The Start ADC signal is set "high" after the programmable phase shift is done counting before the state goes back to the next sample
The Start_ADC signal is sent to the ADC module to start the conversion of the ADC, and from the timing diagram of the ADC, this is later called the CNV signal as seen in figure 4.4.

With a deeper simulation of the system involving the ADC module, the simulation in the figures below shows the response of the ADC signals CNV and SCK both marked in yellow, as well as a simulated AMUX signal. The Start ADC signal is sent to the ADC module to start the conversion of the ADC; the CNV is as expected at the start of the conversion and is also synced with the ASIC clock. The same applies to AMUX, which emits the output at every rising-edge Asic clk

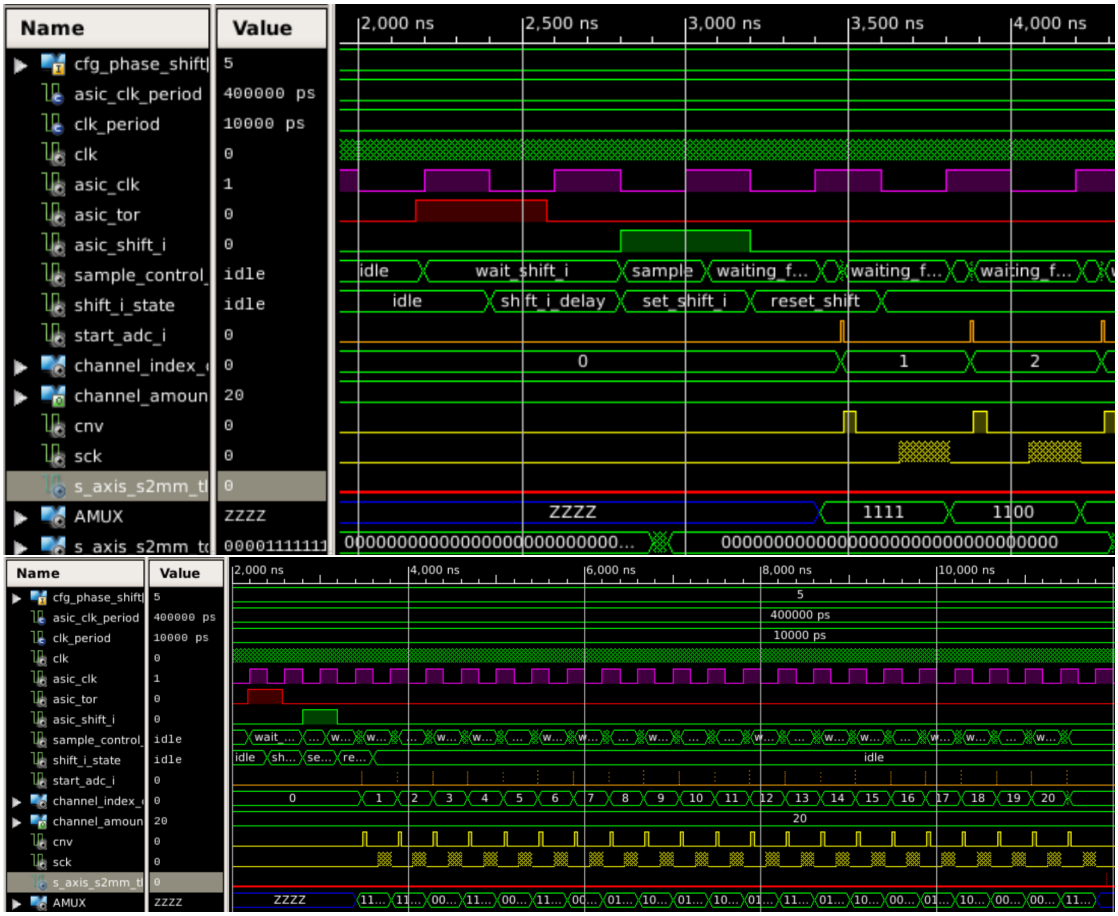

Figure 4.13: Bottom figure shows full 20 channel readout, and the top figure is zoomed in at the start of the process between 2-4us.

5 System Verification

This chapter presents the verification process of the X-ray detection system developed in this thesis. It includes a description of the test plan and its implementation.

The main goal of this verification process is to ensure that APOCAT is fully integrated with the ROSSHIP system and that all hardware and features are fully functional. Additionally, the performance of the radiation detection system will be evaluated to ensure that it meets the requirements specified in chapter 1.1. Functional testing is designed to verify that the system performs its intended functions correctly. Performance testing measures the system's performance characteristics, such as sensitivity, linearity, and resolution. This chapter also describes the test setup and equipment used in the verification process, and the results obtained from the process are presented in the next chapter.

The verification tests have been executed per the test plan 5.2 shown further down in this chapter, where each test has its own identity, which can be followed further in the verification chapter and the results chapter. Figure 5.4 shows a simplified test setup. The ROSSHIP system is connected with a jumper cable to the SiPMs, a 5 V power supply, and an Ethernet cable to a computer, visualized further in the IDEAS-testbench software. As a stimulus to the scintillators, radioactive sources are used, and an oscilloscope is used to monitor test pins from the FEB through a test rig. Finally, a black blanket covers the scintillators to prevent any light from entering. A calibration pulse will provide the test on individual channels to see if the system is responding to the pulse, where a final test is then to use a radioactive source and collect the data throughout the system.

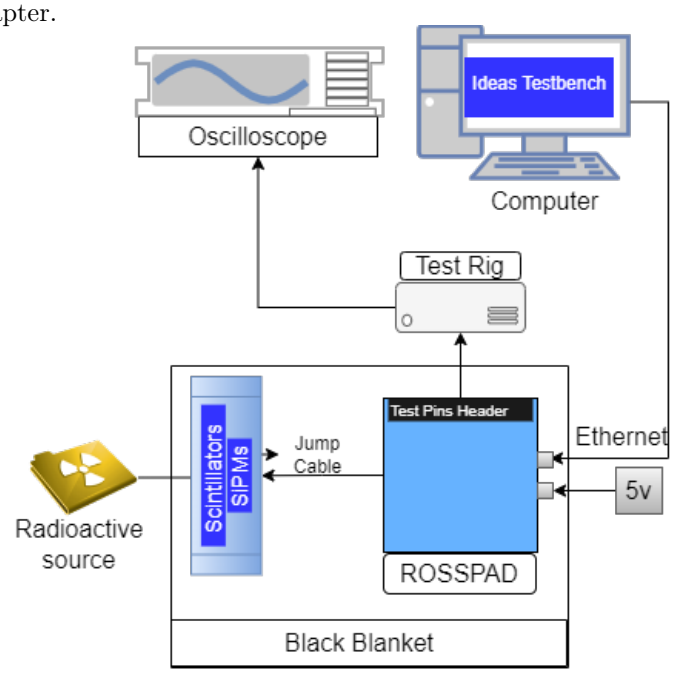

Figure 5.1: Schematic for test-setup

5.1 Test Plan

Radiation Sources

The scintillator detectors were illuminated using radiation sources. An example of a radiation source used in this study is shown in figure 5.2. The radiation source is a small amount of Cs^{137}, placed close to the scintillators. Other sources used for spectral visualization are Am^{241}, Co^{57}, Co^{60} and Na^{22}. The Am241 has a photo peak at 59.5 keV and is a relatively strong source in terms of intensity compared to the others. The Co^{57} peak is twice the energy from Am^{241} at 122.1 keV. Na^{22} has two peaks where one is very steep at 522 keV and a very small one at 1275 keV, which will not be used for calibration purposes due to its small amount of energy release. Co^{60} will be used for higher energy measurements due to its photo peaks at 1.173 MeV and 1.331 MeV.

Figure 5.2: Schematic for test-setup

Table 5.1: Calibration sources used in this thesis and their photo peak energy

Calibration Source	Expected Energy (keV)
Am^{241}	59.5
Co^{57}	122.1
Na^{22}	511
Cs^{137}	662
Co^{60} peak 2	1173
Co^{60}	1333

Table 5.2: Test plan for the ROSSHIP system

Ref:	Functionality	Target specification	Measure
		Initial testing	
TP-010	Visual inspection	Detection of potential soldering defects	Visualization using a Microscope
TP-011	Smoke Test	System shall be powered up from 1V up to ±5V with stable current increase.	Measure test pins for Vdd to Gnd
		Functional testing	
TPF-010	Interface verification		
	Power distributon	-Power Supply for APOCAT at 3.3V	Measure test pins for DVDD/ AVDD to VSS
	Firmware module verification	-Test VHDL code with simulation tools	Stimuli the modules with a test case.
	Configuration of register verification through SPI	-Registers can read and write the correct values	SCK, MISO, MOSI, CS
TPF-011	Hardware testing	Test the implemented hardware works as expected	
	Channel Functionality	-Channel integrity verification -DAC functionality	Measure all channel outputs
	ADC verification	ADC sample verification	Measure on outputs: AMUX, CNV, TOR, SHIFT_I
	Detector Bias	Confirm stable and precise bias voltage output	Measure AMUX with oscilloscope
	Configuration settings	Adjust the APOCAT configurations to fit the application setup	Oscilloscope readout with adjustment of config settings
		Performance testing:	
TPF-012	Calibration		
	Baseline	Find the baseline through each individual channel	Measure average of sampled signal (AMUX).
	Noise	Find the systems Noise through each individual channel	Measure standard deviation of sampled signal (AMUX).
	Channel Gain Variations	Channel Gain Variations within the ASIC	Measurement and calculation of sampled signals(AMUX)
	Equivalent Noise Charge (ENC)	Find the systems ENC	Measure through calculations
	Dynamic Range	Find DnR and resolution of the system	Read and calculate through plot
TPF-013	Spectroscopy		
	Singel Channel Spectroscopy readouts	Obtaining readouts with radiation source	Measure through each channel to verify functionality
	Gain calibration with sources	Find the gain linearity function to convert ADC value to keV	Spectrum with several radiation sources
	Pulse height analysis	Find the FWHM and ENL for the channel	Spectrum analysis with python
	All channel Pulse height Spectroscopy	Obtaining readouts with radiation source	Spectrum from all channels

5.1.1 Test Setup

The FEB was fitted with a test point header to utilise the digital signals generated by the ROIC. This header can be directly connected to the digital reader of an oscilloscope using a specially designed test rig, allowing for easy visualisation of the signals as shown in figure 5.3. To prevent any light from entering, the SiPMs are covered with a black blanket. A realisation of the lab setup is visualised in figure 5.4, where the ROSSHIP system is powered up, and the test rig is connected to an oscilloscope and the black blanket covering the SiPMs.

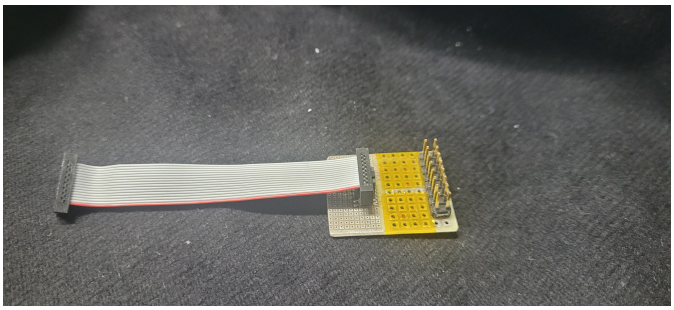

Figure 5.3: The test rig enables digital readout from the oscilloscope and can be connected straight to the FEB test header with the jump cable, as shown in the next figure.

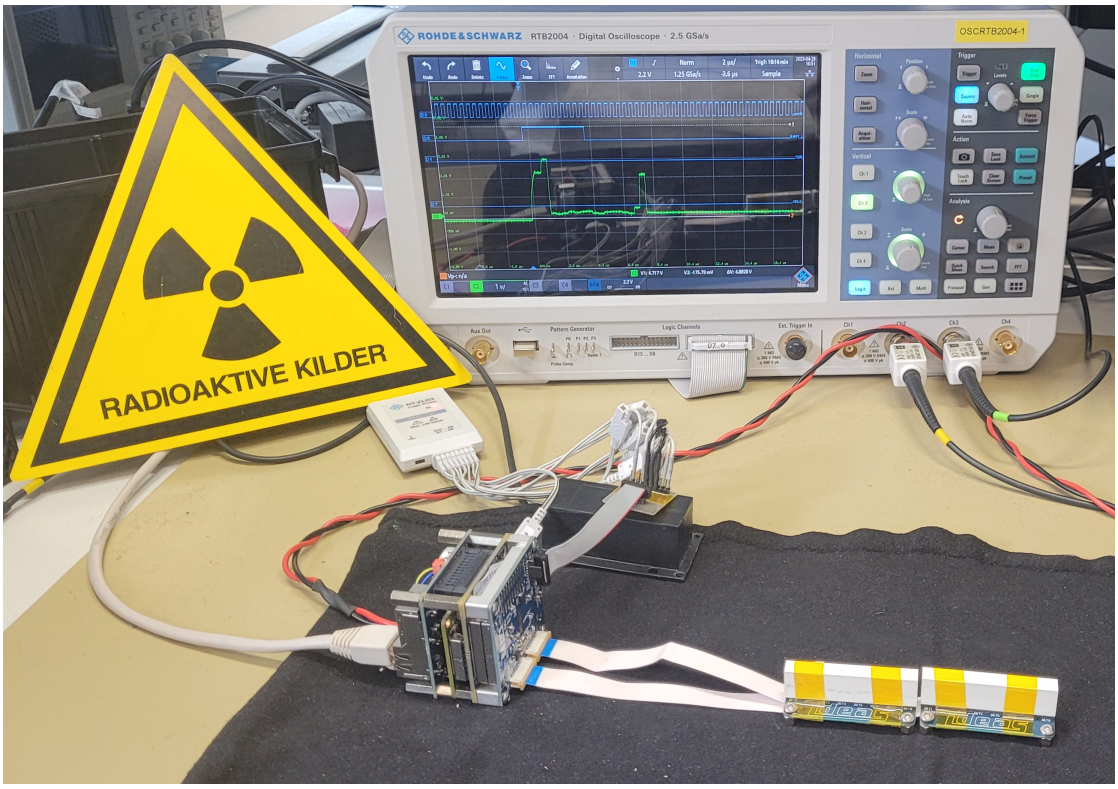

Figure 5.4: Test setup shows the ROSSHIP with the two SiPMS connected with the jump cables. The ROSSHIP is connected to a 5v power supply and an Ethernet cable. Also, the test-Rig is connected for digital signal visualisation on the oscilloscope.

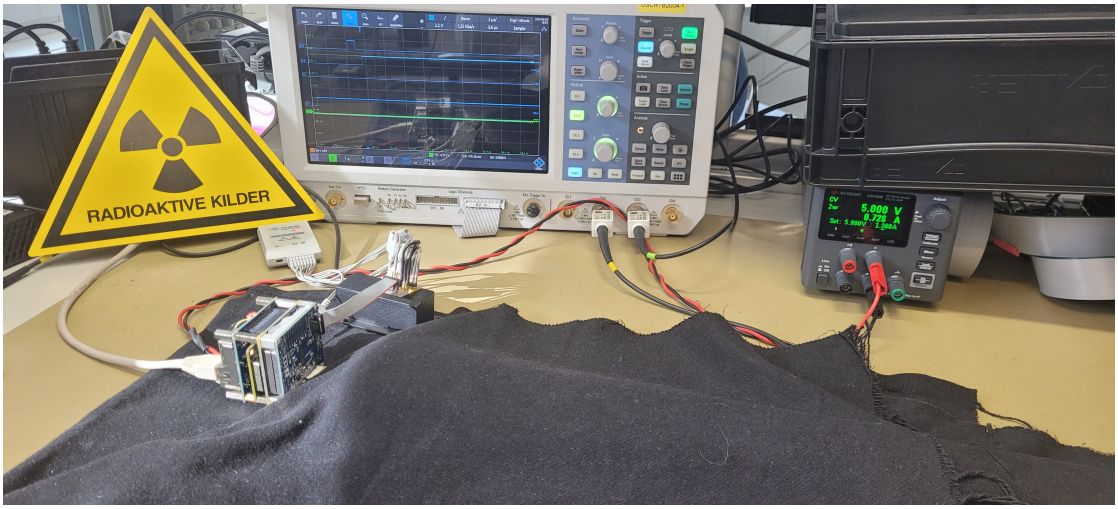

Figure 5.5: In the test setup, the SIPMs are covered with a black blanket to prevent any light from entering, and the source is placed on top of the blanket.

5.2 Initial Testing

The initial testing is to verify that the electronic hardware is not filled with system startup errors, such as electronic shorts. After this, the system is ready for a functionality test.

5.2.1 TP-010 Visual Inspection

The visual inspection process is an essential step in verifying the quality of soldering on the FEB. It involves examining soldering joints and wire bonds to ensure accurate and secure connections. The inspection aims to detect issues such as tombstoning, solder bridges, and misaligned wire bonds. By using a microscope, the soldering joints are carefully examined. The test is considered successful if all soldering joints meet the visual inspection criteria.

5.2.2 TP-011 Smoke Test

A smoke test must be performed to quickly identify any significant issues or faults in the system. The system is connected to a power supply, and the voltage is gradually increased from 1V to 5V while observing the current drawn by the circuit. If the current remains stable and there are no signs of smoke or burning smells, the test is considered passed. However, if the current suddenly spikes or there are any signs of smoke or burning smells, the test is considered failed, and further investigation is required to identify and resolve any issues. In the worst case, components need to be replaced.

5.3 Functional Testing

Functional testing ensures that the system meets its intended requirements and operates correctly. This section outlines the tests that will be performed to verify the system's functionality, including interface verification, hardware testing, detector bias configuration settings, and other tests as necessary.

5.3.1 TPF-010 Interface Verification

Power Supply Verification

This test aims to verify the proper distribution of power within the system. By measuring the voltage test pins on the FEB, we can assess the voltage levels and ensure they meet the required specifications. The voltage supplied to APOCAT is of particular interest, as it confirms the

integrity of the connections between the boards, including the interface and connector boards. The test is passed by measuring a voltage of 3.3 V as it confirms electrical connectivity within the system.

Firmware modules verification

The firmware module verification involves the simulation of the modules made in VHDL. The new module for controlling the new FEB must be tested and verified before the system can be tested physically. Testing with simulation tools allows us to verify the functionality of the design in a virtual environment before deploying it on actual hardware. Test benches will be made for the specific modules, with input stimulus to test if the scenarios work as intended. The virtual part is considered passed if the corresponding modules for the FEB act as intended for the given stimuli.

Configuration of Register Verification through SPI

To confirm that APOCAT's configuration registers can be programmed and read correctly through the SPI interface, a value should be written to one of the registers in the IDEAS-Testbench. The output log from the IDEAS-Testbench can be used to verify that the operation is working. A readout from test points on the FEB through an oscilloscope can be used to confirm if the data is correct. A comparison of a write and read operation on a registered address will ensure that the valid data is stored in the register.

5.3.2 TPF-011 Hardware Testing

Channel Functionality

To perform a functionality test of the APOCAT system channels, a calibration pulse can be sent using the DAC on each channel. By varying the charge on the DAC for each channel, the output pulses on the corresponding channel can be observed and visualised in the IDEAS-Testbench or oscilloscope. This test helps to verify that the DAC is responding correctly throughout the system and that the pulses are transmitted across all the channels. The output can be visualised on different spectrums depending on the charge given. By performing this test, the integrity of the chain throughout all the channels can be verified, ensuring that the system is functioning as expected.

This test also sets the basis for the configuration setting test, where an error in the output pulse

can tell whether a setting may need to be analysed further. The test is passed if all channels respond to the expected charges.

Verification of ADC sampling

Verify the functionality of the ADC sample shown in chapter 4.6.3, one approach could be:

- Setup the ROSSHIP with IDEAS-Testbench
- Connect Oscilloscope-probe to CNV, AMUX(multiplex output), TOR(Trigger signal) and SHIFT_I for visualization.
- Send a calibration pulse through one of the channels
- Visualise TOR activates the signal chain
- Adjust CFG_PHASE_SHIFT so that CNV samples are approximately in the centre of each channel.
- Check the multiplexed output of the 20 channels (AMUX signal) for the channel that received the calibration pulse.
- Verify that the ADC samples all the channels correctly
- Interpret the test results to ensure the ADC sampling meets the required performance specifications.

Detector bias

The detector bias circuit provides a stable and precise bias voltage to the SiPMs. The detector bias circuit uses a 12-bit digital-to-analog converter (DAC) with a resolution of 25 mV. A 12-bit DAC can provide 4096 (2^{12}) different output levels, with each level representing a voltage step of 25 mV. This gives a total range of 102.4 V (4096 x 0.025V). One approach for setting the bias voltage is to increase the voltage level on the DAC while observing the oscilloscope until a stable signal is found, which is the criteria for a passed test.

APOCAT configuration settings approach

Numerous configuration settings are available to optimise the APOCAT system for different detector setups. However, finding the appropriate configuration for a specific setup requires adjusting several settings.

The APOCAT datasheet should be consulted to identify the optimal configuration settings. However, a test-and-fail approach can be used if these settings are unclear or unavailable in the datasheet. This approach involves using the IDEAS-Testbench and an oscilloscope to adjust the settings and observe the resulting output.

Shaper settings:
One critical setting that requires adjustment is the shaper setting. The programmable shaping time and the pulse shape from the detector determine the pulse peaking time. However, finding the correct configuration for this setting is not always obvious and may require visual inspection using an oscilloscope.

To achieve the appropriate configuration together with the CsI(TI) scintillator, a 2 µs peaking time is to be chosen because it enhances the detection of lower energy signals such as X-rays and gamma rays. Other available pulse peaking times include 50 ns, 150 ns, and 300 ns, but 2 µs peaking time was determined to be the most suitable for the desired application. Additionally, a high gain setting is required to amplify the signal, although the recommended value for this setting is not explicitly provided in the APOCAT datasheets and requires further investigation.

The G_EN_2US setting in APOCAT offers a choice between high-rate and lower-rate scintillator use cases, with the lower rate option enabled. In addition, enabling the 2 µs peaking time with G_EN_2US may improve the signal-to-noise ratio in certain cases. For example, when scintillation light output is low, or the detector operates in a low-rate environment, a longer peaking time allows more charge integration, improving sensitivity to low-energy events. Also, in some cases, the G_EN_2US setting and longer peaking time may reduce the need for a high gain setting, particularly in low-energy detection scenarios. However, further investigation may be required to determine the optimal gain setting for a given setup.

CSA gain and CMIS attenuation settings: The CSA gain and CMIS attenuation settings are essential for amplifying the input signal in the APOCAT system. Adjusting these settings can help find the charge given to the system by sending calibration pulses and measuring the resulting voltage.

To adjust the CSA gain and CMIS attenuation settings, it may be necessary to use an oscilloscope to observe the system's response to calibration pulses. By increasing or decreasing these settings, it is possible to optimise the system's performance for different detector setups.

The optimal CSA gain and CMIS attenuation settings may vary depending on the specific de-

tector setup and environmental factors. Therefore, carefully testing and adjusting these settings is essential to ensure the system meets the required performance specifications.

Hold settings

The APOCAT system includes an internal sample and hold circuit that needs to hold the output signal for a sufficient duration to allow the AMUX to circle through all the channels. The system has global settings for holding the signal, sensing time after a trigger, and resetting the signal. These settings must be adjusted carefully to ensure the system works optimally for the specific application.
To inspect the output of the shaper, an oscilloscope can be used to observe the output signal before being sampled by the ADC (AOUT) versus the output on AMUX. This helps to verify that the hold settings are appropriately adjusted and that the system's performance meets the required specifications.

Overall, using a systematic approach and testing the different configuration settings, optimising the APOCAT system for different detector setups and ensuring that it meets the required performance specifications is possible.

5.4 Performance Testing

The performance tests are performed to measure the system's performance characteristics such as sensitivity, linearity, and resolution, where the test is done in two different configuration modes.

In the first mode TPF-012, the system will be tested with detectors connected but without any source present. This test measures the system's baseline, noise, and channel gain variations characteristics. By measuring these characteristics, we can determine whether the system works as intended with the new ROIC. A plot of the data values obtained for each channel can be used to visualise the baseline, noise, and gain variation within the ROIC for each channel.

In the second mode TPF-013, the system will be tested with detectors connected and detector bias applied. This test measures the system's sensitivity, linearity, and resolution characteristics. Known radiation sources will be used as stimuli for the SiPMs and produce signals for detection. The system response will be measured for different radiation source intensities and energies to determine the system's sensitivity, linearity, and resolution.

Both performance test modes will be data sets to analyse, and the results of the performance tests will be analysed in the next chapter to ensure that the system meets the required specifications and performance criteria.

5.4.1 TPF-012 Calibration

The calibration test allows us to evaluate the performance characteristics of the system with the presence of a detector. By measuring metrics such as baseline, noise, gain, dynamic range, and linearity, we can ensure that the system operates within the expected specifications and accurately detect and measure signals from a detector.

Baseline and Noise

The Baseline(Pedestal) calculation for each channel can be found by taking an average of all pulses sampled. A forced readout can obtain the baseline and noise from when the system "lays" at rest. Where forced triggers trigger the system to obtain a readout so that the system collects data even when no actual signal is present. The mean value of the readout is the baseline, while its standard deviation is the noise.

As for the equation below, where $r_k(n)$ represents the sampled value of the signal at index n for channel k. The equation computes the mean value of the signal across all N samples for a particular channel k, which represents the baseline value of the signal.

$$\overline{r_k} \stackrel{def}{=} \frac{1}{N} \sum_{n=1}^{N} r_k(n) \tag{5.1}$$

noise: Noise refers to the fluctuations in the baseline signal and can be characterised by its standard deviation ($\widetilde{r_k}$). By measuring the noise for each channel, we can ensure that the system is operating with the expected level of precision and within an acceptable range which does not affect the detection of low-energy signals.

$$\widetilde{r_k} \stackrel{def}{=} \sqrt{\frac{1}{N(N-1)} - \sum_{n=2}^{N} r_k(n) - \overline{r_k}^2} \tag{5.2}$$

Channel Gain Variations

The gain variation is a measure of how much the gain of each channel in the ROIC varies. This variation can occur due to manufacturing processes or other factors that affect the performance of the ROIC. This measurement aims to determine how consistent the performance of each channel is and identify any potential issues with the ASIC. In addition, the measurement identifies channels that may require calibration or adjustments to align with the rest of the channels.

Using the calibration pulse from APOCAT for charge injection, a number of (n) pulses can be sent through each channel to find and measure gain variation from channel to channel. The gain is the ratio of the input charge to the output signal amplitude. We can measure the gain for each channel to ensure that it is stable and consistent across all channels.

The gain of a single channel can be calculated by applying n number of calibration pulses. The baseline $\overline{r_k}$ is subtracted from the mean value of the pulses. Two measurements are taken with different given charges (Q), and then the two measurements are subtracted and divided by the difference in charge, as shown in the equations below.

$$S_k(n) = r_k(n) - \overline{r_k} \tag{5.3}$$

The gain calculation of each channel gain is found by:

$$g = \frac{\partial S_K}{\partial Q} \tag{5.4}$$

The gain represents the gain of each channel of the ASIC, and since the DAC is used as the input pulse, it is in units of LSB/charge (least significant bit per coulomb). From the APOCAT data sheet, the internal capacitance on the GCU is 50pF, and the DAC range is 1.1V. The maximum charge sent through the system can be calculated as:
max charge $= 50 \cdot 1.1V = 55pC$.
Dividing this by the number of available least significant bits (LSBs) of the DAC (1024) gives a charge/LSB value of 0.0536657 pC/LSB. Therefore, we can calculate the corresponding charge by setting the DAC value to a certain number. For example, a DAC value of 200 corresponds to approximately 10.7 pC charge.

Equivalent Noise Charge

Equivalent Noise Charge ENC) describes the noise performance of the signal processing system. It represents the amount of charge necessary to produce a signal-to-noise ratio (SNR) of 1, which is the minimum SNR required for a signal to be detected above the noise floor. Meaning the lower the ENC value, the better the noise performance of the system.

$$ENC[C] \stackrel{def}{=} \frac{\widetilde{r}}{\hat{g}} \tag{5.5}$$

Dynamic range

The dynamic range can be tested by sending charge injection for the whole range and visualising the result in the IDEAS-Testbench histogram. By measuring the system's response to a range of calibration charges, we can determine the upper and lower limits of the system's dynamic range. Since we know the conversion rate from DAC value to charge, we can find the dynamic range in terms of charge. [14, ch.5]

$$\text{DNR} = \text{maximum signal level} \;/\; \text{Baseline} \tag{5.6}$$

Resolution The resolution of a system refers to its ability to measure and distinguish small changes in the input signal accurately. In this context, the resolution is the smallest detectable change in the input charge that produces a noticeable change in the output ADC value. The dynamic range test determines the input charge range, and the ADC bit resolution is based on the number of available bits in the ADC. Calculation of the resolution can be done with the following equation.

$$\text{Resolution} = \text{Input range} \;/\; (\text{ADC range}) \tag{5.7}$$

5.4.2 TPF-013 Spectroscopy

Various tests can be conducted under different conditions to test the system's performance with radiation sources. One test involves exposing the system to a known radiation source and analysing the resulting spectrum using spectroscopy techniques. Analysing the spectrum can evaluate performance metrics such as resolution, linearity, and energy calibration. This helps to ensure that the system is capable of accurately detecting and measuring radiation signals from a source. In addition to spectroscopy tests, other radiation tests can be performed, such as measuring the system's response to different radiation types and energies. The test will take both single channel readout and a multichannel readout, but the focus has been on a single channel, so the multichannel readout is to show that it gets the right spectrum. The test approaches for exposing the detectors with radiation sources readout would be:

- Setup the ROSSHIP system with SiPMs and the usage of IDEAS-Testbench.
- Cover the SiPMs to prevent any light from entering.
- Connect Oscilloscope-probe to AMUX(multiplex output), TOR(Trigger signal) and AOUT(Signal before ADC sample) for additionally inspection.
- Set up the system with the appropriate configuration settings for the radiation source.
- Place a known radiation source near the system.
- Verify the triggering by visualising the source using an oscilloscope.
- Check the IDEAS-Testbench for the presence of a peak in the histogram.

In addition, further investigation of some data may be needed. The data must be sampled and analysed using Excel and Python.

Single Channel Pulse shape Spectroscopy

With the correct configuration settings, a readout with a radiation source will start triggering the system with pulses. Each channel must be tested to verify that all channels respond correctly to a radiation source. An Oscilloscope can be used to confirm that the system is receiving triggers by visualisation when applying a source near the detector. This also assures that the correct configuration settings are applied or need tuning. During the test, a known radiation source is used, and its corresponding peak will appear in the histogram in IDEAS-Testbench. To ensure accurate measurements, the threshold is adjusted to eliminate noise triggers. The

test is successful when the spectrum of the known source is displayed in the histogram with a reasonable resolution. This indicates that the system is properly detecting and measuring the radiation from the source. After sampling an (x) amount of events, the data will be saved and converted to a readable format for further inspection. The test is considered fully passed when all the sources are sampled and data evaluated to reasonable measurements.

Gain measurement using radiation sources

The data collected from the different sources in the single channel readout will be compiled into a table, presenting the actual energy values of the radiation sources, along with the corresponding ADC values obtained from the measurements. Additionally, these values will be plotted to establish a relationship between ADC values and charge. The resulting plot is expected to show a linear curve, enabling the determination of a linearity gain equation. The equation will also verify the obtained baseline from the baseline test in TPF-012 by identifying the point on the gain curve where it intersects the x-axis at the y-axis zero point. The ADC values will be adjusted using the gain equation and then re-plotted to display an energy spectrum in keV. By comparing the corrected histogram with the expected energy levels, it can be determined if the gain correction successfully brings the histogram to a reasonable energy scale, indicating a passed test.

Pulse shape analysis

By further investigations of the gain corrected data, the Cs^{137} is to be used as a reference for the system, and improved parameters such as the mean values of the peak, its standard deviation, the FWHM, and ENL is done using Python scripts. The data from Ideas-Testbench is given in BIN files. Therefore the data needs to be converted to CSV/Excel files which are read in Python and plotted in a histogram for analysis. In the energy spectrum, the peaks are to be located and analysed. However, only the peaks that meet certain criteria will be displayed. These criteria can be defined based on specific requirements, such as peak amplitude, FWHM criteria, or peak shape. Peaks that meet the specified criteria will be shown, while others that do not will be disregarded. This approach allows for a focused analysis of the relevant peaks in the energy spectrum, ensuring that only reliable and significant information is considered.

After the interested peaks are displayed, their mean value and standard deviation are calculated based on the specified criteria requirements. The Full Width at Half Maximum (FWHM) ap-

proach is presented in equation 2.4, and the complete code for the analysis can be found in the appendix 9.9. The Energy Non-Linearity (ENL) is then calculated as a percentage by comparing the measured value to the expected value for each peak. To assess the system's performance, the calculated parameters are compared with the system requirements specified at the beginning of this thesis (Chapter 1.1). This ensures that the system meets the desired specifications and performance targets. All the relevant parameters and their corresponding values are summarised in a resulting table.

All channel shape height Spectroscopy

The all-channel readout is done by activating all channels for readout and triggers. Then, a new test of the Cs^{137} source is to be taken. The test shows the functionality of the summing channel and is confirmed with a summed measurement analysis of all other channels to confirm they are the same. Of course, using all channels for readout and triggers means more noise contribution due to all the channel activation and might need a deeper analysis. Still, the point here is to show the system is fully operative with both the summing channel and all channel readouts.

6 Results

In this chapter, we will be sharing the outcomes of the verification process. This includes the results of the initial, functional and performance testing, which will be presented in the form of text and figures. Each result is labelled with its corresponding test plan name. At the end of this chapter, we will provide a comprehensive table that summarizes whether each test has passed or failed

6.1 Initial Testing Results

6.1.1 TP-010 Visual inspection

The visual inspection was conducted using a microscope in the laboratory after the soldering process was completed. The soldered ROIC was visually assessed, as shown in the image below. The quality of the soldering work was evaluated by experienced professionals at IDEAS, although my direct involvement in the soldering process was limited.

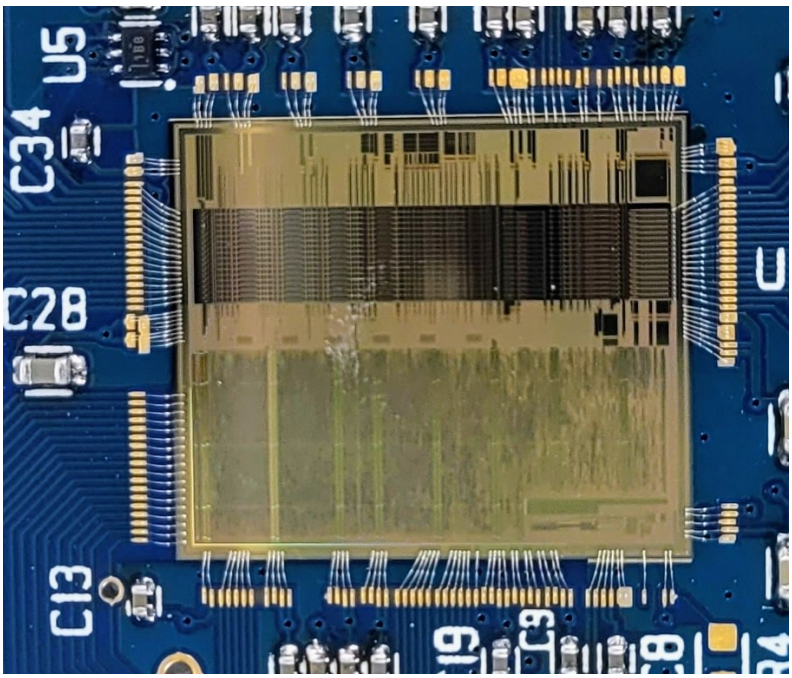

Figure 6.1: Visualization of the front-end board soldering of APOCAT

6.1.2 TP-011 Smoke Test

The test was carried out while visualising the power supply current with a steady increase in the voltage supply. Tests were conducted without any signs of smoke or the smell of burned devices. The current keeps a constant increase throughout each increase of voltage.

6.2 Functional Testing Results

6.2.1 TPF-010 Interface Verification

Firmware module verification

The simulations were performed using test benches for the module ROSSPAD_OS_wrapper from chapter 4.9. This involved running the VHDL code in a simulated environment to verify the functionality and behaviour of the design. The test benches provided input stimuli and captured the output responses, allowing for thorough testing and validation of the module functionality. Verification aspects were addressed by conducting simulations as shown previously in chapter 4.6.2. Also, the details of the VHDL code used for simulations can be found in the appendix (9.4).

Configuration of register verification through SPI

To confirm that APOCAT configuration registers can be programmed and read correctly through the SPI interface, a value was written to one of the registers in the IDEAS test bench. The output log from the testbench, shown below, was then used to verify the operation.

```
2023-04-01 18:09:33.648: Sent: ASIC SPI Register Write ASIC ID: 3, format
    ↪ : 1, address: 90, length: 20, data: [02 00 00]
2023-04-01 18:09:33.778: Recv: ASIC SPI Register ASIC ID: 3, address: 90,
    ↪  length: 20, data: [02 00 00]
2023-04-01 18:10:22.718: Sent: ASIC SPI Register Read ASIC ID: 3, address
    ↪ : 90
2023-04-01 18:10:22.868: Recv: ASIC SPI Register ASIC ID: 3, address: 90,
    ↪  length: 20, data: [02 00 00
```

The figure says that the test bench output where the data [02 00 00] was successfully written to register at address 90 for the ASIC(APOCAT). The subsequent read operation also returned the same data [02 00 00], indicating that the write operation was successful and the data was correctly stored in the register. The result is also shown in the screen dumps from the oscilloscope, where the value 0x41 was written to the register, and the same value was read in the read operation, which confirms that the read operation was successful. The register still holds the value 0x41.

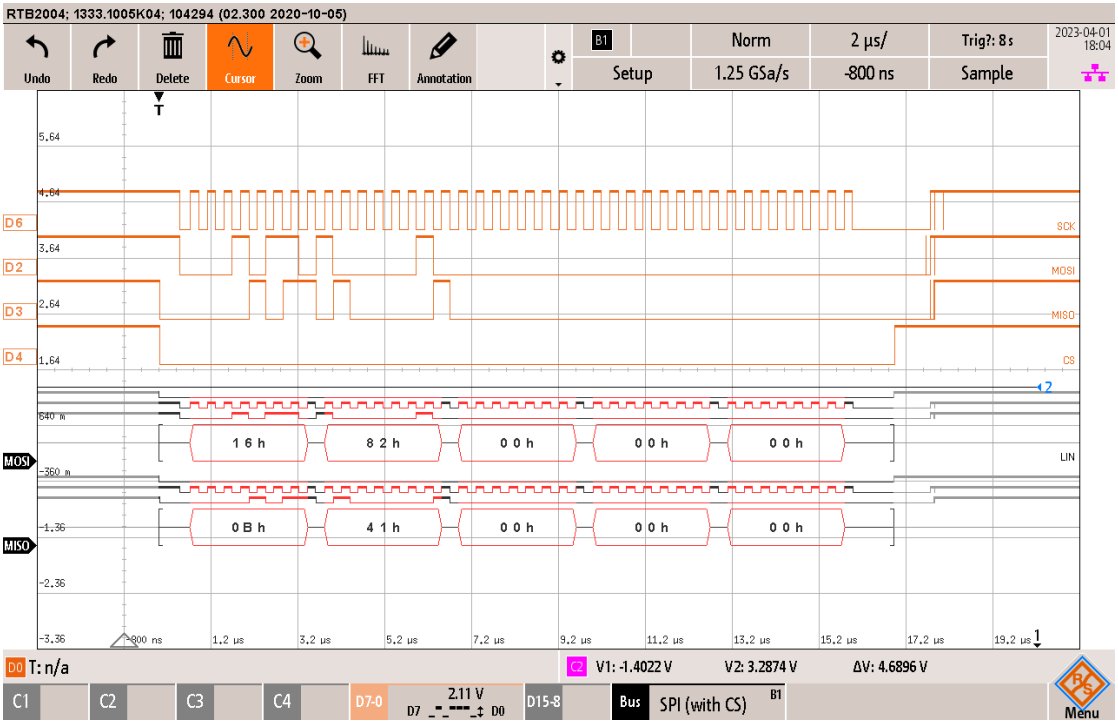

Figure 6.2: SPI write operation

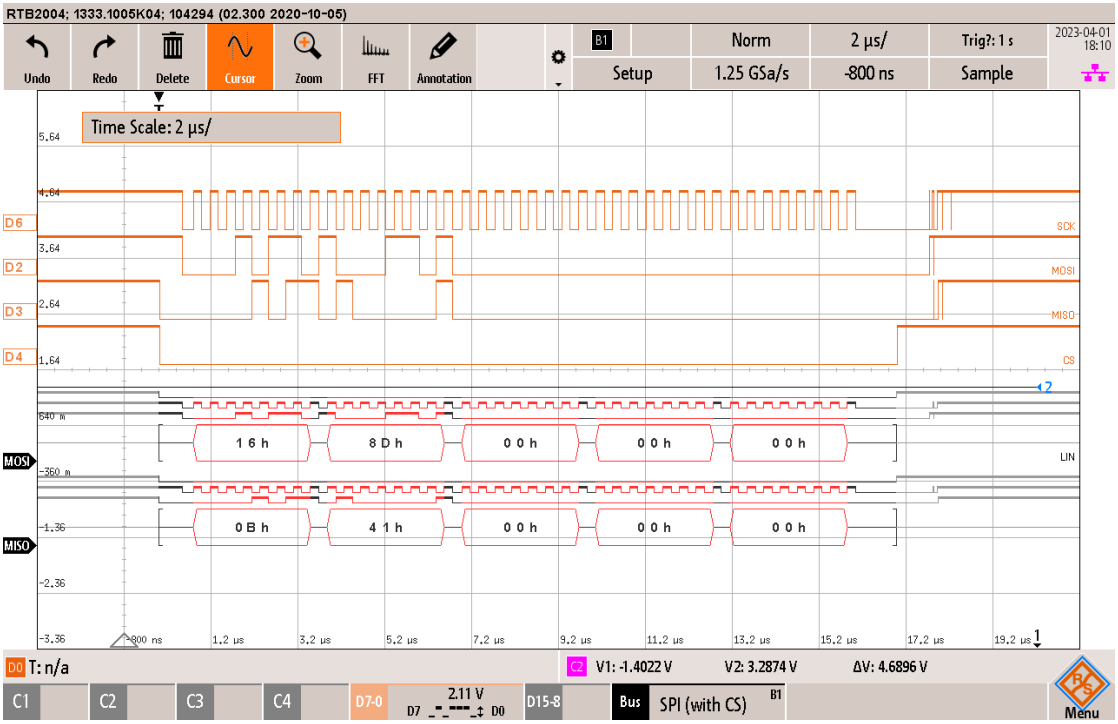

Figure 6.3: SPI read operation

6.2.2 TPF-011 Hardware Testing

Verification of ADC Sampling

To verify the functionality of the ADC sample shown in chapter 4.6.3, a calibration pulse was sent through one of the channels as seen in the screenshot 6.4 from the oscilloscope. The cfg_phase_shift were adjusted so that CNV(the spikes in the figure) were to sample approximately in the centre of each channel. A trigger event is setting TOR high, followed up by Shift_I. The AMUX signal in purple shows the multiplexed output of the 20 channels, where channel 5 is the channel the pulse is sent through. The last three signals correspond to the gain calibration unit, a PT100 element and the value of the internal ADC input. Also, the ADC needs an extra (N+1) "channel", which is the channel not numbered since the ADC send serial data bits which correspond to the previous conversion as seen in the figure 4.4.

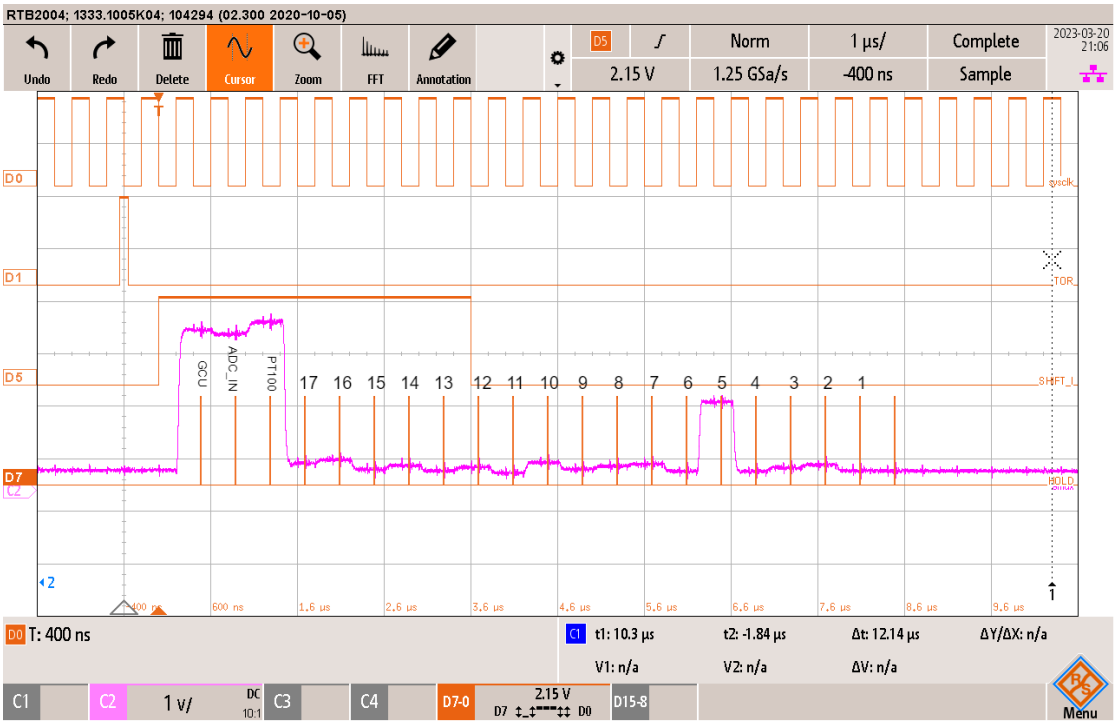

Figure 6.4: Timing of the ADC sampling visualised on the oscilloscope, signals shown from top to bottom, Clock, TOR and Shift_I and in purple the multiplex output AMUX .
The spikes shows each CNV signal for the ADC, with a adjusted cfg_phase_shift setting

Detector bias

The detector bias circuit provides a stable and precise bias voltage to the SIPMs. The detector bias circuit uses a 12-bit digital-to-analog converter (DAC) with a resolution of 25 mV. A 12-bit DAC can provide 2^{12} or 4096 different output levels, with each level representing a voltage step of 25 mV. This gives a total range of 102.4 V (4096 x 0.025V). An oscilloscope was used to visualise the output as the detector bias was increased. A stable signal was found at around 25V.

APOCAT configuration settings

The following settings were found by adjusting the settings and observing the resulting output using an oscilloscope. The start-setting where the slow shaper's 2us peaking time. Also, from the APOCAT datasheet, a combination of peaking time setting for a 2 µs configuration is for the fast shaper to be at 1 µs. The activation of the G_EN_2US gave no reason to use any additional gain, and together with the CMIS attenuation on max(1/20), it could even have been less gain if possible.

Table 6.1: Summarize of the most important APOCAT Configuration Register settings

Setting	Note	Value
Shaper and Gain settings		
G_EN_2US	Scintillator use case, 1= lower-rate	1
Slow Shaper	Chosen slow shaper peak time	2 [us]
Fast Shaper	Chosen fast shaper peak time	1 [us]
CMIS Attenuation	The attenuation of the common mode feedback signal	1/20
CSA Gain	Amplifier is providing a gain of 1	1/1
HOLD settings		
Sense Time	Duration of sensing time for the hold. Interval between trigger and hold in mulitples of 50ns periodes.	70
Hold Time	Duration of the internally generated HOLD signal in multiples of 50-ns periodes.	220
Reset Time	Reset after ended HOLD signal in multiples of 50-ns periodes	6

Hold settings The internal sample and hold circuit must maintain the output signal value for a sufficient duration to allow the AMUX to cycle through all channels. If the hold signal is too brief, as illustrated in the figure below, the output signal on the channel will be truncated prematurely.

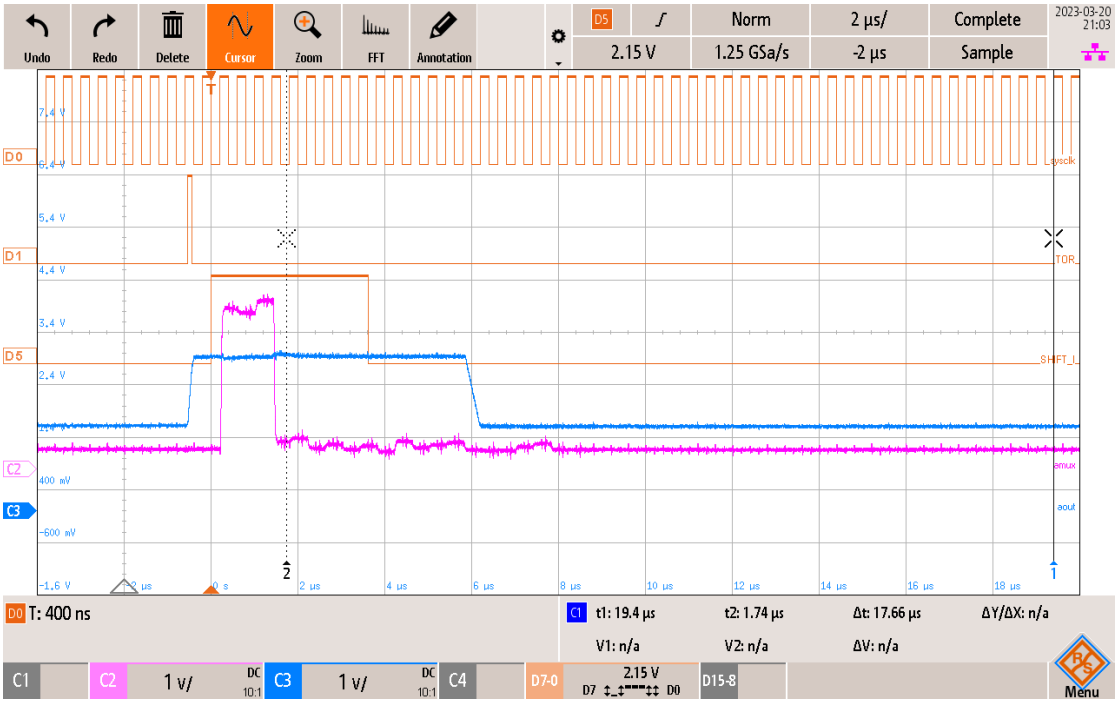

Figure 6.5: The hold signal holds the output signal aout on channel 4 until around 6 us, which is too short for the AMUX to multiplex the correct signal for channel 4

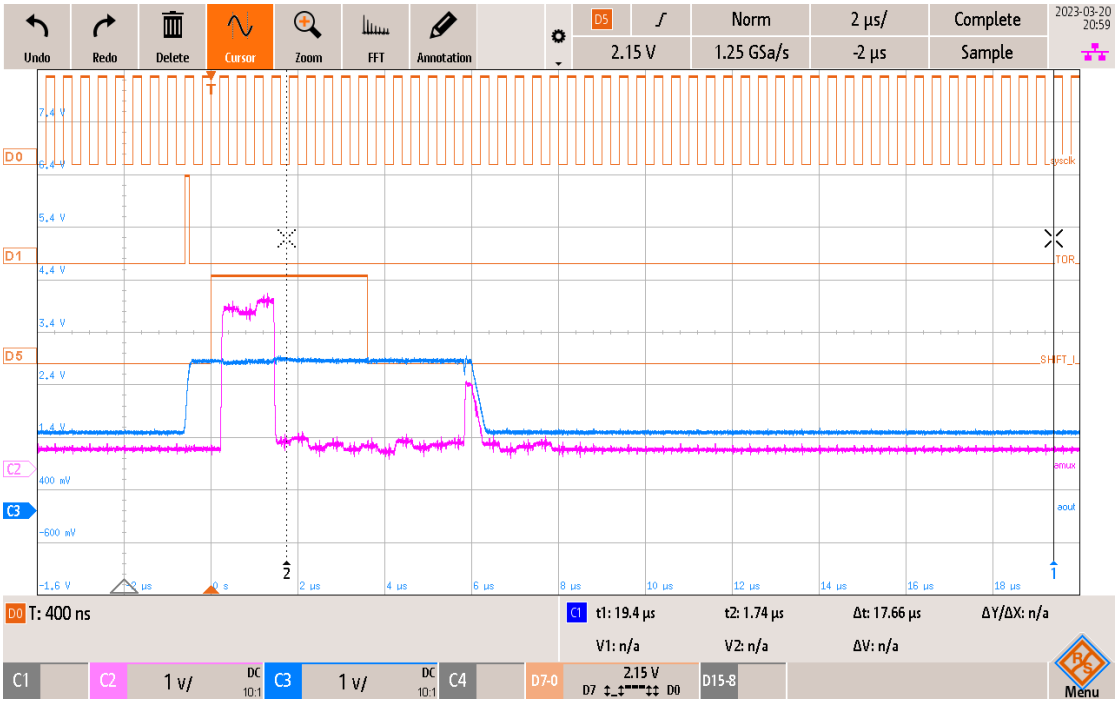

Figure 6.6: With the same setting for hold, a closer look at channel 5 shows where the signal was truncated in the previous figure, indicating the hold signal must hold the output signal for a longer time before resetting

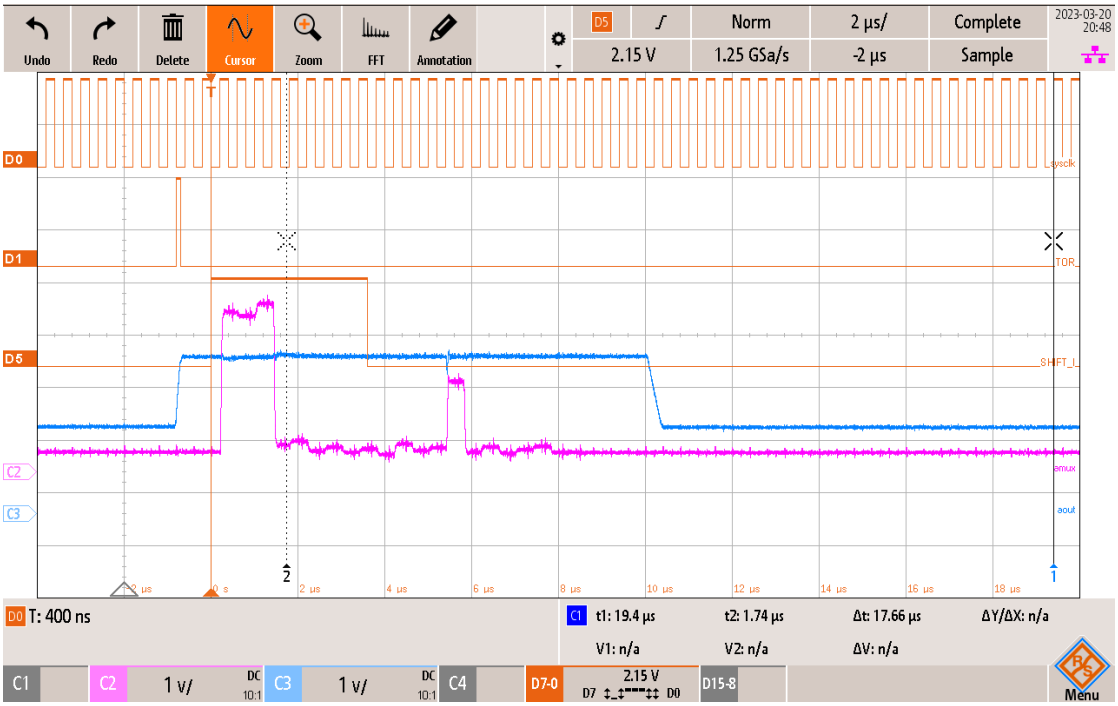

Figure 6.7: After adjusting the hold signal to hold the output signal aout for a longer time, all the signals are multiplexed out of amux and the ADC samples the correct output values.

6.3 Performance Testing Results

6.3.1 TPF-012 Calibration

The Baseline and noise were measured while the system lay at rest. Then, using forced triggers, the system collected data even when no actual signal was present. The measurements were done through the IDEAS-Testbench using scripts (See appendix for the script 9.9 or more details about IDEAS-Testbench in chapter 4.2) to measure the baseline and noise throughout all channels on AMUX. The IDEAS-Testbench software lets the user control the system configuration registers and readout data through scripts based on Python. The script sets each individual channel's configuration settings for enabling forced readouts. Then start a forced readout, which samples each channel's count values to a specific number of pulses. Then the mean and standard deviation are calculated and plotted for each channel. The baseline differs from 600 to 800 in ADC values which are expected. However, some channels have more noise than others, which could be due to variations in cable lengths from the ROIC to the SiPMs. Other noise sources could include SiPM, dark, and bias noise. Conducting noise tests with and without bias and SiPMs may be necessary to investigate this further. Additionally, calculating the cable length and determining if there is any correlation between cable length and noise levels could be helpful.

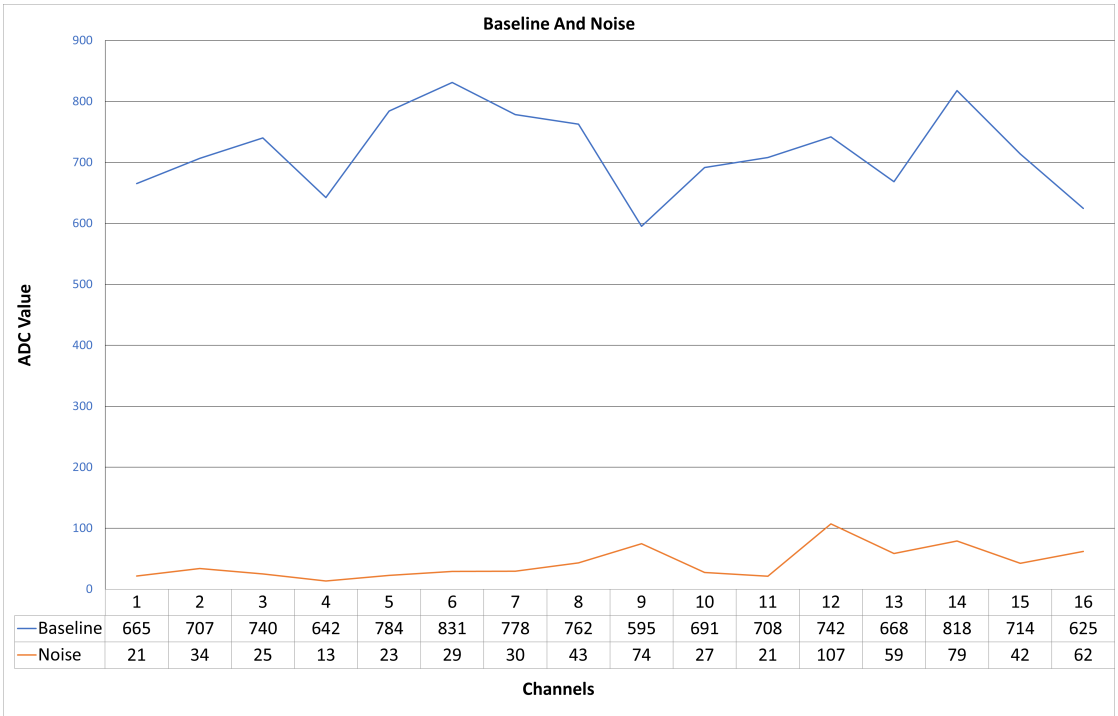

	1	2	3	4	5	6	7	8	9	10	11	12	13	14	15	16
Baseline	665	707	740	642	784	831	778	762	595	691	708	742	668	818	714	625
Noise	21	34	25	13	23	29	30	43	74	27	21	107	59	79	42	62

Figure 6.8: Baseline and noise values for all channels.

Gain variations

The variable Gain represents the gain of each channel of the ROIC in units of LSB/pC (least significant bit per pico coulomb). For simplicity, also here a script was made(Code in appendix 9.9). The measurement was taken by applying two pulses with the charge at 15pC and 30 pC and measuring the mean value of the pulses. The baseline was then subtracted and then divided by the difference in charge.

The gain variation results are as expected, where there are some differences between the channels. Still, it is possible to adjust the gain of channels by increasing their bias voltage, which can lead to better precision in the system. However, the variation in gain is generally within an acceptable range.

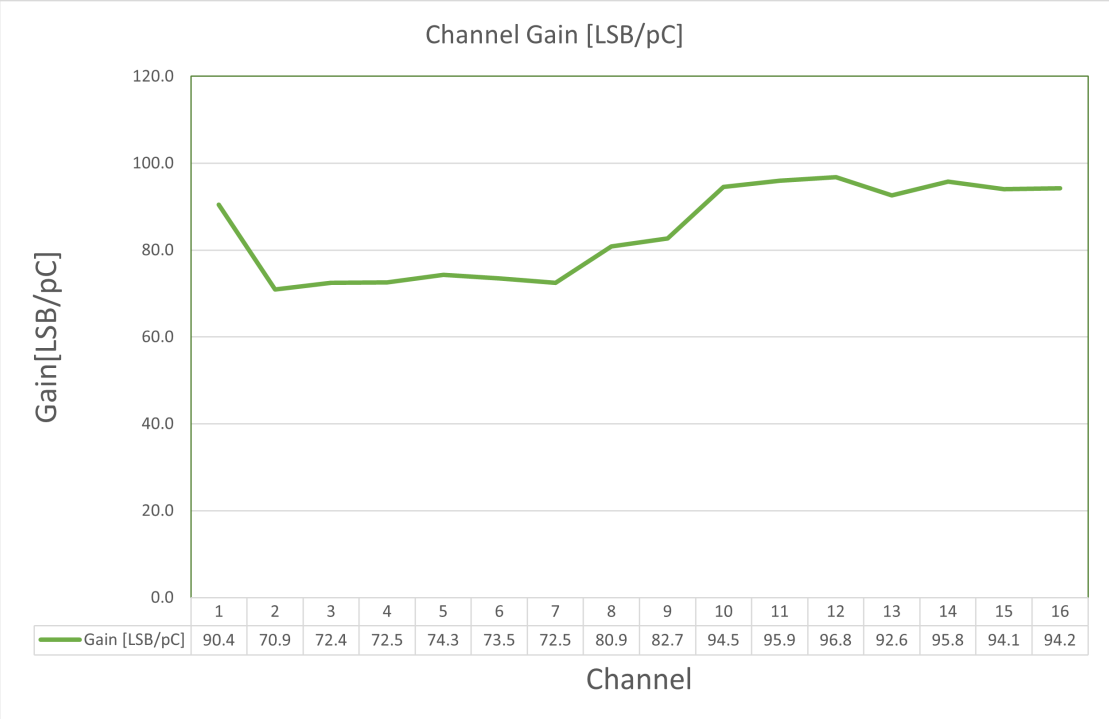

Figure 6.9: Measurement shows gain variation between all channels

Equivalent Noise Charge

ENC was calculated for each channel as follows:

$$ENC[C] \stackrel{def}{=} \frac{\widetilde{r}}{\hat{g}} \tag{6.1}$$

Where for channel one:

$$ENC = \frac{665[LSB]}{90.4[LSB/pC]} = 7.35[pC]$$

Dynamics range

The Dynamic range was found in terms of input charge versus output ADC value by sending a calibration pulse with a given DAC value. The DAC value was converted to charge from the conversion factor from TPF-012, which was 0.0536657 pC/LSB.
The calibration pulse started at the lowest DAC value, giving a pulse without any noise triggers. It was then increased by 100 until the curve stopped increasing and the saturation point was found.

Table 6.2: Table of collected data of calibration pulses with varying DAC values

Source	DAC Value	Capacitance (pF)	Charge (Q) (pC)	ADC Value Range
Calibration	115	50	6.18	1270
Calibration	215	50	11.55	1910
Calibration	315	50	16.92	2540
Calibration	415	50	22.29	3190
Calibration	515	50	27.66	3840
Calibration	615	50	33.03	4500
Calibration	700	50	37.60	4860
Calibration	715	50	38.4	4885

A calculation of DNR in terms of db where the S_{max} represent the maximum ADC value and the S_{STD} is the baseline in ADC value.

$$DNR = 20 \cdot \log_{10} \frac{S_{max}}{S_{STD}}$$

$$DNR = 20 \cdot \log_{10}((4885/665))$$

$$= 17.3\,\text{db}$$

The collected data allowed for the determination of the system's dynamic range. The dynamic range, expressed in dB, represents the ratio of the maximum signal power to the noise power in the system. The dynamic range of 17.3 dB was calculated, indicating the system's ability to distinguish between the desired signals and the inherent noise.

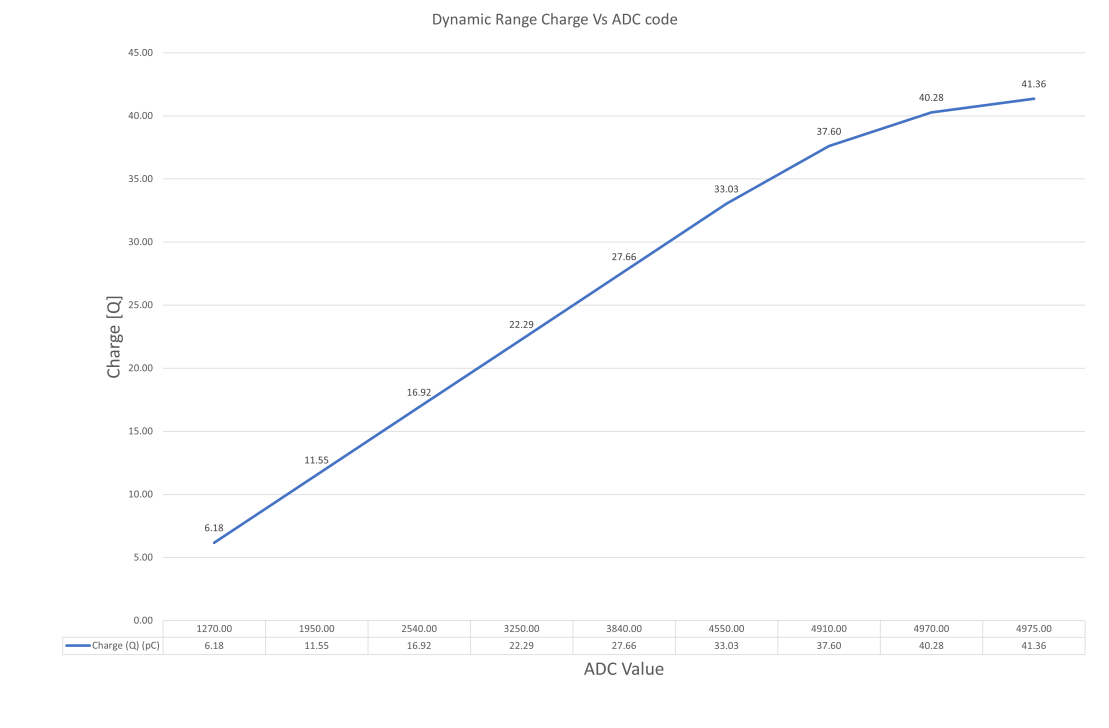

Figure 6.10: Dynamic range where data were plotted as input Charge vs the ADC output value.

Resolution The resolution represents the smallest detectable change in the input charge that produces a noticeable change in the output ADC value. From the dynamic range test, the input range is the highest value measure minus the smallest, and the ADC range is the number of available bits.

$$\begin{gathered}\text{Resolution} = \text{Input range} \;/\; (\text{ADC range}) \\ \mathit{Resolution} = \frac{32.22 pC}{4096} = 0.0079\,\text{pC}\end{gathered} \tag{6.2}$$

6.3.2 TPF-013, Spectroscopy

Single channel spectroscopy readout

Several radiation sources were used as stimuli for the SiPMs to verify the spectroscopy readout. The sources used had different energies and peaks, as shown in the figure below. The test followed the approach mentioned in chapter 5.4.2. All channels were verified as fully functional, and the figure below shows how channel 1 displayed the sources after the measurements. The APOCAT configurations were kept constant for the lower energy readout, and a single-channel readout was used to avoid noise triggers from other channels. A lower threshold was set at the triggering channel for the lower energy sources, while for higher energy sources such as Co^{60}, a higher threshold was used to show the spectrum without too many noise triggers from lower energies. The figure shows the peaks in ADC values from the different sources and where the limits of the mean value were calculated. The sources were sampled one at a time, and their pulse shape was plotted using Python (script shown in the appendix 9.9). The pulse shapes obtained from the sources exhibit the expected shapes, indicating that the system can detect the distinct pulse signatures of each source. Furthermore, the Compton edge in some of the source's pulse shapes indicates the system is sensitive to Compton scattering events.

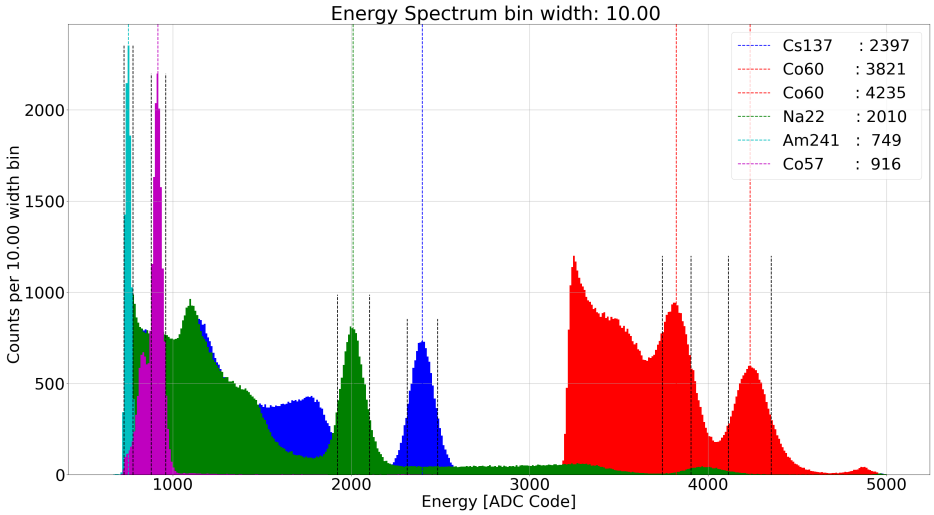

Figure 6.11: Spectroscopy measurement with five different sources shows the number of counts vs ADC code
$NA^{22}, Co^{60}, CS^{137}$ is captured with 800k events but to make Co^{57} and Am^{241} fit the page they have 200k and 100k events. Also, the threshold of the Co^{60} is very high in difference to the other sources, which is why it looks cropped.

Gain calibration with sources

The gain conversion was found when converting the ADC values to energy in terms of keV. The table below shows the different sources and their measure ADC from the system. A polynomial equation was derived by plotting the source energies against the ADC Value, representing the gain for the channel. The given equation was used to find the value in keV for this channel. The gain calibration also corrects the baseline and improves the accuracy of the measurement.

Table 6.3: Gain calculation for channel 1 with five different sources for visualisation of data in keV

Source	Am^{241}	Co^{57}	Na^{22}	Cs^{137}	CO^{60} p2	CO^{60}
Measured ADC (x)	749	916	2010	2397	3821	4235
Acually PEAK in Kev	59.5	122.1	511	662	1173	1333

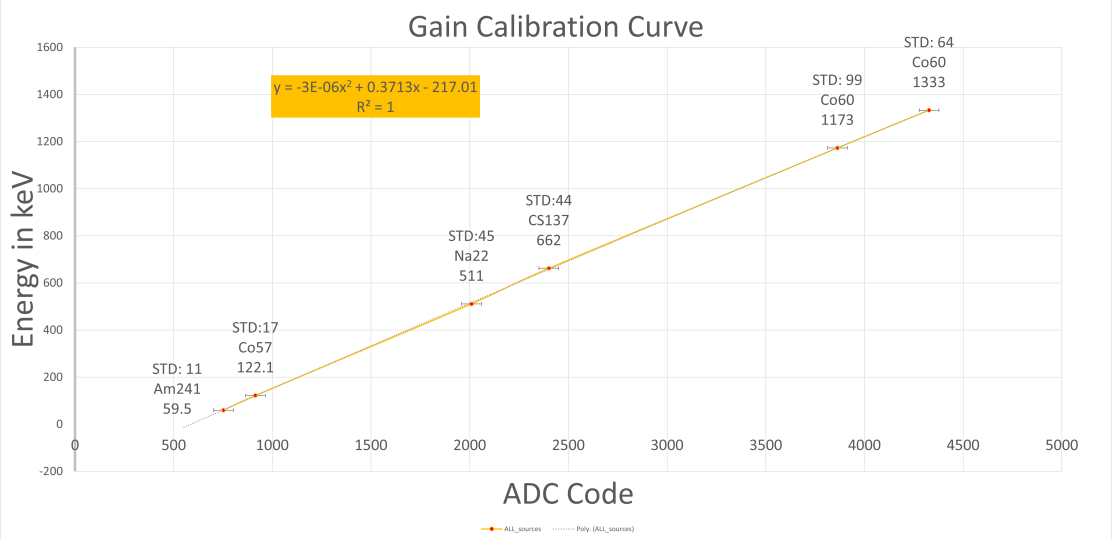

Figure 6.12: 5 different sources is used to calculate the Gain equation for channel one

After applying the gain correction, the histogram of the data shows the peaks in keV, which allows for identifying the peaks based on their actual energy values. The gain correction process aims to account for any non-linearities or variations in the system's response, ensuring that the observed energy values are as accurate as possible. While the energy peaks may not align perfectly with their expected values, the gain correction helps bring them closer to their true energies. This means that despite slight deviations, the resulting values are sufficiently close to

identify and analyse the peaks. The figure is also normalised to the highest peak of each source. All sources now show 800k events.

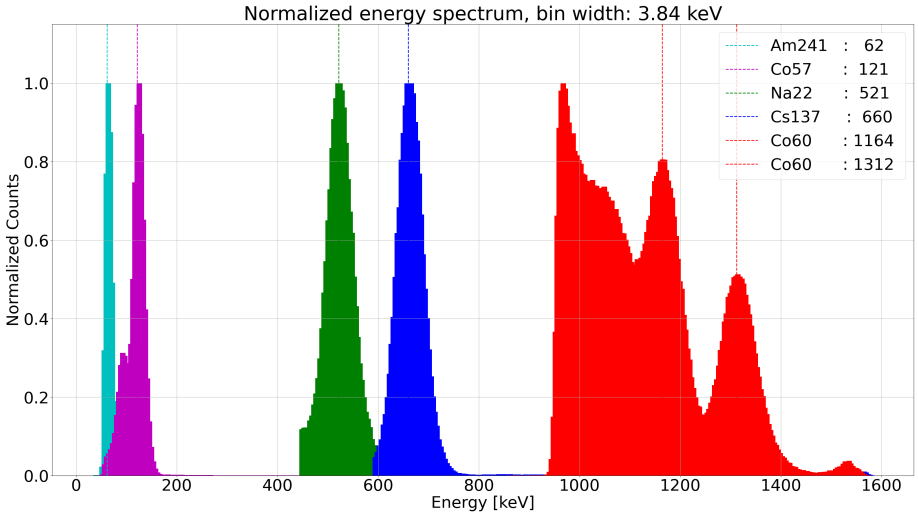

Figure 6.13: Spectroscopy measurement is now plotted with a gain correction and converted to keV. The five different sources are identified with their energy and show the measured peaks
All sources are captured with 800k events but now linearised to each source's highest peak to fit the page. Threshold of the Co^{60} is very high in difference to the other sources.
The Na^{22} and Cs_137 are cropped only to show the photo peak.

Pulse shape analysis

The Cs^{137} spectrum analysis reveals essential information about the detected radiation. The mean peak value of 660 indicates that the measurement aligns closely with the expected energy level. A well-defined Compton edge in the spectrum suggests a high occurrence of Compton scattering events. The count rate, which is high in this case, further supports the observation of significant Compton scattering events. The standard deviation of the peak provides a measure of the spread of the measured energy values, reflecting the range of energy values within the spectrum. The FWHM measurement, which quantifies the peaks' width, is below the expected value of 10%. The FWHM is determined by locating the peak value and identifying the left and right bins where the intensity drops to half. While the current method provides an estimation, a Gaussian fit could offer a more accurate determination of the FWHM. Overall, the Cs^{137} spectrum analysis provides valuable insights into the detected radiation, indicating that the system is reliable and capable of accurately detecting and analysing the radiation.

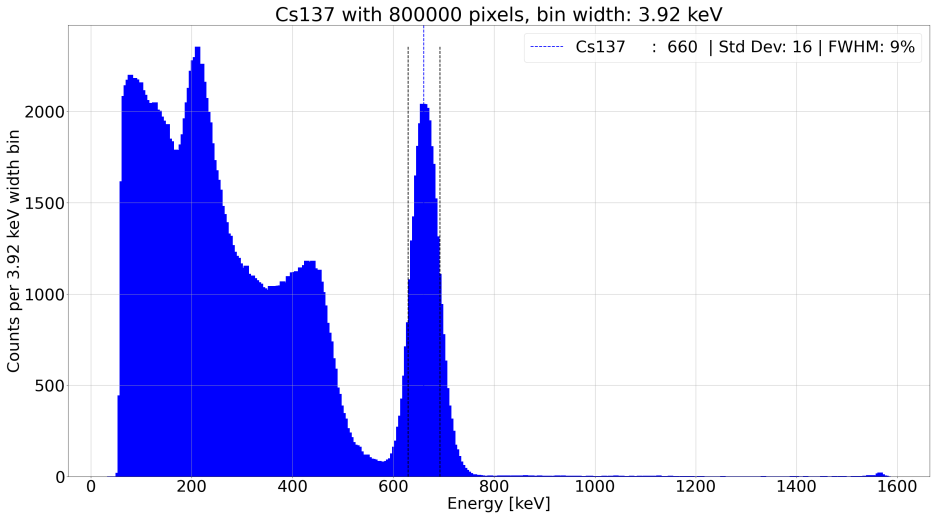

Figure 6.14: Spectroscopy with a Cs^{137} source shows the expected peak at 660keV with a standard deviation of the peak of 16 keV and with a 9% FWHM

Pulse shape analysis CO^{60}

To demonstrate the system's capability with higher energy sources, a Cobalt 60 (Co^{60}) source was used, which produced two clear peaks at energy levels of 1.16 MeV and 1.31 MeV, identifying the radiation source as $Co60$. The threshold was set higher than the other sources only to detect gamma rays that had energy above a certain point, An event of around 1540 keV was also observed, likely due to a cosmic event. The ADC was not at maximum code and did not correspond to a clear bin peak. The output buffer went into saturation of 3 volts on the AMUX, resulting in different bin resolutions depending on the charge given.

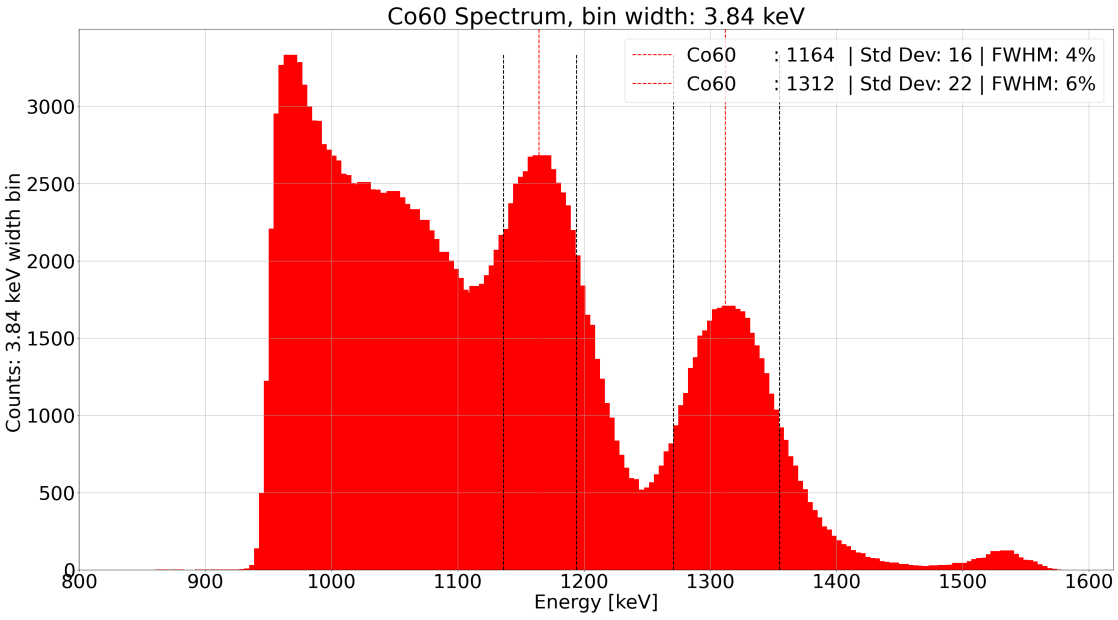

Figure 6.15: Spectroscopy with a Co^{60} source shows the expected peak for the source at around 1.16MeV and 1.31 MeV. The FWHM for the 1.16 MeV peak is set to a higher level since 1.31 MeV's Compton shelf fills its peak area.

Energy Non-Linearity

The energy non-linearity (ENL) of the system was measured using data from several calibration sources as shown in figure 6.13, and the results are summarised in the table below: These results indicate that the system has good energy linearity, with an average ENL within the target specification of less than 2%.

Table 6.4: Energy Non-Linearity for channel one where five different sources measured values versus the expected gives an ENL in percentage

Calibration Source	**Measured ADC**	**Expected Energy (keV)**	**Measured Energy (keV)**	**ENL (%)**
Am-241	752	59.5	61	2.5
Co-57	916	122.1	122	-0,08
Na-22	2010	511	511	1.7
Cs-137	2397	662	661	-0,15
Co-60 peak 2	3821	1173	1164	-0,77
Co-60	4235	1333	1312	-1,5
Average ENL				0,28

All channel Pulse shape Spectroscopy

To test the readout for all channels, all channels were enabled for triggering. The threshold for all channels was set to 430 DAC. The figure presented here shows the sum of all 16 channels, meaning that if a trigger occurred in channel 1, the values from all channels were considered simultaneously. Therefore, the baseline contributions from all other channels are also visible and are the main contribution to the measurement. The figure is zoomed in on the range between 1800 and 3500 ADC. The data for all channels confirms that the system also works with all channels activated and has not been analysed further than this. A gain correction would remove the baseline contribution from the other channels for an accurate interpretation of the data. By removing the baseline contribution, the focus can be on the relevant signal, allowing for more accurate analysis and interpretation of the data. The summing channel was verified to provide the same result as the summing of all channels, to be the same as the figure below. The observed peak for Cs^{137} exhibits a width of approximately 200 ADC code value indicates the lack of alignment among the channels, results in a broader peak. Aligning the channels and applying all-channel gain correction would resolve this issue.

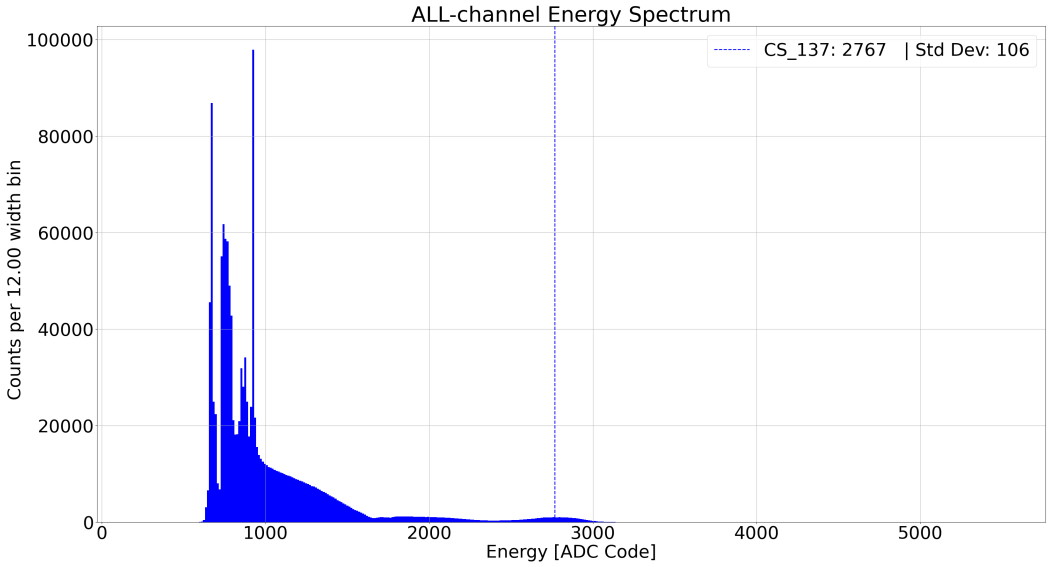

Figure 6.16: All channel Spectroscopy with a Cs^{137} source shows a baseline contribution of all the different channels, the peak at 2759 ADC is seen if zoomed in. Therefore the baseline correction is necessary to get a readable spectre.

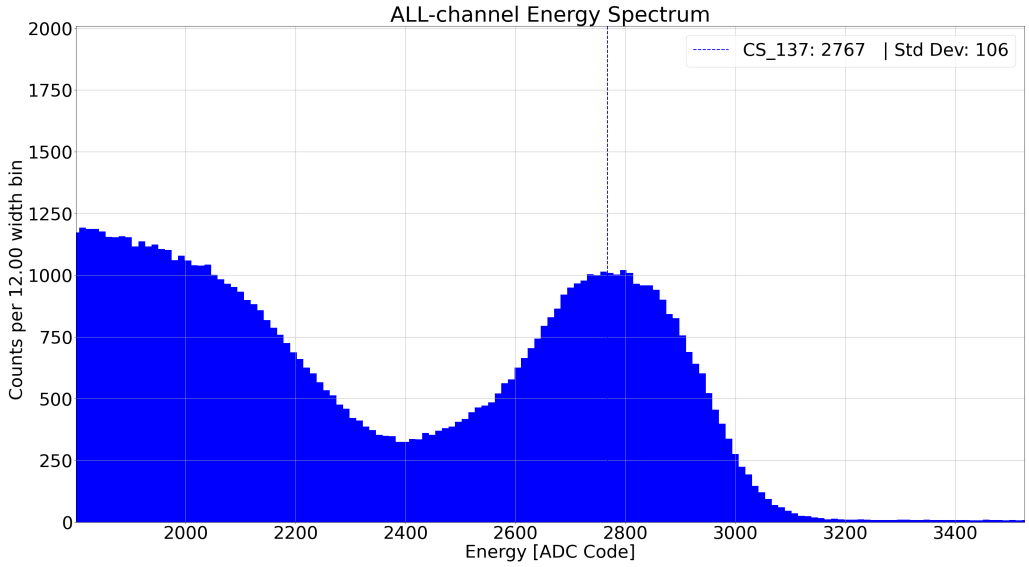

Figure 6.17: All channel Spectroscopy with a Cs^{137} source shows a sum of all channels readout.

6.4 Test Plan Results

Table 6.5: Test plan results

Ref:	Functionality	Target Specification	Result	Note
	Initial testing			
TP-010	Visual inspection	Detection of potential soldering defects	Pass	
TP-011	Smoke Test	System shall be powered up from 1V up to ±5V with stable current increase.	Pass	No noticeable current spikes
TPF-010	Interface verification			
	Power distribution	-Power Supply for APOCAT at 3.3V	Pass	Measured 3.3V between VDD and GND
	Firmware module verification	Test VHDL code with simulation tools	Pass	Rosspad_os_wrapper module is reacting as expected to stimuli ref: 4.6.3
	Configuration of register verification through SPI	Registers can read and write the correct values	Pass	Tested fully operative.
TPF-011	Hardware Testing			
	Channel Functionality	Channel integrity verification	Pass	All channels was tested and found fully functional
	ADC Verification	ADC sample verification	Pass	ADC samples as expected
	Detector Bias	Confirm stable and precise bias voltage output	Pass	Found stable at 25 volt
	Configuration settings	Adjust APOCAT configurations settings	Pass	A configuration setting is found for the CsI(tl) Scintillators
TPF-012	Calibration			
	Baseline	Find the baseline for all channels	Pass	Found for all channels with acceptable parameters
	Noise	Find the noise for all channels	Pass	Found for all channels with acceptable parameters
	Channel Gain Variations	Channel Gain Variations within the ASIC	Pass	Found for all channels with acceptable parameters
	Equivalent Noise Charge (ENC)	Find the systems ENC	Pass	Found for the configuration setting used
	Dynamic Range	Find DnR and resolution of the system	Pass	Only done for ch 1
TPF-013	Spectroscopy			
	Single Channel Spectroscopy readouts	Confirm single channel functionality	pass	Displays a fully functional spectrum.
	Gain calibration with sources	Find the gain linearity function to convert ADC value to keV	pass	Displays a fully functional spectrum in keV
	Pulse shape analysis	Find the FWHM and ENL for the channel	pass	See table below
	All channel Pulse height Spectroscopy	Show all channel functionality	pass	Displays a fully functional spectrum.

Table 6.6: Summed ROSSHIP parameters for channel 1

Parameters	ROSSHIP
Baseline [ADC value]	**665**
Noise [ADC value]	21
Gain [LSB/pC]	90,4
ENC [pC]	7.3
FWHM at 662 keV	9%
ENL	0,28 %
DNR [db]	17.3
Resolution [pc]	0,0079

7 ROSSPAD Comparison

Test results were performed on the original ROSSPAD system using the SIPHRA ROIC, where simple tests with default configuration were used. The basic configuration is not optimised for the CsI(tl) Scintillators. Still, to present a better understanding of whether the APOCAT parameters are accurate enough, this simple test is taken into consideration. The ROSSPAD configuration in this test only focuses on channel one for comparison with the ROSSHIP results. All other channels were disabled. Measurements were taken for analysis with calibration pulses and by placing different sources close to the scintillator.

ROSSPAD Baseline and Noise values were measured by the same methods as for ROSSHIP.

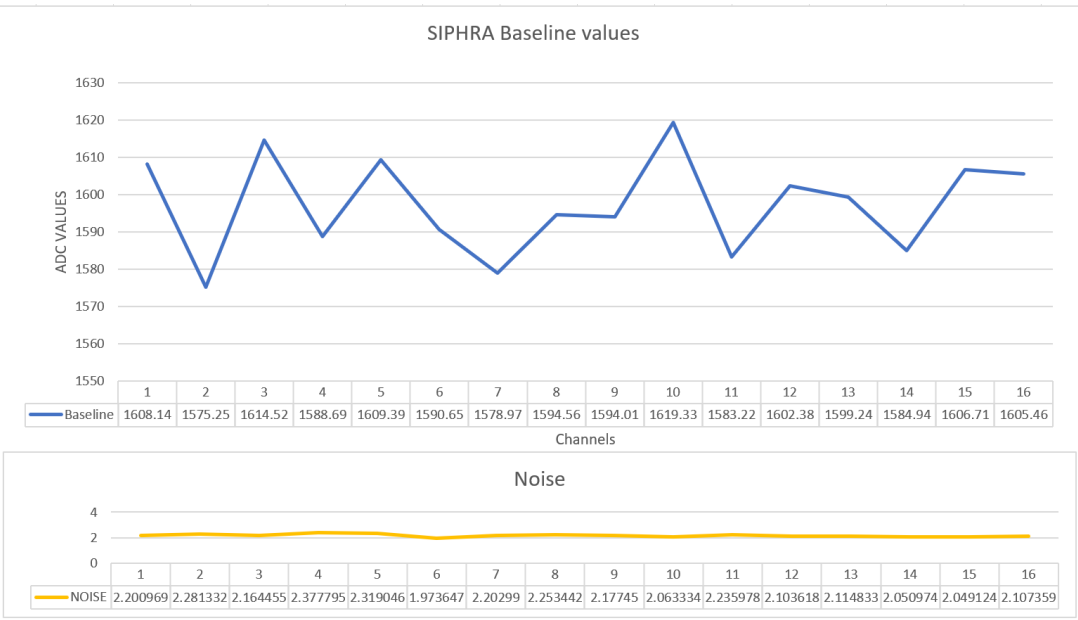

Figure 7.1: Baseline values for each channel for the ROSSPAD

ROSSPAD Dynamic Range

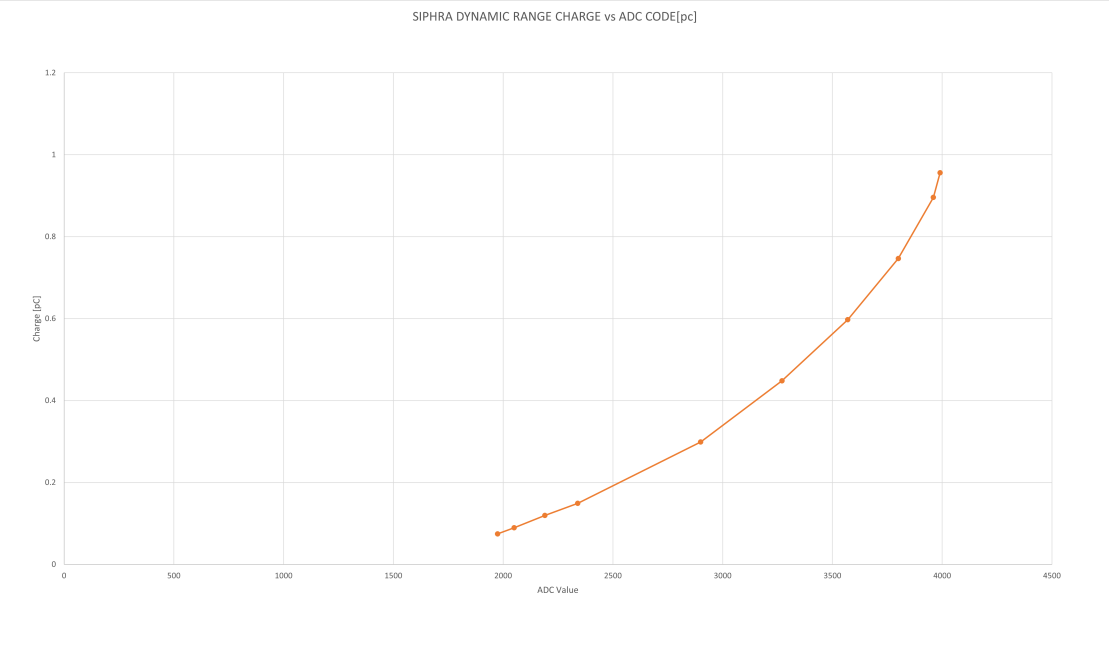

Figure 7.2: The dynamic Range for channel one shows a slight deviation towards linearity, indicating the system is not fully optimized.

The value of 7.9 dB represents the ratio of the maximum signal power to the noise power in the system.

$$DNR = 20 \cdot \log_{10} \frac{S_{max}}{S_{STD}}$$
$$DNR = 20 \cdot \log_{10} \frac{3990}{1608}$$
$$= 7.9\,\text{db}$$

The resolution represents the smallest detectable change in the input charge that produces a noticeable change in the output ADC value.

$$\text{Resolution} = \text{Input charge range} \;/\; (\text{ADC range})$$
$$\text{Resolution} \; = 0.8811pC/4096 = 0.000215128pC$$
$$= 0.215128fC$$

ROSSPAD Gain Calibration Curve

For the gain calibration curve for the ROSSPAD system, for simplicity, only three sources were used for calibration, including Am^{241}, Cs^{137}, and the first peak of Co^{60}.

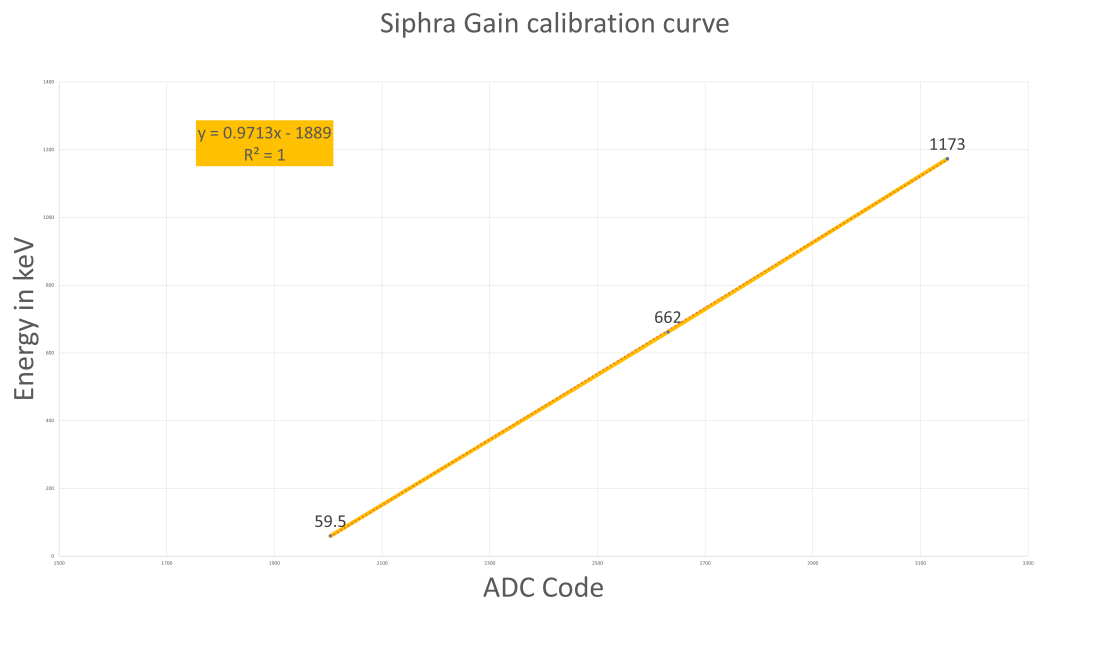

Figure 7.3: ROSSPAD gain calibration curve

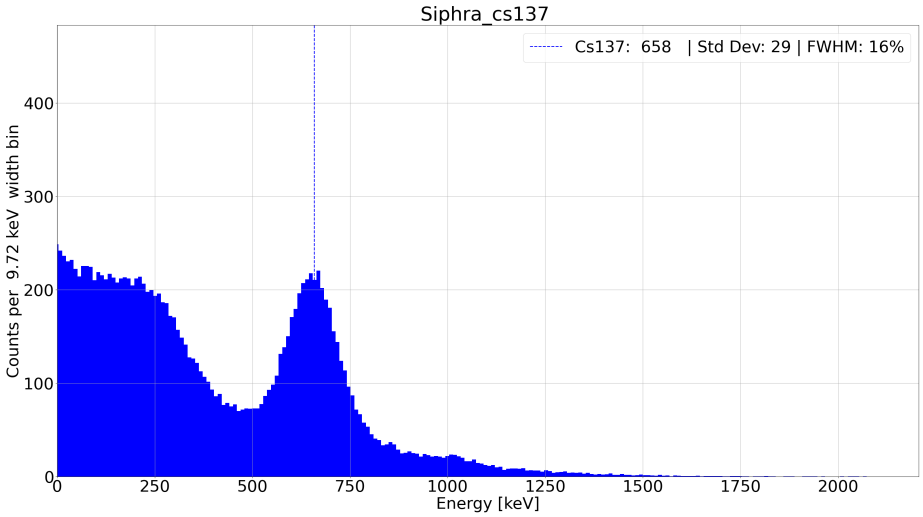

Figure 7.4: ROSSPAD system measuring the Cs^{137} source

Table 7.1: Comparison table for new ROSSHIP vs ROSSPAD for Channel 1

Parameters	ROSSHIP	ROSSPAD
Baseline [ADC value]	**665**	1608
Noise [ADC value]	21	2.28
Gain [LSB/pC]	90,4	72
ENC [pC]	7.3	22
FWHM at 662 keV	9%	16%
ENL	0,28 %	0,6
DNR [db]	17.3	7.9
Resolution [pc]	0,0079	0.000215

7.1 Comparing SIPHRA and APOCAT

Performance parameters: The results obtained from ROSSPAD were based on a default configuration optimised for a different scintillator. Although the same scintillators were used in the test, it is essential to consider that the settings may not have been fully optimised for their performance. Therefore, while the results provide an initial assessment, they may not accurately reflect the true potential of the scintillators in the ROSSPAD system. Optimising the settings specifically for the scintillators used in the test would be necessary to ensure a fair and accurate comparison. This would allow a more comprehensive evaluation of their performance and capabilities within the ROSSPAD system. Additionally, it is important to note that the results obtained from ROSSPAD and ROSSHIP are based on two different ROIC configurations. These configurations include variations in digital processing, shaping time, gain settings, and other parameters. Due to these differences, a direct comparison between the two systems may not fully reflect the true potential of each detector.

The dynamic Range for ROSSPAD shows a slight deviation towards linearity, indicating the system is not fully optimised. As a result, it may affect the system's accuracy, precision, or overall performance, such as the FWHM exceeding the desired limit of 10%. Despite the observed deviation in linearity for ROSSPAD, which indicates a need for further optimisation and may impact system performance, it is important to note that there is still a significant difference in the dynamic range between the two systems. They differ by about 9 dB, roughly three times the power ratio (3dB). This means that APOCATs can better distinguish the signal from noise, particularly towards the noise floor. This allows APOCAT to capture and process signals that are approximately three times weaker in relation to noise compared to the SIPHRA system. This would give an improvement in sensitivity and potentially more accurate measurements.

The ROSSHIP system has an ENC of 7 pC, which means it is expected to provide better signal detection and energy resolution for lower-energy gamma rays, such as the Am^{241}. The lower noise floor allows for more accurate measurement and detection of weaker signals. On the other hand, the ROSSPAD is expected to be more suitable for higher-energy gamma rays, like those emitted by Co-60.

With the given configurations ROSSHIP can handle a wider range of input charges. A larger input charge range allows ROSSHIP to accommodate higher-energy events. On the other hand, ROSSPAD's smaller input charge range indicates its suitability for lower-energy events or signals with smaller amplitudes. While it may have a narrower input charge range, it can still provide precise measurements and resolution within that range, thanks to its better resolution capability.

Choosing between ROSSHIP and ROSSPAD depends on the energy range, signal amplitudes, and level of optimisation needed for the detector. Both systems can be improved through the proper configuration. Adjusting parameters can enhance sensitivity and resolution. Consider inherent characteristics and potential for optimisation when selecting between the two for a specific application and detector.

8 Conclusion

The ROSSPAD system now features APOCAT, which is integrated into the newly developed front-end board known as ROSSHIP(Readout System Spectroscopic High-resolution Pulse-height.) The ROSSHIP systems demonstrate the ability to perform pulse shape spectroscopy using a line scanner configuration. In addition, the APOCAT offers the system great versatility with its peaking time possibility and the gain settings of the system. Although the system features a line-scanning CsI (tl) scintillator, others are possible due to the versatility offered by APOCAT.

The target specifications for this thesis have been achieved, where the line-scanning configuration provided an energy range from 50 keV to 1.5 MeV. Furthermore, the energy non-linearity was found to be 0.28%, where the target was below 2%. Finally, the energy resolution gave a 9% full-width half maximum at 662 keV. In addition, the system demonstrated reliable threshold functionality over the entire dynamic range allowing it to detect and register energy signals above the predetermined threshold.

Due to the limited time available for analysis, the focus has been on single-channel readouts. However, a full-channel readout has been confirmed as fully functional. To improve the accuracy of measurements of the all-channel readout, a more comprehensive analysis should be conducted by repeating the tests performed for single-channel analysis and aligning the gains of all channels.

The ROSSHIP system offers several options that can be used for feature work, including the counter configuration as the biggest contribution, where four counters for each channel, each with its configurable threshold setting. The counters in the system were successfully programmed and read out through the SPI interface. However, a new firmware implementation with a redesigned data frame is required to achieve a comprehensive solution.

Overall it can be concluded that the developed system is an excellent high-resolution spectroscopy measurement detector system for X-rays and gamma rays. The system demonstrated exemplary energy range, linearity, threshold, and resolution performance. The achieved results indicate its capability to detect and analyse radiation sources accurately. Additionally, the Energy Non-Linearity (ENL) is well below the specified threshold, and reliable threshold functionality further supports its suitability for precise measurement. These results validate the system's ability to

meet high-quality and accurate spectroscopy measurement requirements. Still, also its adaptability allows it to excel in various detector configurations, such as SiPM arrays with imaging capabilities.

The system is currently undergoing a process where it is being prepared for sale, but a complete system Datasheet and user manual on how to use the system with IDEAS-Testbench are needed. We believe this advanced spectroscopy system will significantly impact various fields, facilitating new discoveries and driving innovation. It will be a valuable asset for exceptional science and industrial applications.

References

[1] Lucio Cerrito, *Radiation and Detectors: Introduction to the Physics of Radiation and Detection Devices*. Springer International Publishing, 2017, ch. 1 , 4.

[2] R. S. Woolf, J. E. Grove, B. F. Phlips, and E. A. Wulf, "Development of a CsI:Tl calorimeter subsystem for the All-Sky Medium-Energy Gamma-Ray Observatory (AMEGO)," in *2018 IEEE Nuclear Science Symposium and Medical Imaging Conference Proceedings (NSS/MIC)*, 2018, pp. 1–6.

[3] Nicholas Tsoulfanidis, *MEASUREMENT AND DETECTION OF RADIATION*, 2nd ed. Taylor & Francis LTD, 1995, ch. 10, 4.

[4] Glenn F Knoll, *Radiation Detection and Measurement*, 4th ed. Wiley India Pvt. Ltd., 2009, ch. 9 , 16 ,17.

[5] Mouser. SiPM. [Online]. Available: https://no.mouser.com/ProductDetail/onsemi/MICROFJ-60035-TSV-TR1?qs=byeeYqUIh0NZJG9dg5%252B6Ug%3D%3D

[6] M. Renschler, "Characterisation of 64 channel SiPMs arrays for the silicon elementary cell add-on," Master's thesis, KIT - Department of Physics at Karlsruhe Institute of Technology, 2016, collected 25.1.2023

.

[7] Broadcom. (2019) Technology of broadcom-sipm. Collected 25.3.2023

. [Online]. Available: https://docs.broadcom.com/doc/Introduction-to-Silicon-Photomultipliers

[8] I. Dirk Meier. (2016) Siphra 16-channel silicon photomultiplier readout asic. Collected 25.3.2023

. [Online]. Available: http://doi.org/10.13140/RG.2.1.1460.8882

[9] J. Mangan, D. Murphy, R. Dunwoody, A. Ulyanov, J. Thompson, U. Javaid, C. O'Toole, M. Doyle, M. Emam, J. Erkal, G. Fontanesi, J. Kyle, F. Marshall, R. R. Nail, F. Okosun, J. Reilly, S. Walsh, D. de Faoite, L. Salmon, L. Hanlon, D. McKeown, W. O'Connor, K. Stanton, R. Wall, B. Shortt, J. Vanreusel, D. Palma, L. Ha, and S. McBreen, "The environmental test campaign of GMOD: a novel gamma-ray detector," in *International Conference on Space Optics — ICSO 2020*, B. Cugny, Z. Sodnik, and N. Karafolas, Eds.,

vol. 11852, International Society for Optics and Photonics. SPIE, 2021, p. 1185214. [Online]. Available: https://doi.org/10.1117/12.2599225

[10] IDEAS. (2019) Roic for high-rate, high-resolution x-ray and gamma-ray spectroscopy with scintillators. Collected 25.3.2023
. [Online]. Available: https://ideas.no/products/ide3381/

[11] W. Gan, Y. Deng, H. Li, J. Wu, H. Zhang, J. Chang, C. Chen, Z. Zhang, B. Chen, L. Feng, J. Guo, Y. Hu, Y. Huang, Z. Li, Y. Peng, D. Wang, H. Wang, J. Wang, D. Wen, Z. Wu, Z. Zhang, and E. Zhao, "ASO-S: Advanced Space-based Solar Observatory," in *Solar Physics and Space Weather Instrumentation VI*, S. Fineschi and J. Fennelly, Eds., vol. 9604, International Society for Optics and Photonics. SPIE, 2015, p. 96040T. [Online]. Available: https://doi.org/10.1117/12.2189062

[12] Trenz Electronic. TE0720 TRM. [Online]. Available: https://pdf1.alldatasheet.com/datasheet-pdf/view/1244272/TRENZ/TE0720.html

[13] Analog Devices. LTC2325-12 ADC. [Online]. Available: https://www.analog.com/en/products/ltc2325-12.html

[14] Marcel J.M. Pelgrom, *Analog-to-Digital Conversion*. Springer International Publishing, 2010, ch. 3 , 5.

9 APPENDIX

9.1 Schematic and Layout

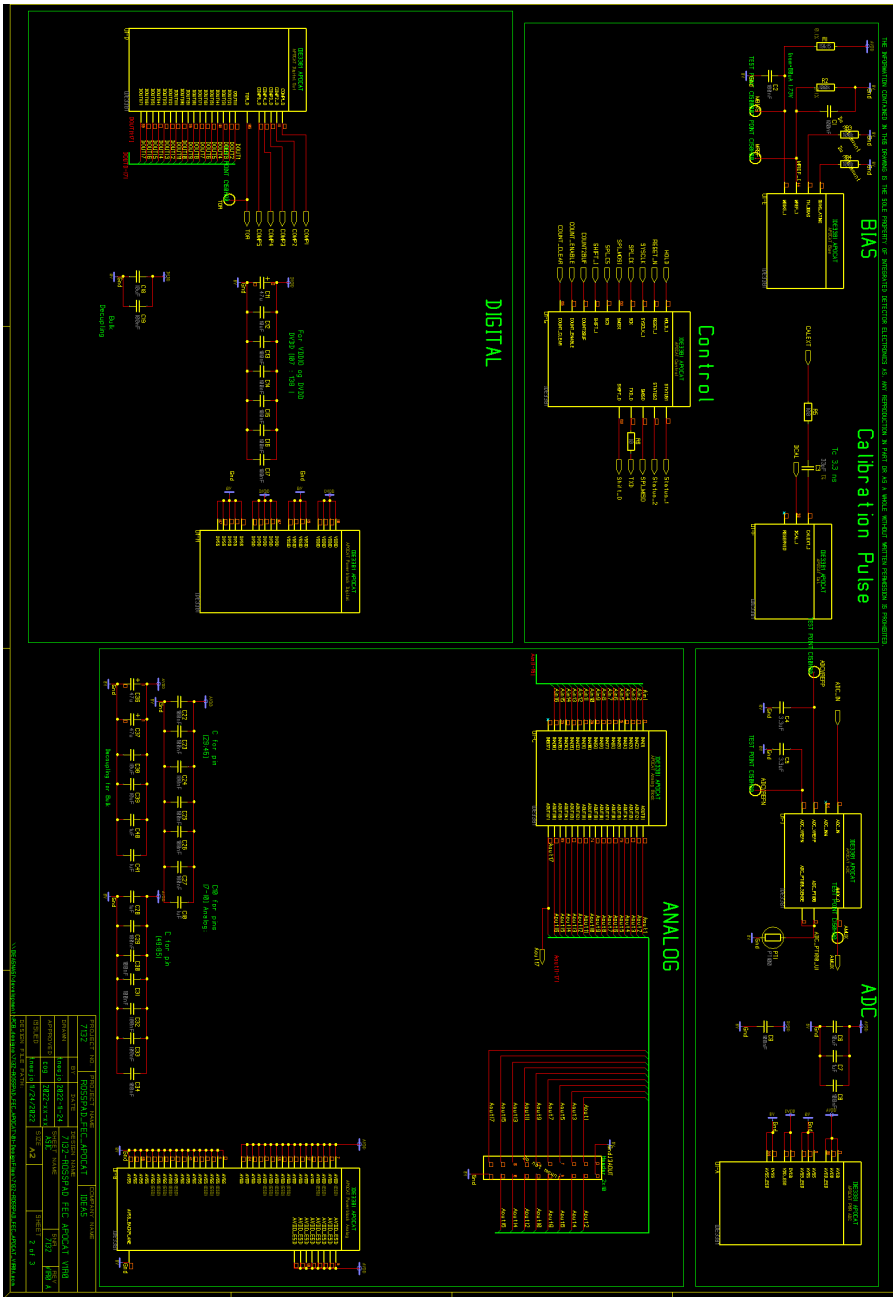

Figure 9.1: Blokkskjema for ASIC schm

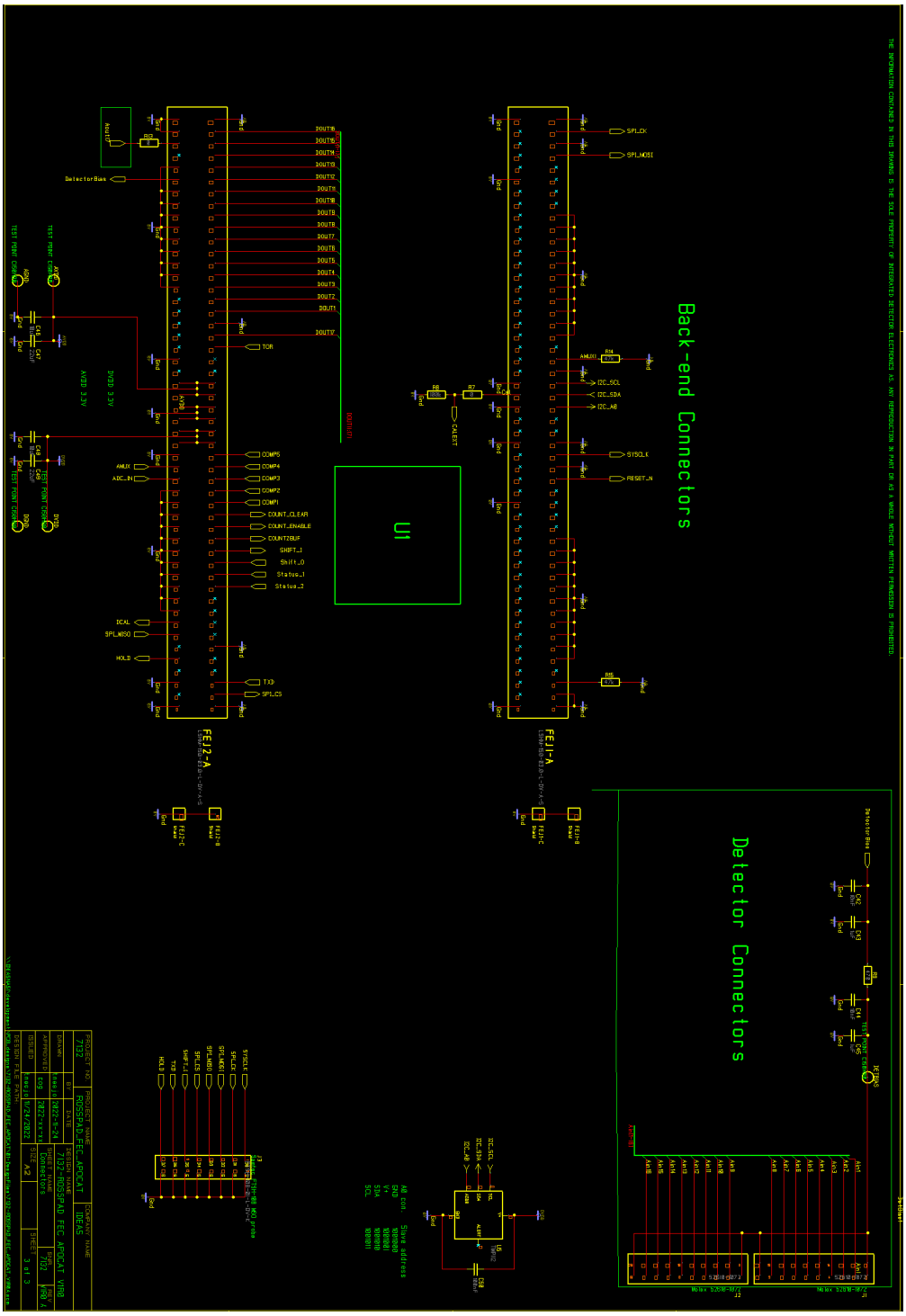

Figure 9.2: Blokkskjema for Connectors

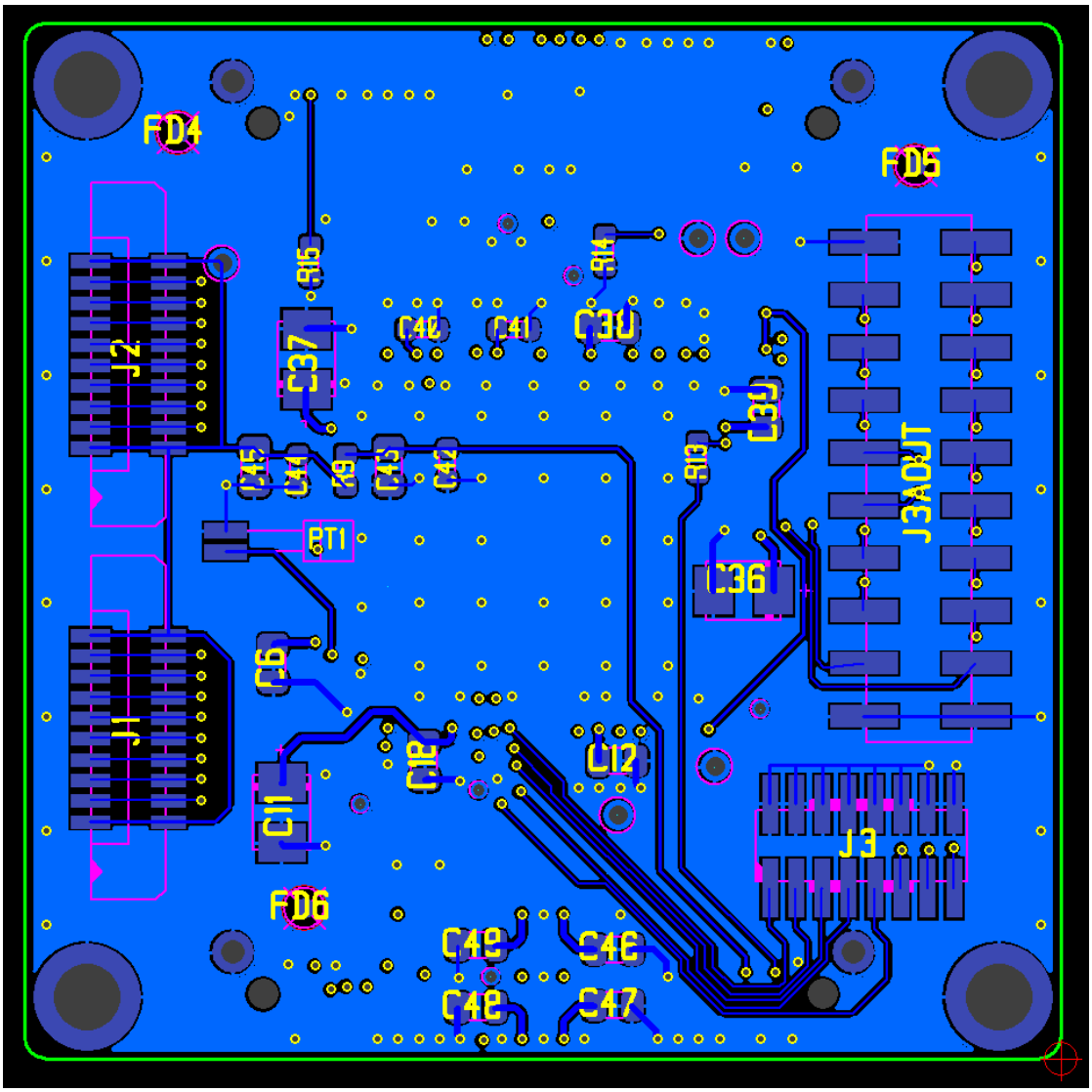

Figure 9.3: Layout bottom side

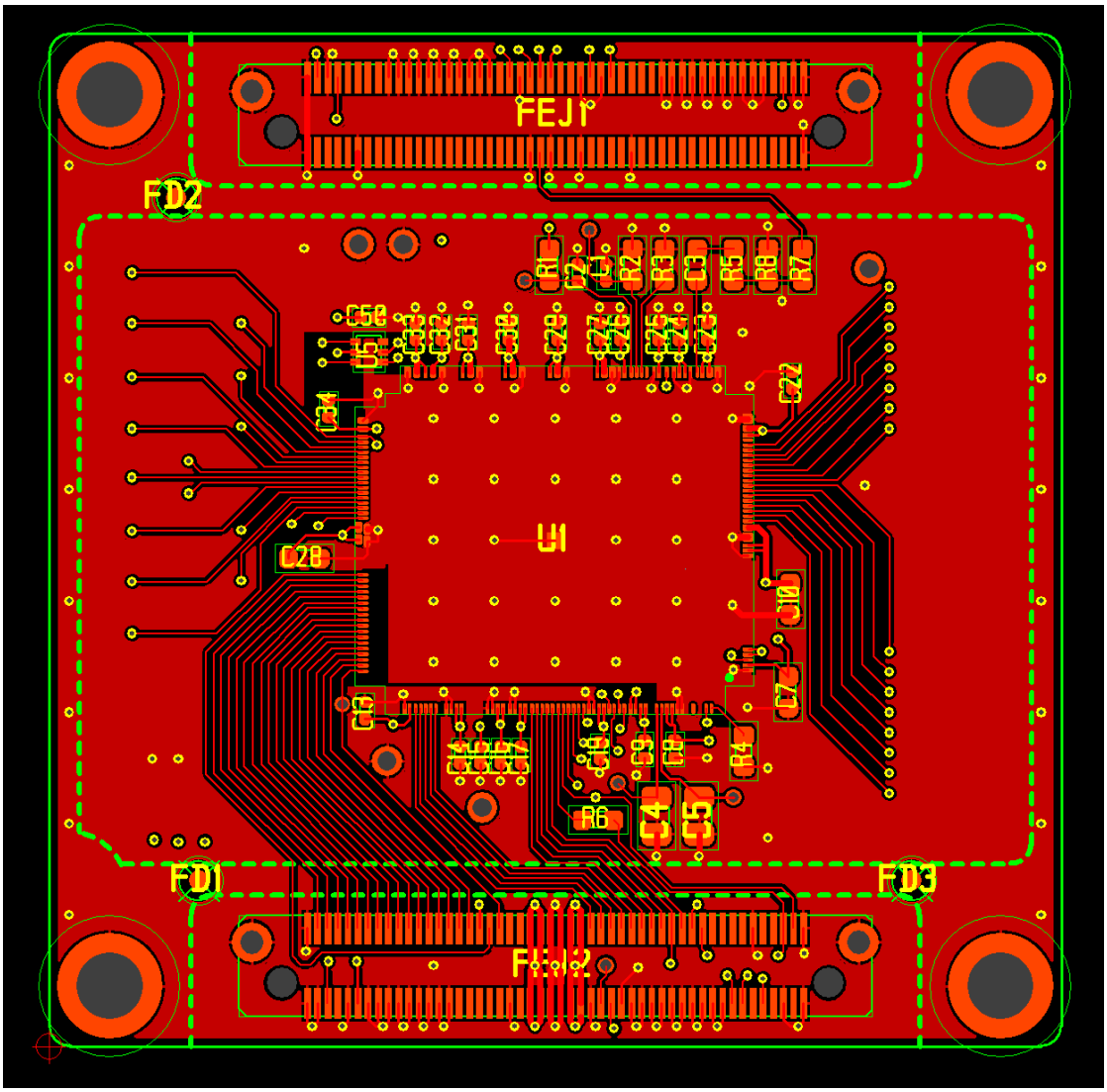

Figure 9.4: Layout Top side

9.2 VHDL Modules

Figure 9.5: System Top module shown with all signal
Asic signal connects to the processing systems

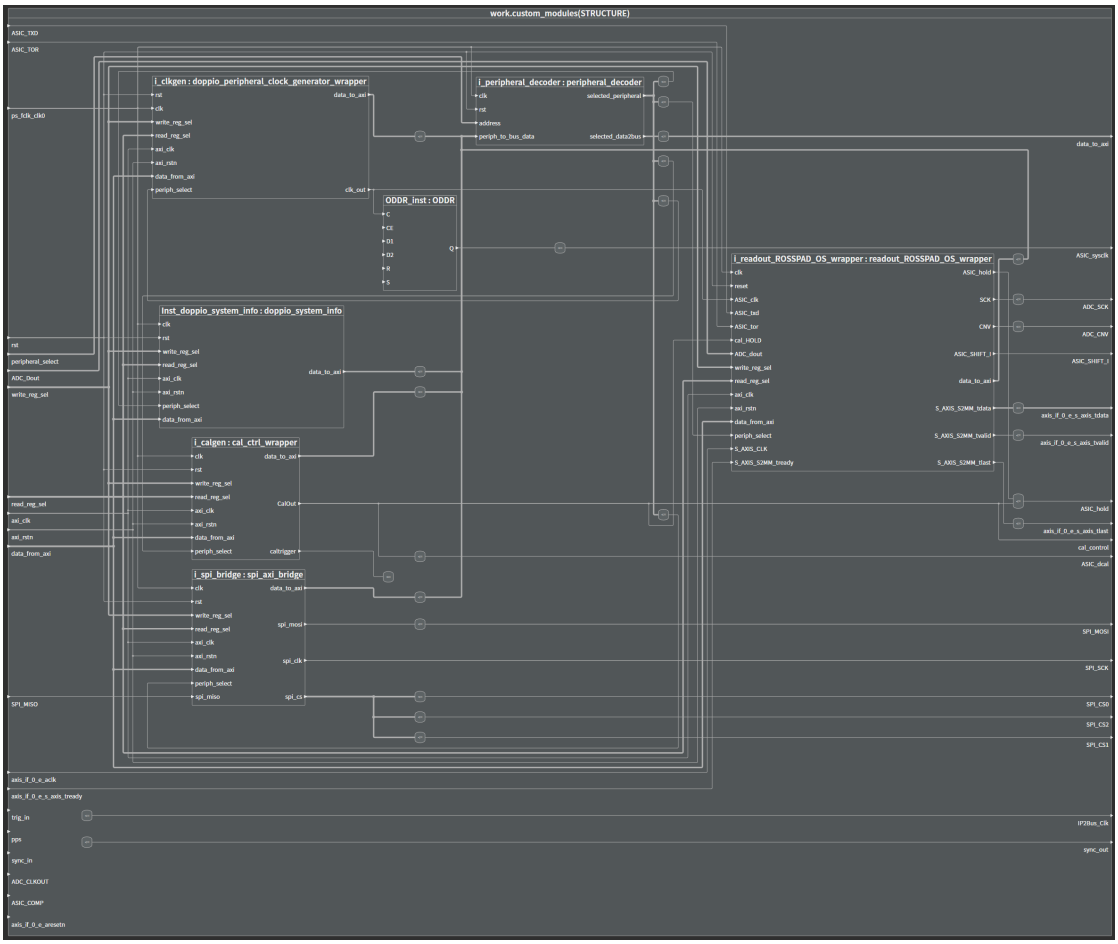

Figure 9.6: Custom module connects the Spi, cal control,clk and periphial modules with the Rosspad wrapper module

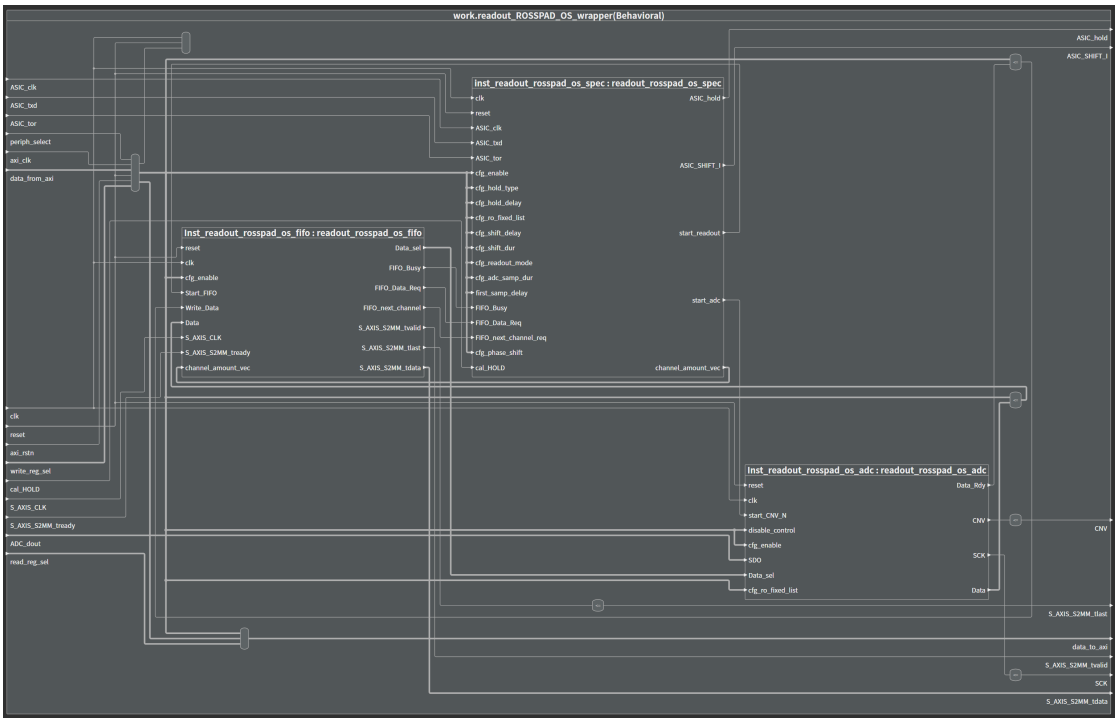

Figure 9.7: The Wrapper module connects the Fifo, ADC and Spectroscopy module

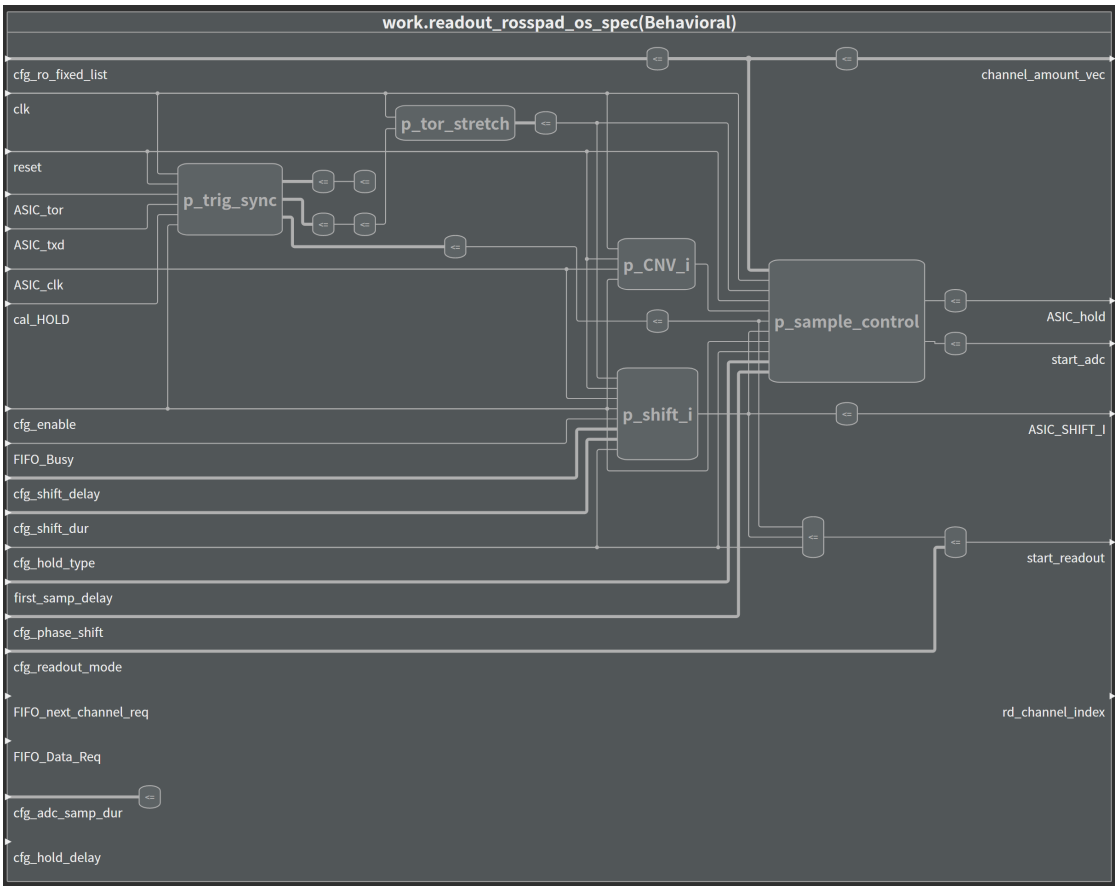

Figure 9.8: Spectroscopy readout module shows the state machine for activating the ADC module

9.3 APOCAT FEB

The front end board design where the top and bottom side are shown in figure, 9.9 shows the Front side with connectors to the SIPMs, test points, etc. While on the Bottom side shows connectors to the Controller board as well as the APOCAT.

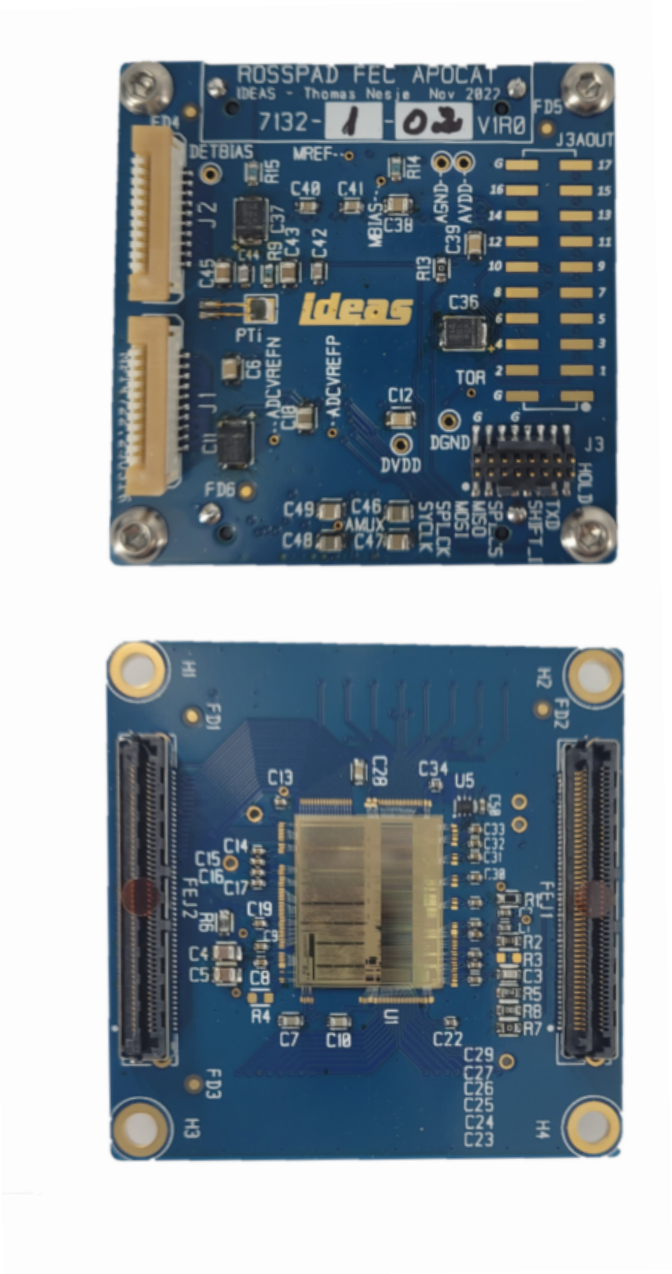

Figure 9.9: The Front end BOARD top and bottoms side, with the implemented APOCAT

				Project name:	7132-ROSSPAD_FEC_APOCAT_V1R0	REV A			
				Last edit date:	2022-12-07				
#	Qty	Kitted	Reference	Description	Value	Specifications	Mounting	Manufacturer	Mfg's Part Number
1	23	Labkit	C1 C13 C14 C15 C16 C17 C19 C2 C22 C23 C24 C25 C26 C27 C29 C30 C31 C32 C33 C34 C50 C8 C9	Capacitor ceramic SMD 0402	100nF	16V X7R			
2	5	Labkit	C10 C28 C40 C41 C7	Capacitor ceramic SMD 0603	1uF	16V X7R			
3	3	20	C11 C36 C37	Capacitor tantalum B-case EIA3528-21	47u	6.3V 20% ESR=70m		AVX	TCJB476M006R0070
4	7	Labkit	C12 C18 C38 C39 C46 C48 C6	Capacitor ceramic SMD 0805	10uF	6.3V X5R			
5	1	10	C3	Capacitor ceramic SMD 0603	33pF	16V NP0 **1%**			
6	2	40	C4 C5	Capacitor ceramic SMD 0805	3.3uF	6.3V X5R			
7	2	10	C42 C44	Capacitor ceramic SMD 0603	10nF	100V NP0			
8	2	10	C43 C45	Capacitor ceramic SMD 0805	1uF	100V X7S 10%		Murata	GRM21BC72A105KE01
9	2	Labkit	C47 C49	Capacitor ceramic SMD 0805	22uF	6.3V X5R			
10	2	6	FEJ1 FEJ2	Dual row 100 pole hermaphroditic 0.5mm pitch	LSHM-150-03.0-L-DV-A-S			Samtec	LSHM-150-03.0-L-DV-A-S-K-TR
11	2	10	J1 J2	FFC connector 10p 1mm pitch, vertical	52610-1072			Molex	52610-1072
12	1	4	J3	For MSO logic probe adapter	FTSH-108-01-L-DV-K			Samtec	FTSH-108-01-L-DV-K
13	1	5	PT1	Platinum RTD Temperature Sensor -200'C to +600'C	PT100			Innovative Sensor Technology	P0K1.202.3K.A.010
14	1	10	R1	Resistor SMD 0603	19k6	0.1% 25ppm 1/10W Thick film			
15	2	Labkit	R13 R7	Resistor SMD 0603	0	1% 1/10W Thick film			
16	2	Labkit	R14 R15	Resistor SMD 0603	47k	1% 1/10W Thick film			
17	1	10	R2	Resistor SMD 0603	100k	0.1% 25ppm 1/10W Thick film			
18	1	Labkit	R5	Resistor SMD 0603	100	1% 1/10W Thick film			
19	1	Labkit	R6	Resistor SMD 0603	10	1% 1/10W Thick film			
20	1	Labkit	R8	Resistor SMD 0603	100k	1% 1/10W Thick film			
21	1	Labkit	R9	Resistor SMD 0603	470	1% 1/10W Thick film			
22	1	Stock	U1	ASIC, 16 channels for PMT/SiPM	IDE3381			Ideas	IDE3381
23	1	5	U5	Temperature Sensor I2C / 2-wire	TMP112			TI	TMP112AIDRL
24	1		~~J3AOUT~~	~~Header 2x10, 2.54mm pitch~~			**Do not mount**		
25	2		~~R3 R4~~	~~Resistor SMD 0603~~	~~100k~~	~~1% 1/10W Thick film~~	**Do not mount**		

Figure 9.10: The Bill of Material for the FEB

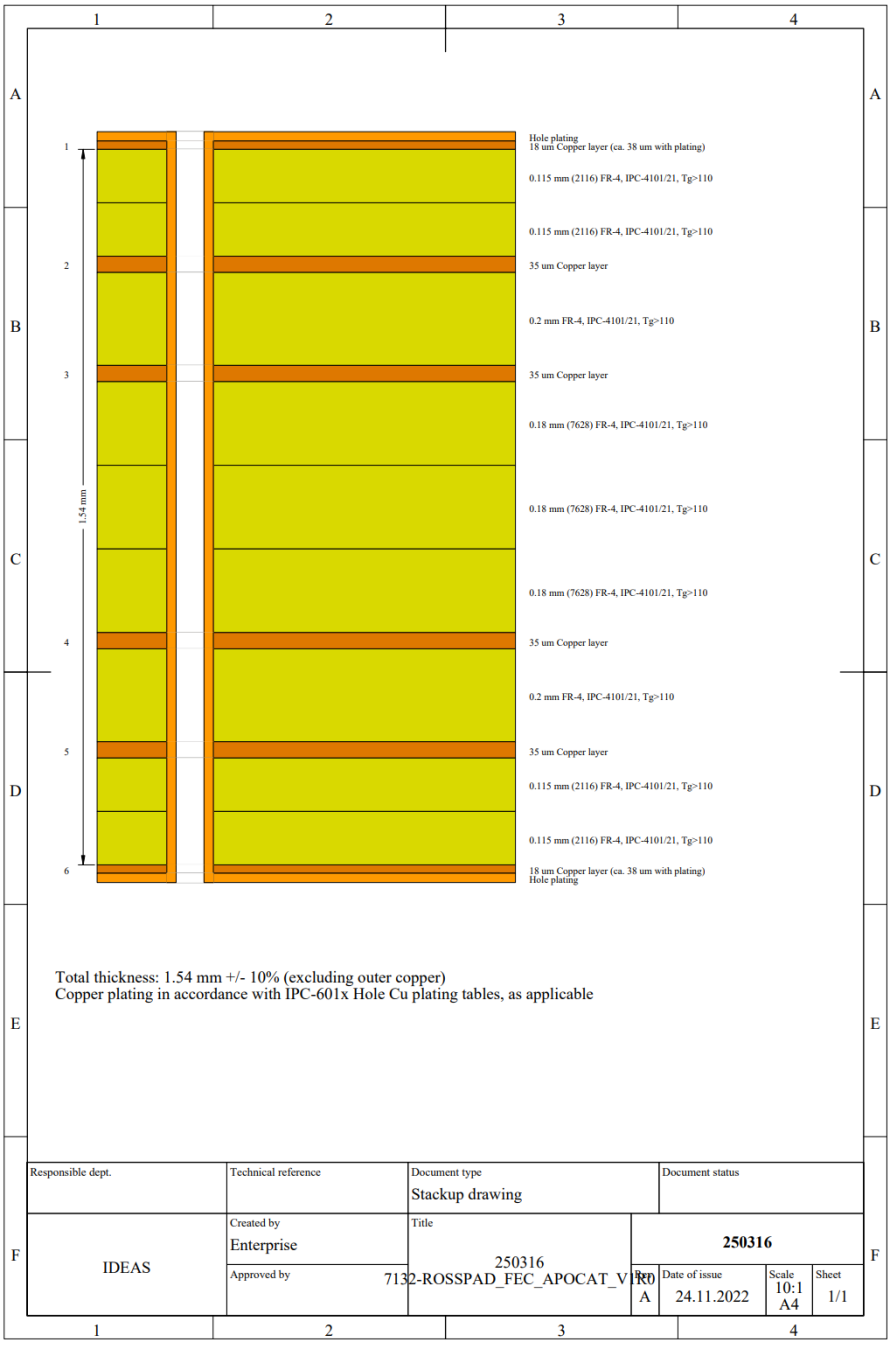

Figure 9.11: Stackup for the FEB

9.4 VHDL kode

9.5 ROSSPAD_SPECTROSCOPY module

```
entity readout_rosspad_os_spec is
    port(
        clk                  : in  std_logic;  -- System clock
        reset                : in  std_logic;  -- Synchronous active high reset
        ASIC_clk             : in  std_logic;  -- Must be the same as the ASIC sys_clk

        ASIC_txd             : in  std_logic;  -- ASIC txd signal
        ASIC_tor             : in  std_logic;  -- ASIC trigger OR signal
        ASIC_hold            : out std_logic;  -- ASIC hold signal

        ASIC_SHIFT_I         : out std_logic;  -- Token-bit for analog multiplexer
        cfg_enable           : in  std_logic;  -- Enable the module
        cfg_hold_type        : in  std_logic;
        -- 0 = internal hold EXT ADC (SHIFT IN) , 1 = external hold INT ADC

        cfg_hold_delay       : in  std_logic_vector(15 downto 0);
        -- Amount of clock cycles until external hold signal is set,
        cfg_ro_fixed_list    : in  std_logic_vector(19 downto 0);
        cfg_shift_delay      : in  std_logic_vector(31 downto 0);
        -- Delay of SHIFT_I in clock cycles

        cfg_shift_dur        : in  std_logic_vector(31 downto 0);
        -- Duration of SHIFT_I in clock cycles

               cfg_readout_mode      : in  std_logic_vector(1 downto 0);
         -- Readout Mode, 00 -> All Channel Spectroscopic,
               cfg_adc_samp_dur      : in  std_logic_vector(7 downto 0);
               first_samp_delay      : in  std_logic_vector(7 downto 0);

        -- Delay of the first sample
               cfg_phase_shift       : in  std_logic_vector(15 downto 0);
        -- Phase shift in number of clk cycles
               FIFO_Busy                   : in  std_logic;
        FIFO_Data_Req                : in  std_logic;
        FIFO_next_channel_req          : in std_logic;
               start_readout               : out std_logic;
        start_adc                   : out std_logic;
               rd_channel_index         : out std_logic_vector(3 downto 0);
        channel_amount_vec       : out std_logic_vector(31 downto 0);
               cal_HOLD                : in  std_logic
    );
end readout_rosspad_os_spec;
```

Listing 1: Entity for the Spectroscopy module

```
architecture Behavioral of readout_rosspad_os_spec is
type SHIFT_I_state_type is
    (
        IDLE,
        Shift_I_DELAY,
        SET_SHIFT_I,
        RESET_SHIFT
    );
type SAMPLE_CONTROL_STATE_TYPE is
    (
        IDLE,
        WAIT_SHIFT_I,
        SAMPLE,
                waiting_for_asic_clk,
                counting_clk
    );
type CNV_state_type is
    (
        SET_LEVEL,
        WAIT_HIGH_LOW,
        WAIT_LOW_HIGH
    );

type data_array_type is array (19 downto 0) of std_logic_vector(13 downto 0);
signal SAMPLE_CONTROL_STATE : SAMPLE_CONTROL_STATE_TYPE;
signal data_format          : std_logic_vector(7 downto 0)  := x"CE";
signal field_len            : integer range 0 to 65535      := 0;
signal timestamp_count      : std_logic_vector(31 downto 0) := (others => '0');
signal samp_num             : std_logic_vector(15 downto 0) := (others => '0');
signal source_ID            : std_logic_vector(7 downto 0)  := x"00";
signal trigger_type         : std_logic_vector(7 downto 0)  := x"02";
signal channel_ID           : std_logic_vector(7 downto 0)  := x"00";
signal rising_clock_state           : CNV_state_type                := SET_LEVEL;
signal SHIFT_I_state        : SHIFT_I_state_type            := IDLE;
signal datasent_count       : integer range 0 to 65535      := 0;
signal DMA_data_block_size  : integer range 0 to 4095       := 0;
signal timestamp            : std_logic_vector(31 downto 0) := (others => '0');
signal channel_index        : integer range 0 to 31         := 0;
signal channel_amount       : integer range 0 to 31         := 0;
signal data_write_counter   : integer range 0 to 31         := 0;
signal discard_sample       : std_logic                     := '1';
signal adc_sample_delay     : std_logic_vector(15 downto 0) := x"0000"; --:= x"0004";
signal ASIC_hold_i          : std_logic                     := '0';
signal asic_shift_ii        : std_logic                     := '0';
signal shift_wait_count     : std_logic_vector(31 downto 0) := (others => '0');
signal shift_dur_count      : std_logic_vector(31 downto 0) := (others => '0');
signal start_adc_i    : std_logic := '0';
signal start_adc_ii    : std_logic := '0';
signal hold_start_adc        : std_logic                     := '0';
signal cnt_shift            : std_logic_vector(15 downto 0) := (others => '0');
signal start_readout_spect_i : std_logic;
signal start_readout_count_i : std_logic;
signal sample_count       : std_logic_vector(7 downto 0) := (others => '0');
signal channel_index_count : std_logic_vector(7 downto 0) := (others => '0');
signal adc_samp_dur       : std_logic_vector(7 downto 0) := (others => '0');
signal first_sample       : std_logic := '1';
signal ADC_CNV_i           : std_logic                    := '0';
signal ASIC_CLK_RISING     : std_logic                    := '0';
signal ASIC_CLK_Faling     : std_logic                    := '1';
signal start_adc_i_sync : std_logic := '0'; -- synchronized version of start_adc_i

ASIC_SHIFT_I <= asic_shift_ii ;
start_readout_spect_i  <= asic_shift_ii when cfg_hold_type = '0' else HOLD_rise_o ;
EXT_ADC_internal hold(shift_i), 1 = external hold med INT_ADC
start_readout     <= start_readout_spect_i when cfg_readout_mode = "00"  else start_readout_count_i;
ASIC_hold           <= ASIC_hold_i;
adc_samp_dur    <= cfg_adc_samp_dur;
channel_amount  <= channel_counter(cfg_ro_fixed_list);   ---- -1
channel_amount_vec <= std_logic_vector(to_unsigned(channel_amount, channel_amount_vec'length));
start_adc <= start_adc_i;
```

Listing 2: Start of Behavioural for the Spectroscopy module

9.6 Shift_in FSM

```
--============== PROCESS: SHIFT IN FSM ================--
 p_shift_i : process(ASIC_clk)
begin
    if falling_edge(ASIC_clk) then
        if reset = '1' or cfg_enable = '0' or cfg_hold_type = '1' then
            SHIFT_I_STATE <= IDLE;
            asic_shift_ii <= '0';
            shift_wait_count <= (others => '0');
            shift_dur_count <= (others => '0');
        elsif cfg_enable = '1' then
            case SHIFT_I_state is
                when IDLE =>
                    asic_shift_ii <= '0';
                    shift_wait_count <= (others => '0');
                    shift_dur_count <= (others => '0');
                    if tor_stretched = '1' and FIFO_Busy = '0' then
                        SHIFT_I_STATE <= Shift_I_DELAY;
                    end if;
                when Shift_I_DELAY =>
                    shift_wait_count <= shift_wait_count + "01";
                    if shift_wait_count = cfg_shift_delay then
                        asic_shift_ii <= '1';
                        SHIFT_I_STATE <= SET_SHIFT_I;
                    end if;
                when SET_SHIFT_I =>
                    shift_dur_count <= shift_dur_count + "01";
                    if shift_dur_count = cfg_shift_dur then
                        asic_shift_ii <= '0';
                        SHIFT_I_STATE <= RESET_SHIFT;
                    end if;
                when RESET_SHIFT =>
                    asic_shift_ii <= '0';
                    shift_wait_count <= (others => '0');
                    shift_dur_count <= (others => '0');
                    SHIFT_I_STATE <= IDLE;
            end case;
        end if;
    end if;
end process;
```

Listing 3: Shift in FSM

9.7 Sample Control state FSM

```
--===== PROCESS: Sample Control FSM ROSSPAD_OS =======--
p_sample_control : process(clk)
begin
    if rising_edge(clk) then
        if reset = '1' or cfg_enable = '0' then
            SAMPLE_CONTROL_STATE          <= IDLE;
            sample_count     <= (others => '0');
        elsif cfg_enable = '1' then
            case SAMPLE_CONTROL_STATE is
            when IDLE =>
                                ASIC_hold_i <= '0';
                                first_sample <= '1';
                start_adc_i      <= '0';
                sample_count     <= (others => '0');
                                cnt_shift <= (others => '0');
                channel_index    <= 0;
                    if tor_stretched = '1' and cfg_hold_type = '0' then
                    SAMPLE_CONTROL_STATE <= WAIT_SHIFT_I;
                end if;
                        when WAIT_SHIFT_I =>
                                sample_count  <= (others => '0');
                                cnt_shift <= (others => '0');
                                if asic_shift_ii = '1' then
                                  SAMPLE_CONTROL_STATE <= Sample;
                                 end if;
                        when SAMPLE =>
                                ASIC_hold_i <= '0';
                                start_adc_i <= '0';
                                cnt_shift <= (others => '0');
                if first_sample = '1' and sample_count = first_samp_delay then
                                  SAMPLE_CONTROL_STATE <= waiting_for_asic_clk;
                    sample_count  <= (others => '0');
                elsif first_sample = '0' and channel_index <= channel_amount  then
                                     SAMPLE_CONTROL_STATE <= waiting_for_asic_clk;
                elsif channel_index = channel_amount + 1 then
                -- required to sample one extra, see LTC2325-12 datasheet
                    SAMPLE_CONTROL_STATE <= IDLE;
                    start_adc_i   <= '0';
                else
                    start_adc_i   <= '0';
                    sample_count  <= sample_count + "01";
                end if;
            when waiting_for_asic_clk =>
                                cnt_shift <= (others => '0');
                if ASIC_CLK_RISING = '1' then
                    SAMPLE_CONTROL_STATE <= counting_clk;
                end if;
            when counting_clk =>
                                sample_count  <= (others => '0');
                cnt_shift <= cnt_shift + 1;
                if cnt_shift = cfg_phase_shift then
                                        ASIC_hold_i <= '1';
                                        first_sample  <= '0';
                                        channel_index <= channel_index + 1;
                    start_adc_i <= '1';
                    SAMPLE_CONTROL_STATE <= SAMPLE;
                end if;
            when others =>
                                sample_count  <= (others => '0');
                                cnt_shift <= (others => '0');
                SAMPLE_CONTROL_STATE <= IDLE;
            end case;
        end if;
    end if;
end process;
```

Listing 4: Sample controll state FSM

9.8 VHDL Testbench

```
    clk_process: process
    begin
                clk <= '0';
                wait for clk_period/2;
                clk <= '1';
                wait for clk_period/2;
    end process;
    ASIC_clk_process: process
    begin
                ASIC_clk <= '0';
                wait for ASIC_clk_period/2;
                ASIC_clk <= '1';
                wait for ASIC_clk_period/2;
    end process;
    procedure set_reg_0(data_in : in std_logic_vector(31 downto 0) ) is
       begin
          periph_select <= '1';
          write_reg_sel <= x"2000_0000";
          data_from_axi <= data_in;
          periph_select <= '0';
          write_reg_sel <= (others =>'0');
          data_from_axi <= (others =>'0');
    end procedure;
       set_reg_1(x"00000000");        -- cfg_hold_type 0 = internal hold, 1 = external hold
           wait for clk_period;
       set_reg_2(x"00000000");        -- cfg_hold_delay
           set_reg_3 (x"000FFFFF");
       set_reg_4(x"00000000");        -- cfg_shift_delay
           set_reg_5 (x"00000009");       -- ( cfg_shift_dur)
       set_reg_6(x"00000019");        -- cfg_phase_shift
       set_reg_7(x"00000000");        --  cfg_readout_mode ,Spectroscopic,
       set_reg_8(x"00000000");        --  cfg_adc_samp_dur
       set_reg_9(x"00000000");        -- disable_control
           set_reg_10(x"00000019");         --- FIRST  SAMPLE deLAY
       set_reg_0(x"00000000");        -- cfg_enable
       wait for clk_period*10;
       set_reg_0(x"00000001");        -- cfg_enable
       wait for clk_period*10;
                ASIC_TOR <= '1';
         wait for ASIC_clk_period;
         ASIC_TOR <= '0';
          wait for 435 ns;
             SDO <= "1111";              -- MSB
             wait for ASIC_clk_period;
             SDO <= "1100";           -- bit 11
             wait for ASIC_clk_period;
             SDO <= "0010";           -- bit 10
             wait for ASIC_clk_period;
             SDO <= "1101";           -- bit 9
             wait for ASIC_clk_period;
             SDO <= "0010";           -- bit 8
             wait for ASIC_clk_period;
             SDO <= "1101";           -- bit 7
             wait for ASIC_clk_period;
             SDO <= "0010";           -- bit 6
             wait for ASIC_clk_period;
             SDO <= "0100";           -- bit 5
             wait for ASIC_clk_period;
             SDO <= "1011";           -- bit 4
             wait for ASIC_clk_period;
             SDO <= "0101";           -- bit 3
             wait for ASIC_clk_period;
             SDO <= "1011";           -- bit 2
             wait for ASIC_clk_period;
             SDO <= "0100";           -- bit 1
    wait;
    END PROCESS;
END;
```

Listing 5: Most essential part of the Testbench code for the ROSSPAD_OS_Wrapper Module

9.9 Python Code

```
class Hist:
    def __init__(self, file_name, chosen_data_from=2,chosen_data_to=None,
    min_pixel=0, max_pixel=5500, direct=1, doPrint=False, end_row = 2000000, delimiter=';' ):
        self.delimiter = delimiter
        csv.register_dialect('custom', delimiter=self.delimiter)
        with open(file_name, 'r') as f:
            reader = csv.reader(f, dialect='custom') #  -
            header = next(reader)  # skip the header
            step_size = 1  # select every data point
            self.data = np.array([row for row in reader][:end_row])
            if chosen_data_to is None:
                self.pix_data = self.data[1:, chosen_data_from:chosen_data_from+1:step_size].astype(float)
            else:
                self.pix_data = self.data[1:,chosen_data_from:chosen_data_to:step_size].astype(float)
                self.pix_data = self.pix_data.flatten()

     def apply_gain(self, x):
        return -3E-06*x**2 + 0.3731*x - 217.28  # Calc gain function ROSSHIP

    def analyze(self, min_width=0.5, distance=10, height=0.5, min_fwhm=1, max_fwhm=800,
            plottitle=None, plot=True, add_noise=True, add_gaussian=True, gain=False, scale_data=False, color='b'):
        if gain:              # Calc bin width in keV and gain data
            gain_data = self.apply_gain(self.pix_data)
            w = (3 * np.std(gain_data) / (len(gain_data) ** (1/3)))                 #GAIN
            bin_edges = np.arange(min(self.pix_data), max(self.pix_data) + w, w)
            bin_edges_gain = self.apply_gain(bin_edges)
            bin_widths_keV = np.diff(bin_edges_gain)
            counts, edges = np.histogram( gain_data, bins=bin_edges_gain, density=False)  # GAIN DATA
            counts_per_w = counts / bin_widths_keV  # Counter per bbin in kev
        else:  # Calc raw data with counts per width bin
            w = int(3 * np.std(self.pix_data) / (len(self.pix_data) ** (1/3)))  # UTEN
            bin_edges = np.arange(min(self.pix_data), max(self.pix_data) + w, w)
            counts, edges = np.histogram( self.pix_data, bins=bin_edges, density=False)  # uten gain
            counts_per_w = counts / w

        ## FIND THE PEAKS
        peaks, _ = find_peaks(counts_per_w, distance=distance, height=height*max(counts_per_w), width=min_width)
        max_peak = np.max(counts_per_w[peaks])
        for peak_bin in peaks:
            # #calculate FWHM
            half_max = counts_per_w[peak_bin] / 2
            left_bins = np.where(counts_per_w[:peak_bin] < half_max)[0]
            right_bins = np.where(counts_per_w[peak_bin:] < half_max)[0]
            if right_bins.size:
                right_bin = right_bins[0] + peak_bin
                distances = right_bin - peak_bin
```

```
47                  if left_bins.size:
48                      left_bin = left_bins[-1]
49                  self.fwhm = int(edges[right_bin] - edges[left_bin])
50              else:
51                  self.fwhm = np.nan
52              if not np.isnan(self.fwhm) and self.fwhm >= min_fwhm and self.fwhm <= max_fwhm:
53              if gain:
54                  self.peaks = gain_data[(gain_data > edges[left_bin]) & ( gain_data < edges[right_bin])]
55                  self.mean = np.mean(self.peaks)
56                  self.std_dev = np.std(self.peaks)
57              elif not gain:
58                  self.peaks = self.pix_data[(self.pix_data > edges[left_bin])
59                              & (self.pix_data < edges[right_bin])]
60                  self.std_dev = np.std(self.peaks)
61              fwhm_percent = int((self.fwhm / self.mean) * 100)
62              peak_label = f'{plottitle:<10}: {self.mean:4.0f}  | Std Dev: {self.std_dev:2.0f}'
63              fwhm_label = f"Peak {plottitle} FWHM: {self.fwhm:.0f} => {fwhm_percent:.0f}%"
64              plt.axvline(self.mean, color=color,  linestyle='dashed', linewidth=2, label=peak_label)
65              plt.vlines([edges[left_bin], edges[right_bin]], 0, max( counts_per_w), colors='k',
66                      linestyles='dashed', linewidths=2 , label=fwhm_label)
67          if plot:
68              if scale_data:
69                  print(f"SCALING DATA from the max peak at {max_peak}")
70                  self.pix_data = self.pix_data / max_peak   # rescale the data between 0 and 1
71                  counts_per_w = counts_per_w / max_peak
72              if plottitle:
73                  if gain:
74                      plt.title( f'{plottitle} with {len(self.pix_data)} pixels,
75                                 bin width: {np.mean(bin_widths_keV):.2f} keV')
76                      plt.ylabel(' Normalized Counts ')
77                      plt.xlabel('Energy [keV]')
78                  else:
79                      plt.title(  f'{plottitle} with {len(self.pix_data)} pixels,
80                                  bin width: {np.mean(w):.2f} ')
81                      plt.ylabel(f'Counts per {np.mean(w):.2f} width bin  ')
82                      plt.xlabel('Energy [ADC Code]')
83              else:
84                  plt.title('Spectrum')
85                  plt.xlabel('Energy')
86              plt.bar(edges[:-1], counts_per_w, width=w,
87                      align='edge', color=color)
88              plt.legend(loc='upper right', bbox_to_anchor=(1, 1))
89              plt.show()
90  return  self.std_dev, self.mean, self.fwhm, self.peaks
91
```

IDEAS Testbench Code

```
    def conf_baseline(asic_id):
    print("ASIC Config Apocat " + str(asic_id) + " - Baseline")
    ch_qc_threshold             = 30
    ch_cmis_detector_ioffset    = 1
    ch_cmis_detector_voffset    = 100
    # Config data channels
    set_threshold(ch_qc_threshold, asic_id)
    cmis_detector_i_AND_V_OFFSETT(ch_cmis_detector_ioffset,ch_cmis_detector_voffset, asic_id)
    _set_field("G_CAL_DAC", 0, asic_id)
    return 0
```

Listing 6: Configures ROSSHIP for baseline test

```

def conf_cal(c_num, c_length, c_int, c_mask):
    tb.writeSysReg(0x0C01,c_pol)
    tb.writeSysReg(0x0C02,c_num)
    tb.writeSysReg(0x0C03,c_length)
    tb.writeSysReg(0x0C04,c_int)
    tb.writeSysReg(0x0C05,0)    # Trigger delay. Not used here.
    tb.writeSysReg(0x0C06,c_mask)
    if c_mask == 1:
        mask = "cal_control"
    elif c_mask == 2:
        mask = "DCAL"
    elif c_mask == 4:
        mask = "HOLD"
    else:
        print("Invalid mask value")
```

Listing 7: Configures the cal pulse generator with the specified attributes

```
def testBaseline(asic_id):
    test_func_txt = "Baseline"
    log_file,log_writer = log_file_open(test_func_txt)
    error_status = conf_baseline(asic_id) # configure ASIC for baseline test
    # initialize module for baseline test
    tb.writeSysReg(0xE020, 0)                    # Readout - Disable
    tb.resetReadoutData()
    tb.writeSysReg(0xE021, 0)                       # cfg_hold_type - Calibration hold (forced readout)
    tb.writeSysReg(0x0E00, 0)                    # DAC - Calibration
    tb.writeSysReg(0x0E22, 0)                    # DAC - Detector bias
    tb.writeSysReg(0xE020, 1)                    # Readout - Enable
    print("Configuring cal gen.")
    conf_cal(1, BASELINE_CAL_TST_NUM_PULSES, BASELINE_HOLD_WIDTH, BASELINE_INTERVAL, 4)
    send_cal()
    tb.resetReadoutData()
    if (error_status == 0):
        conf_baseline_plot()
        tb.plotClear()
        send_cal()
        counter = 0
        while (tb.getReadoutCount() < BASELINE_TST_NUM_PULSES_LIMIT):
            time.sleep(.1)
            counter = counter + 1
            send_cal()
            if counter > timeout:
                print("Readout timed out!")
                error_status = 1
                break
        global baseline
        baseline = [0 for i in range(0,16)]
        noise = [0 for i in range(0,16)]
        baseline[0:16] = tb.getReadoutMean(asic_id)[19:3:-1]
        noise[0:16] = tb.getReadoutStdDev(asic_id)[19:3:-1]
        M = [[0 for ch_i in range(0,len(baseline))] for plot in range(0,2)]
        x_curve = [[0 for ch_i in range(0,len(baseline))] for plot in range(0,2)]
        noise_plot = [0]*len(noise)
        for ch_i in range(0,len(noise)):
            noise_plot[ch_i] = noise[ch_i]
        M[0] = noise_plot
        M[1] = baseline
        ch_val = [0]*len(noise)
        for ch_i in range(0,len(baseline)):
            ch_val[ch_i] = ch_i
        x_curve[0] = ch_val
        x_curve[1] = ch_val
        tb.plotEx2(x_curve,M,2) # Steps
        print("Save Plot")
        tb.plotSave( get_plot_filename(test_func_txt) )
        baseline = [round(x,2) for x in baseline]
        log_writer.writerow(["ADC values for forced readout on all channels"])
        log_writer.writerow([" "])
        log_writer.writerow(["ASIC"] + ["Channel"] + ["ADC value"] + ["Std Dev"])
        for i in range(0, len(baseline)):
            log_writer.writerow([str(asic)] + [ch] + [str(baseline[i])] + [str(noise[i])])
            ch += 1
            if ch == 16:
                ch = 0
                asic += 1
    log_file.close()
    return test_func_txt,error_status
```

Listing 8: Starts the Baseline Calibration

```
#######__________  Gain CALibrtion ______#########
def gain(asic_id):
    # -------- User Settings --------
    chargeValues                = [15, 30]      # Wanted charge amplitudes.
    numPulses                   = 10000          # Number of calibration pulses (per measurement point).
    numChannels                 = 16             # Number of channels to test.
    timeout                     = 1000
    ch_qc_threshold             = 200
    ch_cmis_detector_ioffset    = 1
    ch_cmis_detector_voffset    = 100
    ######_________________________________________________#################
    ### -------- Plot Settings -------- ###
    tb.plotSetXAxis("Channel")
    tb.plotSetYAxis("Gain [LSB/pC]")
    x = range(0,numChannels)
    y = range(0,numChannels*number_of_ASICS)
    ### changing Asic register for Gain readout _____________________________________________________#################
    #for asic_id in range(0,number_of_ASICS):
    # ================= Calibration settings ==================
    cal_mode = 1        # 0=off, 1=digital cal-pulsing, 2=analog cal-pulsing
    calDAC = 1000         # max value = 4095, LSB = 24.4mV, analog cal-pusling
    int_calDAC = 500      # max value = 255,  LSB = 4.61mV, digital cal-pulsing implemented only for ASIC 0
    mean_all = [[0 for col in range(len(chargeValues))] for row in range(numChannels)]
    global gain_all
    gain_all = [0] * numChannels
    for i in range(0, numChannels): #
        for j in range(0, len(chargeValues)):                   # Going through all pulse amplitudes
            tb.resetReadoutData()
            cal2 = cal2dac(chargeValues[j])                     # Calc cal amplitude
            cmis_detector_i_AND_V_OFFSETT(ch_cmis_detector_ioffset,ch_cmis_detector_voffset, asic_id,i)
            Configure_gain_calibration_unit(asic_id,cal_mode, i, cal2)
            send_cal()                                          # Sending cal pulses
            counter = 0
            while (tb.getReadoutCount() < numPulses):       # Waiting until all readouts have been registered
                time.sleep(.01)
                counter = counter + 1
                if counter > timeout:
                    print("Readout timed out! For Asic:"  + str(asic_id))
                    break
            mean_all[i][j] = round(tb.getReadoutMean(asic_id)[19-i] - baseline[i],3)
            print( "round(tb.getReadoutMean(asic_id)[19-i] is " + str(round(tb.getReadoutMean(asic_id)[19-i])) +" with baseline[i]" +str(
            time.sleep(.5)
            tb.resetReadoutData()
        gain_all[i] = round((mean_all[i][1] - mean_all[i][0]) / (chargeValues[1] - chargeValues[0]),4) # Calc Gain for the asic
        tb.plotSetTitle("Gain for all channels Asic: " +str(asic_id+1))
        tb.plot(x,gain_all)
        log_writer.writerow([asic_id+1]+[i+1]+ [str(mean_all[i][0])] + [str(mean_all[i][1])] + [str(gain_all[i])] )
        _set_field("TER_" + str(i), 0, asic_id)
        #--------  calculation --------
        tb.plotSave(get_plot_filename( str(asic_id+1) ) )
        average = round(sum(gain_all)/len(gain_all),3)
        dev_all = [0] * len(gain_all)
        for i in range(0, len(dev_all)):
           dev_all[i] = (gain_all[i] - average)*(gain_all[i] - average)
        var = sum(dev_all)/len(dev_all)
        stddev = round(math.sqrt(var),3)
        print (' NEW CHANNEL <=========================' + str(numChannels)  +'\n')
        print (' Asic: ' +  str(asic_id+1) + "->  Mean for all channels: " + str(mean_all)  )
        print (' Asic: ' +  str(asic_id+1) + "->  Gain for all channels: " + str(gain_all)  )
        print (' Asic: ' + str(asic_id +1)+  "->  Standard deviation of channel gain: "  + str(stddev) )
        print (' Asic: ' + str(asic_id +1)+  "->  Average channel gain: " + str(average))
    log_file.close()
    print ("Log file named:  " + log_file_name + " created.")
```

Listing 9: Starts the Gain Calibration